CERN/PS/AA 78-3
27.1.1978

APPENDIX B

DESIGN STUDY OF A PROTON-ANTIPROTON COLLIDING BEAM FACILITY

FOREWORD

The idea of studying proton-antiproton collisions in storage rings has tempted physicists for a long time; in fact, the first suggestions in this direction were made before proton storage rings existed. The luminosity that could be hoped for was, unfortunately, not high enough for most experiments.

The development of beam cooling techniques has changed this, because cooling permits the accumulation of antiprotons in a storage ring over a long time, as pointed out by Budker and Skrinsky in 1966. C. Rubbia, during 1975 and 1976, worked out various antiproton collection schemes. His proposal was to inject the antiprotons into the SPS and accelerate them, together with protons, to 270 GeV, which is the maximum energy at which it can store particles continuously.

During 1976, two working groups examined the technical aspects of the scheme and the possibilities of $p\bar{p}$ physics. As a result, an experiment (ICE) on stochastic and electron cooling was initiated, and in parallel a study group was formed to prepare the present detailed design for a $p\bar{p}$ facility, using the SPS as a storage ring. During the study, it appeared that at a little extra cost the antiprotons could also be injected into one of the ISR rings. This feature was therefore added without, however, including any modifications to the ISR that might be required as a consequence.

The participants in this study are listed in Appendix A.

C O N T E N T S

I. INTRODUCTION

1.1 Choice of cooling method

Cooling is necessary for collecting a large number of antiproton batches in a storage ring and for compressing their phase space volume to a size acceptable to the SPS. In the present design, the following figures are relevant :

Phase space area	Accepted by cooling ring	Accepted by transfer channel and SPS
Longitudinal	350 mrad	72 mrad
Horizontal	100π mm.mrad	1.4 π mm.mrad
Vertical	100π mm.mrad	1 π mm.mrad

The figures for the cooling ring refer to a single antiproton pulse; for obtaining the design luminosity of 10^{30} cm^{-2} s^{-1}, about 24,000 pulses must be superimposed in phase space.

Two cooling methods (electron cooling and stochastic cooling) exist. Rubbia's earliest proposals (1975) assumed stochastic cooling; the stacking was to be done in betatron space[1]. The fast initial cooling needed for stacking appeared to be difficult in the presence of an intense stack and so a proposal using two separate rings emerged. With the then existing techniques this solution seemed somewhat marginal.

After the successful experiments by Budker's group at Novosibirsk[2], electron cooling appeared to promise higher intensities. One of its important features is that the cooling rate does not depend on intensity; on the other hand, for obtaining a sufficiently high rate with acceptable electron beam currents, the antiproton energy must be low (e.g. 100 MeV). Since at this energy few antiprotons are produced, deceleration is required and after stacking, the antiprotons would have to be accelerated again for injection into the SPS.

This also resulted in a two-ring design, including complicated beam transfer and radiofrequency systems. This design was evaluated in detail during 1976 and 1977[3]. In parallel, however, stochastic cooling was further studied with the specific aim of arriving at a design with a single d.c. operated ring.

This work resulted in a better understanding of the stochastic cooling theory. Some methods were also discovered that promised better cooling. In particular, stacking was found to be easier in momentum space than in betatron space. A method was devised for precooling each injected pulse separately before adding it to the stack. In the meantime, many experiments were performed at the ISR. Although the cooling rate in these experiments was about three orders of magnitude below what is needed for precooling in the antiproton ring, they tend to confirm the existing theory. The same theory predicts a sufficiently high rate in the antiproton ring, mainly because of the larger revolution frequency spread and the smaller number of particles, but also because many more pick-up electrodes and a higher wide-band output power will be available.

The present design, therefore, is based on stochastic cooling using a single ring.

1.2 General description

Protons of 26 GeV/c from the PS will be directed onto a target. The antiprotons produced there will be focused and injected into the cooling ring that will work at a fixed field corresponding to a nominal momentum of 3.5 GeV/c. Each injected pulse will undergo a first rapid cooling treatment to reduce its momentum spread (precooling). It will then be deposited by a radio-frequency system at the top of a stack which has a slightly lower momentum than the injected beam. The stack is cooled continuously, both longitudinally and transversely. As a result, the particles will slowly migrate to the bottom of the stack, where finally a beam of sufficient density will be formed.

The same radiofrequency system then captures a certain fraction of this stack at a time in a single bunch and accelerates this back to the extraction orbit, which is the same as the injection orbit. This bunch will then be extracted and transferred to the SPS. For the design luminosity of 10^{30} cm^{-2} s^{-1}, six bunches, each containing 1/6 of the stack, will be transferred successively within a fraction of a second.

The ring will be located in a new building to be situated near the transfer tunnel TT2, downstream of the PS Booster complex (Fig. 1.1). The extracted antiprotons will follow the existing tunnels TT2a and TT60. Some of the existing extraction elements of the SPS will be used for injecting the antiprotons. Six bunches of antiprotons will be accelerated by four PS type cavities. The protons will be injected between 10 and 14 GeV/c and the bunches matched to the existing 200 MHz RF system at 18 GeV/c. The latter then takes the protons and antiprotons up to e.g. 270 GeV/c, where they will stay as long as their lifetime permits. The beams will be kept bunched in order to increase the interaction rate at the straight section(s) where the experiments will be performed. A low-beta section will further increase the luminosity.

Transfer to the ISR (ring 1) follows the normal route through TT2. In fact, the beam towards the SPS will cross the PS-ISR beam; a bending magnet at the crossing point is all that is needed to direct the antiprotons towards the ISR.

1.3 Choice of the main parameters

1.3.1 Proton source and primary momentum

The antiprotons could be produced by protons from either the PS or the SPS. At SPS energies, the production rate could be about four times as high as that from 26 GeV/c protons. However, the interference with normal SPS physics would be strong; during the long accumulation periods, the SPS would not be available for other purposes. Simultaneous $\bar{p}$ collection and $p\bar{p}$ experiments in the SPS would also be excluded.

With the PS as a proton source, the collection of antiprotons can go on in parallel with the normal PS, ISR and SPS operation. The PS acceleration cycles for $\bar{p}$ production could be interleaved with cycles for SPS or PS physics or for filling the ISR. A minimum repetition period of 2.6 seconds has been assumed for the present design, but this could of course be increased, depending on other users of the PS machine. Faster repetition is excluded by the precooling requirements.

1.3.2 Diameter of the ring

Single-turn extraction of the protons from the PS will normally produce a pulse with a duration of 2.1 μs. It would be difficult to inject a stream of antiprotons of this duration into a ring smaller than the PS itself, since multiturn injection is not possible because of the large phase space volume occupied by the antiprotons.

However, as will be discussed in Section 5, it is possible to inject the protons from the PS Booster into the PS in such a way that only one quarter of the PS circumference is filled. Thus, the cooling ring may have one quarter of the PS diameter (i.e. 50 m) and still accept all antiprotons produced.

The circumference of the extraction orbit will be made exactly equal to 1/44 of the SPS circumference. This will simplify the rf synchronization between the two machines.

1.3.3 Antiproton momentum

Although it would seem that with 1/4 of the PS circumference the cooling ring could work at up to 7 GeV/c, this appears to be impractical for several reasons :

a) As may be seen from Fig. 1.2, a relatively large fraction of the circumference is needed for injection, extraction, cooling and diagnostic equipment. This alone would prevent the use of a momentum higher than 3.5 GeV/c.

b) The output power needed for the precooling stage increases with the square of the momentum. It would be difficult to increase it much beyond the figure foreseen at present (25 KW, 150-400 MHz bandwidth).

c) The 152° bend in the transfer line to the SPS requires only a small addition to the existing tunnels if the momentum is 3.5 GeV/c. Any increase would result in more interference with the SPS programme because of the extra civil engineering work that would be needed.

For these reasons the figure of 3.5 GeV/c has been chosen, even though it is well below the usual SPS and ISR injection momenta.

1.3.4 Momentum spread and emittance of the injected $\bar{p}$ beam

The total number of particles accepted is proportional to the momentum spread and to the square root of the emittance in each plane*.

Consideration of the influence of these parameters on the apertures required and on the power needed for the precooling system led to the following figures :

Horizontal and vertical emittance	100π mm.mrad
Momentum spread	$\pm$ 0.75%

Fig. 2.4 shows the actual apertures resulting from this choice. These depend of course on the lattice adopted, which will be discussed in more detail in Section 2.

---

* This is somewhat unusual; with constant phase-plane density at the target one would expect it to increase with the first power of the emittances. It is due to the imperfect matching that can be achieved with a target which is long compared to the β value at its centre.

1.4 Expected performance

The rate at which antiprotons can be accumulated and the luminosity obtained in the SPS are the two most important performance figures. To a certain extent they are independent, since accumulation could go on during normal SPS operation and the time needed is therefore not a critical parameter. Nevertheless, very large accumulation times would be inconvenient and also increase the risk of sudden beam loss due to random failures. Moreover, an accumulation time not longer than the useful lifetime in the SPS would simplify operation.

For this reason, the luminosity estimate is based, admittedly somewhat arbitrarily, on a time of accumulation of 24 hours.

Further assumptions are : a repetition period of 2.6 s and a PS intensity of 10^{13} protons per pulse. The number of antiprotons accepted per cycle will then be 2.5×10^{7}. After 24 hours of operation, taking into account transfer losses, occasional PS stops, etc., the total number of antiprotons accumulated will be 6×10^{11}.

These will be distributed over six bunches and collide in the SPS with six proton bunches.

The luminosity will be :

$$L = \frac{2 N_p N_{\bar{p}} f_r}{M \left[\beta_H \beta_v \, (E_{Hp} + E_{H\bar{p}}) (E_{vp} + E_{v\bar{p}}) \right]^{\frac{1}{2}}}$$

With the values of table 1.1, we find

$$L = 10^{30} \text{ cm}^{-2} \text{ s}^{-1}$$

TABLE 1.1

N_p	total number of p		6×10^{11}
$N_{\bar{p}}$	total number of $\bar{p}$		6×10^{11}
f_r	revolution frequency		43.4 KHz
M	number of bunches		6
β_H	horizontal betatron function	at the interaction point	4.7 m
β_v	vertical betatron function	at the interaction point	1.0 m
E_{Hp}	proton emittances at 270 GeV/c		$6.9 \times 10^{-8}\pi$ rad m
E_{vp}	proton emittances at 270 GeV/c		$3.5 \times 10^{-8}\pi$ rad m
$E_{H\bar{p}}$	antiproton emittances at 270 GeV/c (allowing for blow-up by a factor 1.5)		$3.8 \times 10^{-8}\pi$ rad m
$E_{v\bar{p}}$	antiproton emittances at 270 GeV/c (allowing for blow-up by a factor 1.5)		$1.9 \times 10^{-8}\pi$ rad m

It must be made clear that the luminosity depends on many different features. It is not excluded that the initial value could be smaller and that the design figure would only be reached after an initial development period.

2. LATTICE AND APERTURES

2.1 Introduction

The lattice of the antiproton ring must fulfil the requirements both for storage and stochastic cooling. In contrast with conventional storage rings, the injected beam will have very large transverse emittances and momentum spread. Also the stochastic cooling process requires that "mixing" of a sample of particles occurs due to their spread in revolution frequency. This implies a large average value of the momentum compaction function α_p. Clearly these two characteristics combine to give very large radial beam sizes.

2.2 Injection and storage requirements

To permit the injection of the large emittance, large momentum spread beam, the focusing structure must be such as to minimise the "kick" strength required. For this reason the injection septum must be located in a region where α_p is close to zero. In addition, to avoid perturbing the stacked beam, it must be screened from the injection kicker by means of a moveable shutter. To permit this, the stack and the injected beam are separated in momentum by an amount Δp. This is shown in figure 2.1 and it can be seen that for a shutter thickness t and horizontal beam emittance πE_H, the momentum separation is given by

$$\frac{\Delta p}{p} = \frac{1}{\alpha_p} \left[t + 2 \sqrt{E_H \beta_H} \right]$$

where α_p and β_H are the values of the momentum compaction and betatron functions at the shutter position. Clearly this momentum separation contributes to the apertures required around the ring so that it is important to design the lattice such that $\alpha_p = 0$ at the septum position and its value at the injection kicker (i.e. 90^0 of horizontal phase advance downstream) is as close as possible to the maximum value.

2.3 Stochastic cooling requirements

Each injected pulse of antiprotons is subjected to a fast "pre-cooling" of its momentum spread. As in the case of the injection kickers, the pre-cooling kickers have shutters to confine their effect to the injected beam. Hence they must be located in a region of high α_p. However, each time a particle receives an impulse δp its closed orbit is shifted by an amount $\alpha_p \frac{\delta p}{p}$ and statistically this would blow up the betatron oscillations and counteract the betatron cooling. This effect must be avoided by providing two regions of equal and high α_p separated by a half wavelength of betatron oscillation so that the impulse can be applied in two halves without inducing any betatron motion.

To provide adequate "mixing" of particles, the absolute value of the dispersion in revolution frequency f, given by

$$\eta = -\frac{\delta f/f}{\delta p/p} = \frac{1}{\gamma_t^2} - \frac{1}{\gamma^2}$$

should be at least 0.1 which corresponds to a maximum transition energy $\gamma_{tr} < 2.45$ or an average α_p of 4.2 m in a ring of average radius 25 m.

2.4 Lattice design

In summary the basic requirement on the focusing and bending structure is for a ring one quarter the circumference of the PS, with a nominal momentum of 3.5 GeV/c, a transition energy $\gamma_{tr} < 2.45$ and a large amount of straight section space. To achieve the large average value of α_p with zero at the injection septum, the momentum compaction function should rise as quickly as possible after this and stay at a high value elsewhere in the ring.

Many types of focusing structure were examined: separated function, combined function and hybrid. Two possible solutions were found, namely a triplet type as in the PS Booster or a FODO type. Careful comparison of these showed that although the triplet lattice had lower betatron function values in the bending regions, the peak α_p and large momentum width combined to give excessively large quadrupole apertures. This in turn reduced the available gradient and increased the quadrupole length at the expense of free straight section space.

It has been shown[4] that in a "smooth" FODO lattice with equal bends it is possible to produce a region of $\alpha_p = \alpha'_p = 0$ by adjusting the bending angles in adjacent cells. Two independent variables were required so that choosing one of the bending angles as zero fixed both the phase advance and the remaining bend. Using this approach a lattice was designed which satisfies all the above conditions. The main parameters are given in table 2.1 and the betatron functions are plotted in figure 2.2.

The betatron tunes $Q_H = 2.29$, $Q_V = 2.28$ are in a region of the working diagram which is free of non-linear resonances up to seventh order (Fig. 2.3). Variations of the vertical tune do not affect the momentum compaction function but horizontally the maximum and minimum values change by :

ANTIPROTON RING 12 PERIODS D/2 F D/2 AGS VERSION 75.03 24/11/77 16.44.58

CIRCUMFERENCE = 156.49200 2 HALF SUPERPERIODS STRAIGHT MAGNETS ALL VALUES AT EXIT OF ELEMENTS

NO	ELEM	L(M)	DIST(M)	ANG(MR)	K(1/M2)	BETAV(M)	BETAH(M)	ALPHAV	ALPHAH	MUV/2PI	MUH/2PI	ALPHAP(M)	ALPHAP
INITIAL			0.0000			10.54954	7.12218	0.00000	0.00000	0.00000	0.00000	6.03343	.000000
1	D	.2700	.2700	0.00000	.2180866	10.38958	7.24630	.58931	-.46215	.00409	.00600	6.08146	.356211
2	SS1	.4825	.7525	0.00000	0.0000000	9.85109	7.73127	.52674	-.54296	.01169	.01627	6.25333	.356211
3	BP1	1.4450	2.1975222	.54630	0.0000000	8.15361	9.63145	.61878	-.78297	.03746	.04282	6.82394	.579680
4	BP1	1.4450	3.6425222	.54630	0.0000000	6.36350	12.21956	.58925	-1.02298	.06961	.06391	7.91481	.803150
5	SS2	2.6080	6.2505	0.00000	0.0000000	4.72994	18.09452	.03711	-1.45976	.14845	.09151	10.00942	.803150
6	F	.2700	6.5205	0.00000	-.2940930	4.85729	19.08575	-.40024	.02113	.15748	.09377	10.11839	.062593
7	F	.2700	6.7905	0.00000	-.2940930	5.10840	18.67203	-.87216	1.50022	.16612	.09604	10.01082	-.794019
8	SS2	2.6080	9.3985	0.00000	0.0000000	12.03465	12.03101	-1.76060	1.04619	.21976	.12388	7.92958	-.798019
9	BP1	1.4450	10.8435222	.54630	0.0000000	17.11651	9.38698	-1.66880	.79669	.23581	.14540	6.94607	-.574550
10	BP1	1.4450	12.2885222	.54630	0.0000000	21.44048	7.46404	-1.24916	.54720	.24782	.17276	6.28281	-.351080
11	SS1	.4825	12.7710	0.00000	0.0000000	22.67372	6.97652	-1.30678	.46320	.25131	.18343	6.11341	-.351080
12	D	.2700	13.0410	0.00000	.2180866	23.02201	6.84799	-.02365	.01534	.25318	.18967	6.06703	.007058
13	D	.2700	13.3110	0.00000	.2180866	22.64644	6.95978	1.35259	-.43155	.25506	.19591	6.11723	.365309
14	SS3	1.9935	15.3045	0.00000	0.0000000	17.75216	9.35771	1.10354	-.77133	.27091	.23564	6.84548	.365309
15	SS3	1.9935	17.2980	0.00000	0.0000000	13.84864	13.11033	.65449	-1.11110	.29120	.26444	7.57372	.365309
16	SS3	1.9935	19.2915	0.00000	0.0000000	10.93849	18.21763	.60544	-1.45088	.31709	.28902	8.30196	.365309
17	F	.2700	19.5615	0.00000	-.2940930	10.85223	18.61450	-.28367	-.00849	.32105	.28735	8.31141	-.205455
18	F	.2700	19.8315	0.00000	-.2940930	11.24925	18.22667	-1.19728	1.43463	.32495	.28967	8.24296	-.949916
19	SS3	1.9935	21.8250	0.00000	0.0000000	15.86249	13.17360	-1.62652	1.10015	.34806	.31021	6.24932	-.949916
20	SS3	1.9935	23.8185	0.00000	0.0000000	24.23510	9.25409	-2.05977	.76567	.36377	.33879	4.35566	-.949916
21	SS3	1.9935	25.8120	0.00000	0.0000000	33.30706	7.06815	-2.49101	.43119	.37495	.37600	2.46201	-.949916
22	D	.2700	26.0820	0.00000	.2180866	34.12695	6.95810	-.52950	-.02143	.37622	.38414	2.22444	-.812122
23	D	.2700	26.3520	0.00000	.2180866	33.87268	7.09154	1.46550	-.47542	.37748	.39026	2.02230	-.667256
24	SS4	.5053	26.8573	0.00000	0.0000000	32.41571	7.61609	1.41655	-.56277	.37990	.40123	1.67506	-.667256
25	BP2	2.4650	29.3423340	.30557	0.0000000	22.67174	11.38642	2.27330	-.98415	.39451	.44337	.41877	-.343628
26	BP2	2.4650	31.8272340	.30557	0.0000000	11.14034	17.21082	2.09578	-1.40553	.41950	.47123	.00000	.000000
27	SS4	.5053	32.3325	0.00000	0.0000000	9.14611	18.67523	1.85123	-1.49286	.42747	.47571	.00000	.000000
28	F	.2700	32.6025	0.00000	-.2940530	8.36513	19.08490	1.06193	-.61353	.43240	.47798	.00000	.000000
29	F	.2700	32.8725	0.00000	-.2940930	7.98276	18.68964	.36437	1.46697	.43768	.48025	.00000	-.000000
30	SS3	1.9935	34.8660	0.00000	0.0000000	7.09396	13.51106	.08149	1.13077	.48035	.50027	.00000	-.000000
31	SS3	1.9935	36.8595	0.00000	0.0000000	7.33300	9.67292	-.20139	.79456	.52492	.52816	.00000	-.000000
32	SS3	1.9935	38.8530	0.00000	0.0000000	8.69988	7.17521	-.48427	.45836	.56507	.56662	.00000	-.000000
33	D	.2700	39.1230	0.00000	.2180866	8.83133	7.05211	-.00000	-.00000	.56996	.57268	.00000	-.000000

DP/P	COSMU(H)	Q(H)	QPRIME(H)	BETAMAX(H)	COSMU(V)	Q(V)	QPRIME(V)	BETAMAX(V)	XMAX(H)	GAMMA TR.
0.0000	.61114	2.2907	-2.8139	19.0658	.63782	2.2798	-1.2676	34.1270	10.1184	2.4347
-.0500	.60793	2.2920	-2.8195	19.7266	.62999	2.2831	-1.2776	35.1430	-.4769	2.5487
-.0400	.60923	2.2915	-2.8164	19.5029	.63297	2.2818	-1.2758	34.9568	-.3865	2.5241
-.0300	.61014	2.2911	-2.8143	19.2783	.63518	2.2809	-1.2739	34.7613	-.2935	2.5005
-.0200	.61073	2.2909	-2.8132	19.0543	.63669	2.2803	-1.2719	34.5571	-.1980	2.4778
-.0100	.61105	2.2907	-2.8130	19.0271	.63755	2.2799	-1.2698	34.3454	-.1001	2.4559
.0100	.61105	2.2907	-2.8157	19.2611	.63755	2.2799	-1.2652	33.9029	.1022	2.4143
.0215	.61076	2.2909	-2.8188	19.4787	.63663	2.2803	-1.2624	33.6394	.2223	2.3916
.0300	.61046	2.2910	-2.8220	19.6488	.63556	2.2808	-1.2603	33.4416	.3126	2.3754
.0400	.61001	2.2912	-2.8265	19.8579	.63393	2.2814	-1.2577	33.2063	.4206	2.3569
.0500	.60950	2.2914	-2.8318	20.0758	.63191	2.2823	-1.2550	32.9691	.5303	2.3390

TIME = .215 SECONDS

Table 2.1 Lattice Parameters

$$\Delta\alpha p_{max} = -\ 23\ \Delta Q_H \quad (m)$$

$$\Delta\alpha p_{min} = 8.3\ \Delta Q_H \quad (m)$$

2.5 Off-momentum orbits

A sextupole scheme which to a first order cancels the machine chromaticity in both planes, has been calculated. The sextupole components will be incorporated into the profile of the quadrupoles, and the required strengths are $K'_F = -0.048\ m^{-3}$ and $K'_D = 0.057\ m^{-3}$. With these conditions the residual variation in tunes within a momentum range of ± 3% is such that

$$\Delta Q_H < 4 \times 10^{-4} \quad \text{and} \quad \Delta Q_v < 1 \times 10^{-3}$$

over most of the aperture. An additional small correction to the quadrupole profile will create a slight over compensation of the natural chromaticity near the bottom of the stack in order to suppress the transverse resistive wall instability. This will only be required at the end of cooling, when nearly all particles will be at the bottom of the stack. A normal sextupole type correction would cause an undesirable Q variation across the aperture.

2.6 Apertures

The aperture requirements are based on the need to have a stacked beam with a total momentum width of 2.5%, an injected beam of 1.5%, both with horizontal and vertical emittances of 100π mm.mrad and separated by a momentum "gap" of 1.8% (see figure 2.1). This gives a total acceptance needed of 5.8% in momentum and 100π mm.mrad transverse emittances. The corresponding beam sizes in one quadrant of the machine are shown in figure 2.4. Since the machine lattice has reflection symmetry at the injection region, it was decided to use a split septum magnet which can then serve in common for injection and extraction. The resulting beam apertures in the injection region are also shown in figure 2.4 and the beam geometry around the septum in figure 4.5.

2.7 Intensity-dependent effects

At the end of the stacking period, some intensity-dependent effects may become noticeable. These will be discussed below, assuming the following stack parameters :

$$\Delta p/p = \pm\ 1.5 \times 10^{-3}$$
$$E_H = 1.4\ \pi \text{ mm.mrad}$$
$$E_V = 1\ \pi \text{ mm.mrad}$$
$$N = 6 \times 10^{11}$$

2.7.1 Intra-beam scattering

This is the most important effect. It has been evaluated following Piwinski's theory [5]. The blow-up is a function of the momentum spread and the transverse emittances. For the values above, the blow-up times are

horizontally	:	0.5 h.
vertically	:	23 h.
longitudinally	:	2.4 h.

The horizontal and longitudinal blow-up rates increase rapidly if either $\Delta p/p$ or the horizontal emittance are decreased. The vertical rate depends mainly on $\Delta p/p$ and on the vertical emittance. As it happens, the effect is just small enough to be overcome by the stochastic cooling.

2.7.2 Incoherent tune shift

The direct effect (without images) will be at most

$$\Delta Q_V = -0.0025$$

The contribution from images is somewhat more difficult to estimate because the shape of the vaccum chambers is complicated and not yet completely defined. However, a rough estimate shows that the image effects

will be about 10 times smaller than the direct effect, because of the small dimensions of the stack compared to the vacuum chamber aperture. Partial neutralization of the stack due to ionisation of the residual gas will further reduce this effect.

2.7.3 Transverse instability

The main contribution to transverse instability will come from the frequency shift corresponding to the incoherent space charge effect. To increase the Landau damping, we shall shape the quadrupole profile so as to make the chromaticity slightly positive at the bottom of the stack. A chromaticity value of 0.2 can be obtained locally in both planes without exceeding a Q spread across the stack of 0.01. This spread must be kept small to avoid losses on resonances, since the particles migrate slowly towards the bottom of the stack.

Even with this chromaticity we still expect that the lowest modes will be unstable at the final stack density. An active feedback system covering the range 1-25 MHz will therefore be provided for each plane.

Other contributions to the instability will be less important. Both the resistive wall effect and the low frequency effect of cross-section variations will be negligible. Resonances of cavity-like objects do not seem dangerous because at the high frequencies concerned the Landau damping is sufficiently strong. Only the coupling impedance due to special objects (pick-ups, kickers) may have to be watched. No great problems are expected, however.

2.7.4 Longitudinal instability

The condition for longitudinal stability will be most stringent when 5 batches have been extracted and the last one, still with its initial density, remains. Under this condition, we have according to the Keil - Schnell criterion [6] :

$$\frac{Z_{//}}{n} < 840\ \Omega$$

The contributions to Z/n from the negative mass effect (25 Ω) and from the resistive wall (< 2 Ω) will be negligible. Resonant cavity-like objects do not seem dangerous, but will have to be watched and maybe damped in some cases.

The main contribution will probably come from the kickers for momentum cooling of the stack (see Section 5). Because of the ferrite rings surrounding the beam and the loading by the external circuit, these will appear to the beam as an inductance L and a resistance R connected in parallel. The inductance is proportional to the ferrite cross-section, which is determined by the requirement that at the lowest frequency used for stochastic cooling (250 MHz) the value of ωL should be large compared to R. For instance, with R = 50 Ω, ωL = 500 Ω at 250 MHz, and with 70 rings, the contribution to Z/n from ωL will be 250 Ω, independent of frequency. The parallel R will only reduce this value.

2.7.5 Ion-antiproton oscillations

This effect is discussed in Section 7.1

3. MAGNET SYSTEM

3.1 Magnet design

The magnet system must provide very wide apertures and yet occupy a minimum of azimuthal space. All elements are designed to operate DC but may be laminated or built from plates for ease of fabrication.

Two types of dipole bending magnets are proposed. The large angle magnets in the region of small momentum dispersion occupy most of the free space between consecutive quadrupoles. In this way it is possible to achieve the required deflection at a field level of 1.6 T so that a simple H magnet with flat coils can be used. Elsewhere the very wide apertures together with the need to leave as much free space as possible, led to a window-frame design with a field level of 1.8 T. The cross-sections of these dipoles are shown in figures 3.1 and 3.2 and the main parameters listed in table 3.1.

After allowing for closed orbit deviations, vacuum chamber wall and thermal insulation around the vacuum chamber, the magnet gaps are such that the H and window-frame versions require equal excitations. This is maintained by designing the magnetic circuits with an equal degree of saturation, so that they can be powered in series. The number of excitation turns was then chosen to give a current below 2,000 amps to keep cable costs down. Further considerations include : the number of parallel water cooling circuits, the total ring voltage, coil fabrication costs, and the need to locate about one quarter of the ampère-turns of the window-frame type coil inside the pole gap.

The quadrupoles will be of two types with large and small apertures and all having the same effective length. The distribution of these two types around the ring is determined by the azimuthal variation in momentum compaction.

TABLE 3.1

Dipole Parameters

Type	"H"	Window Frame	
No.	4	8	
Field	1.6 T	1.8 T	
Gap	157.5 mm	140 mm	
Effective length	4.97 m	2.89 m	
Steel length	4.79 m	2.73 m	
Overall length	∿ 5.3 m	∿3.4 m	
Width overall	∿ 1.8 m	∿2.5 m	
Good field ½ width	120 mm	282 mm	
Turns/pole	54	54 (12 in gap coil;42 in main coil)	
Conductor	24 x 24 mm^2	32 x 17.3 mm^2	25.2 x 24.5 mm^2
Hole for cooling water	12.5 mm	7.8 mm	8.5 mm
No. of cooling circuits/pole	3	1	3
Current	1950 A	1950 A	1950 A
Power/magnet	202.8 kW	27.8 kW	93.6 kW
Δp	20 kp/cm^2	20 kp/cm^2	20 kp/cm^2
ΔT	19.6°C	18.6°C	18.7°C
Mean length of one turn	11.2 m	7.7 m	8.2 m
Water flow/magnet	2.5 ℓ/s	0.4 ℓ/s	1.2 ℓ/s
Volts/magnet	104 V	14.2 V	48 V

In order that all F quadrupoles can be powered in one circuit and all D's in another, the focusing strengths of large and small types must be equal at equal currents. Thus the inscribed apertures are chose in the ratio $\sqrt{2}$: 1 and the excitation coils designed with a turns ratio of 2 : 1.

As in the case of the dipoles, the number of turns has been chosen to give an excitation current below 2,000 amps. The resulting quadrupole cross sections are shown in figures 3.3 and 3.4 and the main parameters are given in table 3.2.

The small quadrupole having a fairly low total flux has been designed with a parallel sided pole so as to allow the use of simple, flat, rectangular cross-section coils.

Also, a reduced aperture version of the small quadrupole will be produced for use in the injection beam line. This will have the same excitation coil and external dimensions, but a modified pole profile.

The large aperture quadrupole must have a tapered pole to avoid excessive saturation and in addition it is estimated that due to its length being almost equal to the inscribed diameter, the steel length will need to be equal to the required effective length.

It is proposed to shape the quadrupole profiles to provide the sextupole component which will make the chromaticity zero in both planes (see Section 2.5).

The magnet system will be powered in three separate circuits, one for the dipoles and one each for the F and D quadrupoles. Table 3.3 gives the overall characteristics of these three circuits.

TABLE 3.2

Quadrupole Parameters

	Large	Small	Injection
No.	16	8	8
Strength	1.85 T (F) 1.37 T (D)	1.85 T (F) 1.37 T (D)	4 T
Inscribed radius	208 mm	147.08 mm	75 mm
Effective length	0.54	0.54	0.54
Steel length	$\sim$ 0.54	$\sim$ 0.49	$\sim$ 0.49
Overall length	$\sim$ 0.86	$\sim$ 0.77	$\sim$ 0.77
Width overall	$\sim$ 2.2	$\sim$ 0.96	$\sim$ 0.96
Turns/pole	40	20	20
Good Field $\frac{1}{2}$ width	340	160	80
Conductor dimensions	21.5x18.0 mm^2	14.5x18.2 mm^2	
Hole for cooling water, diameter	8 mm	4.8 mm	
No. of cooling circuits/pole	1	1	
Mean length of one turn	2.6	1.7	
Flow/magnet	0.72 ℓ/sec	0.34 ℓ/sec	
Δp	20 kp/cm^2	20 kp/cm^2	
ΔT	20°C(F) 11°C(D)	18.8°C(F) 10.3°C(D)	5.4°C
Nominal gradient	3.429 T/m (F) 2.542 T/m (D)	3.429 T/m (D) 2.542 T/m (F)	7.41 T/m
Current	1550 A 1150 A	1550 A 1150 A	830 A
Power/magnet	59.2 kW 32.6 kW	26.4 kW 14.5 kW	7.6 kW
Volts/magnet	38.2 V 28.3 V	17.0 V 12.6 V	9.1 V

TABLE 3.3

Power Supply Parameters

1. Dipole Circuit

Magnet Current	=	1950 Amps
Magnet Voltage	=	914 Volts
Magnet Power	=	1.78 MWatts
DC Cables Voltage Drop	=	8.8 Volts
Reserve (including connections)	=	77 Volts
Power Supply	=	2000 Amps 1000 Volts (2.0 MVA)

2. F Quadrupole Circuit

Magnet Current	=	1550 Amps
Magnet Voltage	=	380 Volts
Magnet Power	=	0.6 MWatts
DC Cables Voltage Drop	=	7.0 Volts
Reserve (including connections)	=	63 Volts
Power Supply	=	1750 Amps 450 Volts (0.9 MVA)

3. D Quadrupole Circuit

Magnet Current	=	1150 Amps
Magnet Voltage	=	280 Volts
Magnet Power	=	0.32 MWatts
DC Cables Voltage Drop	=	6.9 Volts
Reserve (including connections)	=	43 Volts
Power Supply	=	1300 Amps 330 Volts (0.5 MVA)

3.2 Magnet fabrication

The fabrication techniques which will be employed for the magnetic circuits must be consistent with the high-precision pole profiles required and the very large magnet cross-sections. Since the total core length of any one type of magnet is rather small, it is unlikely that a large, precision punching die will prove to be an economical solution. Initial studies and discussions indicate that in all cases the most promising technique will be to clamp short stacks (1 to 2 m) of plates or laminations and machine them together. These would then be de-burred as necessary and, in the case of the dipoles, stacked against a curved reference surface before being bolted or welded into cores. With this procedure it is possible and preferable to distribute plates from each machining operation uniformly among the required number of magnet cores, to eliminate systematic differences due to the machining.

The excitation coils have all been designed to be as simple as possible. Wherever the requirements allow, the coils are flat and have rectangular cross-sections. Nevertheless, the small quantities required will probably not justify the development and fabrication of vacuum impregnation moulds. Since however very low radiation levels are expected and with the exception of the H type dipole, the coils are fairly short, it will be possible to insulate the coils by using a double half-lapped layer of B-staged glass-mica tape on the individual turns. The coil will then be clamped and heated to partially cure the turn insulation and fix the mechanical dimensions. After this the ground wrap of glass tape is applied and the assembly can be vacuum potted in an open "bath" type of mould. This technique, already widely used, combines the advantages of the higher voltage holding capabilities of mica tapes with the superior mechanical strength of a pure glass/resin insulation.

3.3 Correction elements

Since the ring will always be operated at the same field level, closed orbit corrections and adjustment of coupling may be achieved by displacing or tilting individual quadrupoles. Similarly, field imperfections may be cured by adding end shims to magnets where required.

Little space would be available in the lattice for chromaticity sextupoles. Since it is believed that the fixed correction to the quadrupole profile described in Section 2.5 will be sufficient for all purposes, we do not propose to incorporate any correction elements.

In the event that small corrections do prove necessary, it will be possible to obtain them by shimming. To this end it is foreseen to include a study of the effects of a range of shims as part of the magnetic measurements programme.

4. ANTIPROTON PRODUCTION AND BEAM TRANSFERS

4.1 General description

The position of the Cooling Ring and a schematic layout of the transfer lines is shown in Fig. 4.1. Protons at 26 GeV/c are extracted from the CPS and pass along the existing beam line in TT2. About 140 m downstream of the extraction point they are deflected to the right and traverse a 20 m long tube leading to the building which houses the Cooling Ring. Here the protons are focused onto a target to produce the antiprotons. In the injection transfer line the 3.5 GeV/c antiprotons are matched to the acceptance of the Cooling Ring. One injection takes place every 2.6 seconds. When enough antiprotons have been accumulated and cooled to a small emittance they are extracted and transferred to the SPS via the existing tunnel TT2a and after a bend of 152^0, down TT60. A short tunnel has to be built for the connection from TT2a to TT60. In TT60 the antiprotons travel along the beam line which normally transports high energy protons from the SPS to the West Hall. The antiprotons are injected into the SPS through the extraction channel in LSS6.

The antiprotons can be directed to ring 1 of the ISR by energizing a bending magnet at the crossing point of the antiproton beam with the beam line in TT2.

4.2 Branch-off from TT2 and transfer to the antiproton production target

The layout of the branch-off from TT2 is shown in Fig. 4.2. Immediately downstream of quadrupole QF 215 two C-type bending magnets are installed which deflect the beam horizontally by 4.5^0 to clear the quadrupole QD 216. Two more bending magnets increase the total horizontal angle to 8.5^0 before the beam traverses the tunnel wall. A small extension to TT2 houses a safety beam stopper, two more quadrupoles and two steering dipoles. The beam level in the cooling ring is 1.9 m above that in TT2 so a vertical deflection is also required. This is achieved by a 15^0 tilt of the four bending magnets which provide the horizontal deflection.

From the extension a 20 m long tube leads to the target tunnel which forms part of the building housing the cooling ring. Details of the layout in this tunnel are shown in Fig. 1.2. Here the rising beam is first made horizontal by a vertical bending magnet and then focused by a quadrupole triplet onto the antiproton production target.

The two C-type bending magnets for the branch-off and the 4 quadrupoles situated in TT2 and its extension are of a standard CERN type. The triplet upstream of the target will use quadrupoles from the neutrino area of the CPS. The other two bending magnets in TT2 and the vertical bending magnet in the target tunnel are of the same type as those for the transfer from the cooling ring to the SPS (see Fig. 4.11).

4.3 Antiproton production

The target in which the antiprotons are produced should be made of a material with a short absorption length so that the source size is kept small and the phase space density is not diluted more than necessary. This is true even though it leads to the choice of a heavy material that may have a lower conversion efficiency.

The target should be a thin cylindrical rod or wire so as to minimize reabsorption of the antiprotons, many of which will escape sideways.

Although it would be possible to focus the primary beam down to a few tenths of a millimetre (and therefore to use a correspondingly thin target), this would lead to excessive heating in the target; it would be quickly destroyed by thermal stresses. From this point of view, it is advantageous to use a material with a high value of $\sigma_B/\alpha E$, where

σ_B = tensile strength

α = coefficient of thermal expansion

E = Young's modulus.

Tungsten appears to be the best choice; its absorption length is also sufficiently small. Calculations[7] show that it will probably be necessary to adopt a target diameter of at least 3 mm. This will reduce the efficiency by a factor 2 compared with a target of 0.5 mm diameter. The latter would, however, probably explode when hit by 10^{13} protons of 26 GeV/c.

It would nevertheless be possible to replace the target every pulse. This would not require an excessive amount of material, but the machinery needed to replace and stretch the tungsten wires would be complicated. This is a possibility for future improvement; the present proposal, however, does not include it.

The antiproton production in Lead has been measured by Dekkers et al.[8] for an incident proton momentum of 23.1 GeV/c and a $\bar{p}$ momentum of 4 GeV/c. At a production angle of 0^0, they found :

$$\frac{\partial^2\sigma}{\partial\Omega\partial p} = 28.7 \pm 4.9 \text{ mb ster}^{-1} \text{ (GeV/c)}^{-1} \text{ per nucleus.}$$

To obtain $\partial^2N/\partial\Omega\partial p$ per interacting proton, excluding elastic interactions, we divide this by the total absorption cross-section σ_{abs} = 1750 mb, as measured by Bellettini et al.[9]. Since the antiproton production increases rapidly with the proton momentum in this region (by a factor two between 19.1 GeV/c and 23.1 GeV/c) [8] we apply a gain factor of 1.5 for 26 GeV/c protons.

The difference in cross-section between 3.5 GeV/c and 4 GeV/c is expected to be small, because of the broad production maximum around 4 GeV/c. Similarly, the dependence on the target material is small[8] and the possible difference between the figures for tungsten and lead is therefore neglected.

For estimating the $\bar{p}$ production, we have therefore used the value

$$\frac{\partial^2 N}{\partial \Omega \partial p} = 0.0246 \text{ ster}^{-1} \text{ (GeV/c)}^{-1} \text{ per interacting proton.}$$

The angular dependence was approximated by a parabolic correction, giving a reduction by a factor two at 100 mr [8]. Since the largest production angle of interest is 50 mr, this is a small effect.

4.4 Target matching

Typical antiproton production angles are much larger than the angular acceptance of the cooling ring; on the other hand, the target diameter can be much smaller than the ring aperture. The optics of the transfer channel must provide the matching.

It was found that for the first part of the matching system, near to the target, the use of steel-core quadrupoles would somewhat restrict the acceptance that could be obtained, because of the limitation on their gradient-aperture product.

It is, therefore, proposed to do most of the matching by means of a small magnetic horn. Detailed calculations have shown that a factor of 1.5 can indeed be gained despite some scattering and absorption in the material of the horn.

Fig. 4.3 shows a cross-section of the horn. It will consist of an aluminium inner conductor with a thickness of 0.5 mm, shaped so as to give the required focusing effect, and surrounded by a cylindrical outer conductor. The current will be pulsed, with a peak value of 145 kA and a pulse duration of 20 μs (capacitor discharge).

The shape of the horn and the target length and position have been adjusted for optimum antiproton collection at 3.5 GeV/c.

For calculating the number of antiprotons per pulse, it is assumed that 10^{13} protons hit the target. The number of $\bar{p}$ accepted has been found by means of a Monte Carlo calculation, taking into account the following effects :

a) protons hitting the target with a Gaussian radial distribution; standard deviation 0.75 mm;
b) angular dependence of production as described in paragraph 4.3;
c) reabsorption of $\bar{p}$ in the target;
d) scattering and absorption of $\bar{p}$ in the horn material.

As a result, it is found that 2.5×10^7 antiprotons per pulse will be accepted in a horizontal and vertical acceptance of 100π mm.mrad each and within a momentum spread of $\pm$ 0.75%.

4.5 The injection transfer line

The antiprotons produced in the target and prematched by the magnetic horn must be transported and matched to the cooling ring. The layout of this beam line is shown in Fig. 1.2. It consists of 8 individually powered quadrupoles arranged in doublets and a horizontal bending magnet to compensate the dispersion of the injection septum magnet. The bending magnet also separates the antiprotons from the primary protons. A proton dump which consists of a water cooled steel cylinder 2 m long and about 300 mm diameter is installed just inside the target tunnel to allow an effective shielding. Collimation of particles outside the acceptance of the transfer channel is provided in the same region.

The 8 quadrupoles for the injection transfer line are a modified version of the small type for the cooling ring (Table 3.2). The two between the target and the dump will be equipped with radiation hard coils. The bending magnet (Bl = 1 Tm) must have a clear aperture of 80 mm and might also require radiation hard coils.

A small number of correcting dipoles is required to steer the beam onto the injection trajectory.

4.6 Injection into the cooling ring

An injection scheme must be designed that does not disturb the stack of antiprotons and allows the injected beam to be driven into the stack. The solution adopted consists of a C-shaped kicker magnet at a position where the momentum compaction function α_p is large so that with a slightly higher momentum, the injected beam is separated from the stack. Since the field of a C-shaped magnet falls off slowly, an efficient screen is required which during the pulse of the kicker protects the stack but which thereafter is removed to give a free passage for the injected beam to be driven into the stack. This scheme is similar to that used for injection into the ISR.

The lattice of the cooling ring is of the FODO type. The bending magnets are positioned so as to leave empty two consecutive half periods with a large α_p where the kicker can be installed and upstream of that at a phase distance of 90^0 two more empty half periods where the septum magnets can be placed. In the upstream empty periods the α_p was forced to be zero in order to keep the strength of the kicker magnet within a reasonable limit.

The layout of the injection elements can be seen in Fig. 1.2. Two kicker magnets each about 2 m long are positioned in periods 3 and 4 close to the central F quadrupole and two septum magnets in periods 1 and 24 around the central D quadrupole. This arrangement allows the same septum magnets to be used for extraction (Section 4.7). The D quadrupole between the septum magnets is of the large type to give sufficient aperture for the injected and extracted beams.

A cross-section of one of the two kicker magnets together with the injected beam and the stack is shown in Fig. 4.4. Because of the changing β-function and α_p the distance between the two beams varies. At the upstream end of kicker magnet 1, it is only 32.8 mm. At the exit of kicker 2 it is more than 60 mm.

Five bunches of antiprotons are injected into the cooling ring over 1 turn (the primary protons occupy one quarter of the CPS circumference). The equidistant bunches have a length of 15-20 nanoseconds and the descent of the kicker pulse must therefore be less than 105 - 20 = 85 nanosec. The flat top must last for at least 440 nanosec. The aperture of the kicker magnets is 240 mm (horizontal) and 100 mm (vertical) and the nominal kick strength 0.04 Tm per magnet. Details of their construction are discussed in Section 4.8.

The trajectory of the injected beam in the straight sections where the septum magnets are situated is shown in Fig. 4.5. The beam approaches the central orbit at an angle of 6.5^0. Taking into account the deflection by the D quadrupole in between the two septum magnets, they must provide 3^0 of bending. D.C. magnets are proposed, with their septa outside the ultra-high vacuum.

4.7 Extraction from the cooling ring

The stack of antiprotons will be extracted in 6 batches which have to be equally spaced around the SPS. As explained in Chapter 5 each bunch has a length of about half the circumference of the cooling ring (250 nanosec). The part of the beam to be extracted is driven into the gap of a C-shaped kicker magnet positioned at large α_p and is then kicked out of the machine. The capture of part of the stack into one bunch and its subsequent acceleration to the extraction orbit is described in Section 5.

The same type of kicker magnet as for injection could be used but would be an expensive solution. It is proposed to build a kicker with an aperture just sufficient for the cooled beam and to move it into place prior to extraction. The movement can be slow since extraction will take place at most a few times per day. An aperture of 40 mm (horizontal) by 20 mm (vertical) is foreseen, which compared to the

large aperture of the injection kicker (240 mm by 100 mm) makes its construction much easier. The extraction kicker must provide a nominal kick strength of 0.04 Tm. The rise time will be 200 nanoseconds and the flat top about 300 nanoseconds. The minimum time between two successive extractions of 30 ms is given by the time required for recharging the power supply for this kicker magnet and the corresponding one in the SPS for injection.

4.8 Kicker magnets for injection and extraction

The kicker magnets must be fast and relatively powerful and therefore must operate at high voltage. Satisfactory experience in the construction of a high voltage kicker has already been gained in the PS with the so-called Full Aperture Kicker (FAK) system; it is proposed that the injection and extraction kicker systems should draw heavily on FAK experience and use identical equipment wherever possible.

The kicker magnets must operate in ultra high vacuum and have strictly limited stray fields so as not to disturb the stack.

4.8.1 Injection kicker

The injection kicker is a static device located in two 2 m vacuum tanks up and downstream of quadrupole QFW4. Each tank contains six identical magnet modules of 0.008 Tm kick strength and 75 ns fall time (95-5%). Thus the total required kick strength of 0.08 Tm can be met with some margin to satisfy operational needs or equipment outage.

The magnet module is of the delay line type, has ten discrete cells and a characteristic impedance of 15 ohms. It is judged that 15 ohms is the lowest impedance which can be considered for reasons of cut-off frequency and pulse distorsion; the adoption of this impedance also allows many FAK designs to be used for the pulse generators.

The magnetic circuit of the magnet is a ferrite C-core which is profiled to improve the field uniformity in the aperture. The high voltage and earth conductors are placed around the back-leg so as to have free access between the aperture and the stack. The magnet capacitance is provided by interleaved high voltage and earth plates attached to their respective conductors. A capacitor plate spacing of 7 mm is proposed, identical to that which has given trouble free operation in the FAK.

The stray field from the injection kicker must not be allowed to disturb the stack. For reasonably acceptable stack blow-up it is desirable that the fast stray field at the stack centre be less than 2×10^{-3} of the kicker field. This requires an efficient moveable eddy current shutter between the kicker aperture and the stack.

A schematic cross-section of the magnet module with its shutter installed in the vacuum tank, is shown in Fig. 4.6. In this arrangement, assuming a stack/injected beam separation of 30 mm, it is still possible to kick the fringe of the injected beam closest to the shutter with 95% of the nominal kick.

Bake out at a temperature of 300°C is foreseen for which titanium or inconel are suitable plate materials.

Twelve 80 kV pulse generators are needed for excitation of the injection kicker modules. These can be identical to those already built for FAK. Because the injection kicker pulse length is much shorter than that of the FAK the PFN cable lengths can be shorter and the pulsed resonant power supply transformers reduced in size.

The main parameters of the proposed injection kicker system are given in Table 4.1.

4.8.2 Extraction kicker

The extraction kicker is a plunging device located in a 0.9 m tank downstream of quadrupole QFW22. Two options exist according to whether the difficulties are to be found in the magnet or pulse generator. The first option is to build the magnet as a 15 Ω delay line, in which case the magnet is large and heavy but the pulse generator is simple (identical to those of the injection kicker). The second option is to build the magnet as a lumped inductance with shunt capacitive compensation external to the vacuum tank. In this case the magnet is light and simple but one of the thyratrons of the pulse generator must be bidirectional because of the substantial reflection at the magnet.

On balance the second option is favoured because it leads to a smaller, lighter plunging assembly, allows better pumping of the ferrite, reduces the vacuum tank size and yet still gives an acceptable kick field rise time of less than 180 ns (2-98%). Further a high voltage bidirectional switch is already under development for the PS/SPS Multibatch Filling Project.

The lumped inductance magnet is a single turn ferrite C-cored device with the earth conductor located above and below the aperture to allow transfer of the stack for ejection. The stray field disturbance on the stack is of less concern than for the injection kicker because pulsing takes place only 5 times in the presence of stack. Horizontal screening plates, attached to the earth conductors, are proposed to reduce the stray field to an acceptable level. A schematic cross-section is given in Fig. 4.7.

As far as possible the pulse generator is the same as used for the inflection kicker. The thyratron at the remote end of the PFN must be bidirectional. Provided that the transmission cable length from the PFN to the magnet is less than about 24 m there is no requirement for

the thyratron at the front end of the PFN to be bidirectional because the magnet reflection can pass whilst the tube is still conducting the main pulse.

The parameters of the ejection kicker system are given in Table 4.2.

TABLE 4.1

Injection Kicker Parameters

Type of module	Delay line
Number of modules	12
Minimum aperture height (mm)	100
Useful aperture width - 95% kick (mm)	225
Module length (mm)	275
Inter-module spacing (mm)	40
Characteristic impedance (ohms)	15
Kick rise/fall time 5-95% (ns)	75
Module kick strength for 80 kV PFN voltage (Tm)	0.008
Remanent field (T)	5.10^{-4}
Module weight (kg)	> 300
Module ferrite weight (kg)	52
Ferrite type	8C11
Capacitor plate spacing (mm)	7
Capacitor plate material	Inconel or titanium
High voltage insulation	97-98% Al_2O_3
PFN voltage for nominal kick strength of 0.08 Tm (kV)	66.7
Kick pulse jitter, absolute (ns)	< 2
Pulse repetition rate (pulses/s)	< 1
PFN charging time (ms)	3

TABLE 4.2

Ejection Kicker Parameters

Type of module	Lumped inductance
Number of modules	1
Minimum aperture height (mm)	20
Useful aperture width - 98% kick (mm)	43
Module length (mm)	750
System characteristic impedance (ohms)	15
Kick rise time 2-98% (ns)	178
Kick variation on flat-top (%)	< 2
Maximum PFN charging voltage (kV)	70
Corresponding kick strength (Tm)	0.08
PFN voltage for nominal kick strength of 0.06 Tm (kV)	52.5
Corresponding peak magnet voltage (kV)	33.4
Half height duration (ns)	< 120
Ferrite weight (kg)	39
Ferrite type	8C11
High voltage insulation	97-98% Al_2O_3
Kick pulse jitter, absolute (ns)	< 6
Pulse repetition interval (ms)	30
PFN charging time (ms)	3
Number of consecutive pulses	6
Maximum transmission cable length (m)	24

4.9 Transfer of antiprotons to the SPS

The extracted antiprotons are transferred to the SPS along the existing tunnel TT2a and after a bend of 152° down the existing beam line in TT60 (see Fig. 4.1). Injection into the SPS uses the elements of the extraction channel in LSS6.

The proposed scheme does not use any part of a beam line that is required for injecting protons into the SPS. This allows the whole channel to be tuned prior to the transfer of antiprotons by using 3.5 GeV/c protons travelling in the opposite direction

The extracted antiprotons leave the cooling ring building through a tube of small diameter in the wall and re-enter TT2 immediately upstream of the branch-off to TT10. The layout of this region is shown in Fig. 4.8. A pair of tilted bending magnets one on each side of the wall brings the beam down to the level of TT2 and makes the two beam lines cross at an angle of 7.5° between the quadrupoles QD 332 and QF 333. Here a bending magnet can direct the antiprotons along TT2 towards ring 1 of the ISR or be turned off allowing the beam to go via TT2a to the SPS.

The transfer along TT2a requires 4 horizontal and one vertical bending magnet and a number of small quadrupoles installed at 20 m intervals.

The connection tunnel to TT60 is built where TT2a and TT3 join. (Fig. 4.9). The horizontal deflection of 152° uses two groups of five bending magnets with an F quadrupole in between to compensate the dispersion. The beam enters TT60 through a small hole in the tunnel wall. The last of the 10 bending magnets is installed just below the TT60 beam line and a vertical bending magnet several metres downstream brings the beam on axis. The vertical deflection required is achieved by tilting part of the ten bending magnets.

The cross-section and main parameters of these magnets are given in Fig. 4.11. The same type will be used both for the deflections in TT2a and for the 26 GeV/c protons downstream of the TT2 branch-off.

A provisional cross-section and parameters of the quadrupole needed up to TT60 is shown in Fig. 4.10.

The apertures in the existing TT60 line are adequate for a beam of 1 to 1.4 π mm.mrad.The beam line was designed for 200 GeV/c and in the upstream part for 400 GeV/c. When used for 3.5 GeV/c antiprotons, the magnets will be operated at about 1% of their normal strength. The power supplies for these magnets will be modified to achieve the required precision and stability at these low current levels.

4.10 Injection of antiprotons into the SPS

For injection of antiprotons into the SPS the extraction channel in LSS6 will be used. A possible trajectory has been calculated which uses the extraction kicker MKE, the electrostatic septum ZS and the thick septum magnet MSE. The ZS provides sufficient deflection so that the thin septum magnet MST need not be pulsed. No closed orbit bump will be applied in order not to run the MKE at too low a voltage.

The aperture of the SPS extraction channel is tightest in the MSE (gap 20 mm) corresponding to a beam of 1π mm mrad vertical emittance.

The pulse form of the MKE is adequate for injecting the 6 bunches of antiprotons. The risetime can be as long as 3.6 microseconds. The nominal deflection is about 1 mrad and only one of the two magnets will be pulsed, in order to avoid too low an operating voltage for the switch tubes. However, the multipulsing at intervals of about 30 ms requires an additional resonant charging supply with six primary capacitor banks.

The ZS deflects about 1 mrad which corresponds to a field strength of 3 kV/cm. For injection of antiprotons its polarity is reversed, by means of a remote switch.

The MSE current of 200 A (0.8% of its maximum) will be provided by a separate small power supply.

4.11 Injection of protons into the SPS

The protons which will collide with the antiprotons are injected into the SPS in the usual way. At the moment of injection the 6 bunches of antiprotons are already circulating in the SPS and would be kicked out of the machine when the inflector is pulsed. This is avoided by displacing the phase of the antiproton bunches with respect to the protons. The amount of the displacement is given by the rise time of the inflector.

The new inflector of the SPS for multibatch injection has a repetition time of not less than 0.5 second. Each proton bunch must, therefore, come from a different CPS pulse and the total time for the transfer is $5 \times 0.65 = 3.25$ seconds.

5. RF SYSTEMS FOR THE CPS AND THE COOLING RING

In this chapter we present a consistent series of RF manipulations designed to meet the needs of the proton-antiproton proposal, up to the point that antiprotons reach the SPS. Further manipulations in the SPS are described in Section 10. One can think of alternatives to many of these procedures. Some of these we can dismiss as incompatible with other links in the chain and others, while offering greater beam stability, have been eliminated because of their cost or complexity.

5.1 Filling one quadrant of the CPS with protons

The circumference of the antiproton cooling ring is one quarter that of the CPS. If the antiprotons produced by the impact of the CPS beam are to fit neatly into the circumference of the antiproton ring, one must find a scheme which crowds as many parent protons as possible into one quarter of the CPS circumference.

The CPS is fed by a four-ring booster. The circumference of each ring is just one quarter of the CPS and equal to that of the cooling ring. Clearly, one must endeavour to superimpose the four beams from the booster in the same quadrant of the CPS. This can be done by a combination of transverse and longitudinal stacking.

First, the beams from each pair of booster rings will be stacked in vertical phase space. In this way, two double strength beams may be formed, each one quarter of a CPS ring long. To cause these two beams to coalesce one must inject them sequentially into the CPS, but at slightly different momenta, onto two different mean orbits and their revolution frequencies will be different. Each beam is then trapped separately with reduced voltage. For this only a few of the PS cavities are needed. The harmonic number will be the same (i.e. 20) for both beams, but one string of five bunches will tend to overtake the other one. At the moment that the two bunch trains fall into register, the RF voltages are switched off and then on again at an increased voltage and at the centre frequency to form buckets which embrace both beams. Detailed calculations show that subsequent filamentation dilutes the combined bunch area by a factor between 1.5 and 1.7, leading to a total bunch area of 30 mrad.

The time constant of the CPS cavities (2 μs) is short enough to perform the proposed voltage gymnastics.

5.2 Acceleration in the CPS

At the cost of an extension of the CPS cycle by a few milliseconds, $\dot{B}$ can be reduced in the parabola and sufficient bucket area made available for this large bunch. The bunch area, twice as big as normally accelerated, should ensure that the beam is stable against longitudinal instabilities in spite of its unusually high intensity.

The five CPS bunches within one quadrant are fast ejected to impinge upon the target where they create antiprotons.

5.3 Debunching and stacking the antiprotons in the cooling ring

The antiproton beam of $\pm$ 7.5 $^{o}/_{oo}$ momentum spread from the production target, is allowed to debunch and then precooled to a momentum spread of $\pm$ 1 $^{o}/_{oo}$ in the antiproton ring. It must then be carried across the vacuum chamber from the injection orbit to be stacked with previous batches, which are in the process of being cooled. All this must be over before the CPS is ready, one cycle later, to create another burst of antiprotons.

In moving the beam its momentum is decreased by about 3% in 100 ms. The voltage required is small, but the bucket area needed to hold $\pm$ 1 $^{o}/_{oo}$ is large. We propose to use a single standard PS cavity with some additional capacitive loading to lower its tuning range to 1.8 MHz. This provides 8 kV, enough to contain the momentum spread. The harmonic number in the antiproton ring will be 1.

5.4 Bunching antiprotons for extraction from the cooling ring

We shall see in Section 10 that the antiproton bunches injected in the SPS must be rather long if space charge ΔQ due to the high line density is to be tolerable. An acceptable bunch length corresponds to half a turn of the cooling ring. Bunches must be formed at a harmonic number of 1 within the stack, and moved to an orbit where they may be extracted towards the SPS. To form and extract the six long bunches needed for the SPS, this must be repeated six times, although in initial tests at low luminosity only one such operation is needed.

The single PS cavity installed in the cooling ring to displace the antiprotons after precooling will be used. To keep the bucket area small enough to contain only one sixth of the beam, the voltage must be very low (92 V for a bunch area of 12 mrad). A larger bunch area would exceed the capacity of the SPS 200 MHz buckets, since 12 mrad in the cooling ring scaled as h/R becomes 1260 mrad in the SPS even before any blow-up has taken place.

The cooled antiproton beam must have a momentum spread of $\pm$ 1.5 x 10^{-3} to remove the beam in six passes with a bucket of 12 mrad. Careful control of the longitudinal acceptance must be exercised to keep the bunches of equal intensity. This can be facilitated by using the stochastic cooling loop to flatten the momentum distribution. Fortunately, such precise voltage control will not be required in early single-bunch transfers.

TABLE 5.1

RF PARAMETERS FOR THE COOLING RING

1) Stacking

γ_{tr}		2.43	
$\Delta p/p$ after initial cooling		1	$^{o}/_{oo}$
Corresponding bunch area at 3.5 GeV/c		45	mrad
Deceleration rate for $\sim$ 3% within 0.1 s		1	GeV/c/s
Energy loss per turn		524	eV
Accelerating voltage	without blow-up during adiabatic trapping	3	kV
Stable phase angle	without blow-up during adiabatic trapping	10	deg

2) Ejection

Total bunch area (6 bunches)	72	mrad
Total $\Delta p/p$ of coasting beam at 3.5 GeV/c	± 1.536	10^{-3}
RF frequency (h = 1, R = 25 m)	1.84	MHz
RF voltage for stat. bucket 12 mrad	92	V
RF voltage for bunch length $\pm 90^{o}$	514	V
$\Delta p/p$ of 12 mrad bunch ($\pm 90^{o}$)	± 6.74	10^{-4}
Length of 12 mrad bunch	$25\pi = 78.54$	m
Longitudinal stability $(Z/n)_{max}$ (12 mrad coasting)	$\sim$ 840	Ω
Longitudinal stability " (12 mrad bunched 180^{o})	~ 2560	Ω

6. STOCHASTIC COOLING

6.1 General description of momentum cooling

Fig. 6.1 illustrates the general principle of stochastic momentum cooling. A pick-up electrode is connected through a linear high-gain, wide-band amplifier to a wide-band accelerating gap (kicker). A particle that passes the pick-up induces a short pulse in it. The electrical delay in the system is such that this pulse arrives at the kicker together with the particle. The latter, is therefore accelerated by the peak value of the pulse. This is called the coherent effect.

At the same time, other particles also create pulses. These are not infinitely narrow, due to the finite system band-width, so that some of them will also influence the particle under consideration. The mean effect of this noise (called Schottky noise) will be zero if the system does not transmit the d.c. component. It will, however, lead to an increase of the energy spread (incoherent effect).

Since the duration of the pulses is quite short compared to the revolution time, and since different particles have different revolution times, each particle will be influenced by a small and continuously changing fraction of the other particles. This quasi-random effect has been analyzed quantitatively[10], and it was found that the blow-up is similar to that which would result from purely random kicks. That is, the mean square energy change is proportional to the time and to the square of the electronic gain. The proportionality factor depends on the amount by which the particles overtake each other on each turn.

Two extreme regimes may be distinguished :

a) "good mixing". On each successive turn, the particle is influenced by different particles, i.e. the typical differences in revolution time between the particles are large compared to the pulse length;

b) "bad mixing". The population of particles seen by a specific particle on successive turns, changes only slowly. This situation exists in the present ring for all cooling systems.

It appears from the theory that a particle is only influenced by those frequency components in the noise spectrum that are nearly coincident with one of the harmonics of its own revolution frequency. In case a), the frequency bands belonging to different harmonic numbers overlap due to the large frequency spread between the particles. Each particle can therefore be influenced by many groups of other particles, each around a different revolution frequency. As a result, it is found that the blow-up effect is the same as that caused by purely random kicks. In case b), the Schottky bands do not overlap, and each particle is only influenced by particles with nearly the same revolution frequency. The blow-up is larger than in case a) and it is proportional to the local density of particles in frequency (or energy) space.

Additional blow-up is caused by the amplifier noise. In contrast with the Schottky noise, which is concentrated in narrow bands around the revolution harmonics, that from the amplifier has nearly equal density at all frequencies. With the present design, its density is well below the Schottky noise density at the frequencies that influence the particles (i.e. the Schottky bands) and so it does not affect the cooling appreciably. However, it is responsible for most of the total output power at the kicker terminals.

Since the coherent effect is proportional to the system gain, but the blow-up to the square, the gain has to be chosen so as to obtain an optimum balance between these two effects[11]. With bad mixing, the blow-up is proportional to the particle density in energy space, so the optimum gain will be inversely proportional to this density.

If the gain were the same for all particles, there would be no

cooling effect; only a general acceleration or deceleration. A concentration of particles (i.e. cooling) results only if the coherent effect pushes the particles in the direction of decreasing gain. This dependence of the gain on energy can be obtained either by shaping the pick-up electrode so that its gain depends on the closed orbit position (e.g. by using a linear transverse pick-up)[12] or by using a sum pick-up and including a filter in the electronics chain, using the fact that the revolution frequency depends on energy. The filter should act in a similar way on all harmonics of the revolution frequency and it should have a constant group delay[13].

6.2 Reasons for using two separate systems

The filter method is preferable for low-density beams (e.g. in the precooling system) where the amplifier noise is relatively important, since a sum pick-up produces as large a signal as can be obtained across the whole aperture. Moreover, a wide-band sum pick-up can be much shorter in the beam direction than a difference pick-up, because the use of a ferrite ring around the beam gives sufficient impedance even with a very short pick-up. (The length of a pick-up with variable gain across the aperture must be of the order of a quarter wavelength in the centre of the passband.) As a result, many more sum pick-ups can be placed in a given space, thus increasing the available signal. For the precooling system, the design includes 100 pick-ups in a straight section of 5 m length. A linear filter will be used so that the gain is linearly dependent on energy, as for a linear transverse pick-up. This is adequate for compressing the energy spread of each injected pulse by a factor 7.5 in two seconds.

For cooling the stack, on the other hand, such a system is not suitable. As discussed above the gain must be inversely proportional to the local particle density in the stack. Since theory shows[11] that a minimum aperture is required for the stack if the density profile versus energy has an exponential shape, we would need a filter with an

approximately exponential response. The ratio of density between the centre of the stack and its edge must be about 20000 for the required performance and this must also be the ratio by which the gain changes over a region in which the revolution frequency changes by 0.25%.

Although such filters can be designed, there is another reason why they cannot be used. This is connected with the feedback from the kicker towards the pick-up, via the beam. The total gain of the loop formed by pick-up-amplifier-kicker-beam-pick-up might exceed unity. This implies either a risk of instabilities or, if gain and phase shift versus frequency are such that the system is stable, a loop gain larger than one would lead to a decrease of the Schottky signals and, therefore, spoil the stochastic cooling. Theory shows[11] that both without a filter (for any pick-up shape), or with a linear filter, the condition for unit loop gain is about equal to the condition for zero cooling effect (i.e. blow-up cancelling the coherent effect). Thus to get useful cooling, the gain must be reduced so that the feedback effect will be small.

With higher-order filters, however, the loop gain would be higher at some frequencies. Such filters are therefore precluded. However, pick-ups with a gain strongly dependent on particle position can now be used, since the precooling has already increased the density enough to make the amplifier noise relatively harmless even with only 30 pick-ups.

6.3 Precooling system

The pick-ups for the precooling system should not see the particles in the stack to avoid overloading the output amplifier with their Schottky noise. Similarly, the precooling kickers should not kick the stack thereby causing blow up. The Schottky noise of the precooling system cannot blow up the stack because it does not overlap with the Schottky bands of the stack. However, the amplifier noise is present at all frequencies and it is much higher on the precooling kickers than

on the stack kickers because of the higher gain needed at lower density.

For this reason, the precooling pick-ups and kickers (which will be of similar construction) must surround the newly injected beam with their ferrite rings; the stack must pass outside. When the precooled beam is displaced by the RF system towards the top of the stack, part of the ferrite must be temporarily removed. A possible way of doing this is suggested in Fig. 6.2.

Obviously, these devices should be located at a point in the lattice where α_p is high, so that the injected beam and the stack are well separated. This, however, means that the kickers will not only change the particle energy, but also excite the horizontal betatron oscillations through components of the amplifier noise that coincide with the betatron Schottky bands. In order to reduce this effect sufficiently, these kickers will be grouped into two equal sub-assemblies, in straight sections that are half a betatron wavelength apart, as shown in fig. 1.2.

At present it is assumed that the pick-ups and kickers will have an impedance of 50 ohms, like those already used in the ISR experiments. The possibility of increasing this impedance will be investigated. This would improve the signal-to-noise ratio and reduce the amplifier output power required.

The linear filter (fig. 6.3) will be made by using a delay line D1 that is shorted at its end, fed by a current source. If the length of the line is such that its delay is half the revolution time at the centre of the particle distribution, it will have zero impedance at all harmonics of the corresponding revolution frequency. In a small region around each harmonic, the impedance will change linearly[13]).

The delay line D1 is shunted by some lumped components (R, L, C) and by a combination of two further lines of the same length, D2 and D3.

The end of D2 is shorted, that of D3 is open. These components serve to reduce the gain between the Schottky bands, in order to decrease the output power due to amplifier noise. The combination D2-D3 behaves like a series tuned circuit, having zero impedance at two intermediate points between each two adjoining Schottky bands. The resistance R causes damping at those frequencies where the total impedance would otherwise become too high. L and C are added in order to make the degree of damping dependent on the harmonic number; this is desirable because the Schottky bands are wider at the high frequency end. The whole is optimized for minimum r.m.s. gain over the entire passband (150-400 MHz), while keeping the phase shift inside the Schottky bands to less than 30°. The resulting r.m.s. gain is 0.92 times the average gain at the edge of the Schottky bands.

Losses in the delay lines modify the characteristics slightly; in particular, around the zero-gain points the gain remains finite. This effect can be minimized by choosing a line of sufficiently large cross-section for D1, and then reduced to a negligible level by a compensating device, not shown in fig. 6.3. For D2 and D3, the losses are not important.

The main parameters of the precooling system are :

Number of pick-ups	100
Number of kickers	2 x 50
Impedance of pick-ups and kickers	50 Ω
System bandwidth	250 MHz
Lower frequency	150 MHz
Upper frequency	400 MHz
Noise figure of input amplifiers (one for each pick-up)	3 dB
Number of particles per pulse	2.5×10^{7}
Momentum spread	± 0.75%
Output power due to Schottky noise	1.8 kW
Output power due to amplifier noise	3.2 kW
Amplifier rating	25 kW

Fig. 6.4 illustrates the cooling expected from numerical computation. In two seconds, about 80% of the particles would be collected inside a momentum spread of ± 0.1%, i.e. 7.5 times smaller than the original one.

6.4 Momentum cooling of the stack

The radiofrequency system will deposit each new precooled pulse at the top of the stack. Allowing for a blow-up during RF stacking by a factor 1.5, the particle density in momentum space will be 5 times as high as the injected density. The ratio of Schottky noise to amplifier noise will therefore be more favourable, so that the number of pick-ups needed is smaller than for the precooling system. Moreover, the system gain at the top of the stack may be about 5 times lower than at the edge of the injected momentum distribution; this results in an output power much smaller than for the precooling system.

The gain of the stack system will decrease strongly towards the bottom of the stack. The gain profile has been determined in such a way that it results in a density profile with maximum slope, while still ensuring a constant particle flux in momentum space towards the stack bottom (i.e. climbing against the density gradient) equal to the average injected flux. Fig. 6.5 shows this density profile, together with some curves that demonstrate the build-up of the stack with time.

The cooling system will use pick-ups with a sensitivity that depends strongly on the horizontal position of the particles (Fig. 6.6). A linear filter similar to the one described for the precooling system, with zero gain at the stack bottom, will be used in addition.

Nevertheless, the gain needed around the stack bottom is so low that the amplifier noise would again be too high in that region if the only means of reducing the gain there would be the pick-up of fig. 6.6, together with the linear filter. In order to improve this, the system is

split up into three sections, with pick-ups displaced horizontally relative to each other. (A fourth section with a linear pick-up for cooling the densest part of the stack is added to these.)

The pick-ups that are most sensitive at the stack bottom are followed by less electronic gain, so that the overall gain profile is still as required. A block diagram is shown in fig. 6.7; the gain of the four sections vs energy in fig. 6.8.

Additional noise filters reduce the gain of sections 1 and 2 below the cross-over point where the next section takes over. In this way, the amplifier noise of these sections is reduced sufficiently in the bottom region of the stack where it would be most harmful. With the density distribution of fig. 6.5, the amplifier noise power density inside the Schottky bands will be at least three times lower than the Schottky noise density anywhere in the stack. The filters used for this purpose do not influence the cooling process much below the cross-over point; their phase shift is therefore irrelevant in that region. These filters will again use delay lines in order to obtain a filter characteristic that repeats itself around each harmonic.

The output power of section No. 3 will be much lower than that of sections 1 and 2, because of its low gain. Therefore it is possible to use a higher bandwidth (1-2 GHz) for this section. This improves the cooling near the stack bottom and keeps the number of particles remaining in the tail of the stack low (see the increased density gradient in this region in fig. 6.5).

Particles of different energy have different times of flight between the pick-ups and the kicker. For the high bandwidth section 3, these differences become comparable with the response time of the system. This explains the peculiar shape of the gain profile of section 3, as shown in fig. 6.8. The effect is small enough not to be troublesome.

The final momentum spread of the stack ($\pm$ 1.5 x 10^{-3}) is so small that it would be difficult to meet the requirements on selectivity of the linear filter, due to the losses in the delay line. For this reason, Section 4 will not use a filter, but it will be equipped with a linear transverse pick-up. The amplifier noise is quite negligible for this section, because of the high particle density and the low system gain. Techniques similar to those already used in the ISR experiments [14] may be applied. The cooling time at the final stack density would be 0.3 h, i.e. small enough to overcome the blow-up due to the intra-beam scattering.

The pick-ups for the stack cooling will be placed in straight sections 17, 18, 19 and 20 where α_p is large. This is needed for obtaining the required pick-up response. The kickers will be in straight section 13 where α_p is zero. The kickers will be in straight section 13 where α_p is zero. They will therefore not excite the horizontal betatron oscillations.

The main parameters of the stack cooling system will be as follows :

Maximum total stack width	$\Delta p/p = 2.5 \times 10^{-2}$
Final half width	$\Delta p/p = 1.5 \times 10^{-3}$

Section	1	2	3	4
Number of pick-ups	14	14	2	1
Number of kickers	50		20	4
Impedance of pick-ups, kickers	50		50	50 Ω
System bandwidth	250		1000	1000 MHz
Lower frequency	250		1000	1000 MHz
Upper frequency	500		2000	2000 MHz
Output power from Schottky noise	850		12	7.5 W
Output power from amplifier noise	725		3	0.5 W
Power amplifier rating	5000		50	20 W

6.5 Betatron cooling

It would be difficult to reduce the betatron amplitudes to an appreciable extent during the precooling of each injected pulse, because the amplifier noise would be too high in comparison with the betatron signal from a transverse pick-up. Moreover, it is preferable to do betatron cooling on the stack, because this relaxes the vacuum requirements (multiple scattering) and counteracts the blow-up by intra-beam scattering.

Reduction of the initial oscillation amplitudes by a factor 8.5 horizontally and 10 vertically is required. The cooling time should not be too long, in order to allow the collection of small stacks with the final emittance in a few hours, if required.

It appears that these requirements are not too difficult to satisfy and that we could even consider to cool only the bottom part of the stack. A stack of 6×10^{11} particles within the final momentum spread would have a cooling time constant of 0.5 h with an optimum gain system working between 1 and 2.5 GHz.

We could, however, greatly improve this by additional cooling during the stacking process. At lower densities than the final one, the cooling is correspondingly faster if we adjust the gain accordingly. For the horizontal cooling, this is achieved if more or less automatically, if we use the same pick-ups as for the momentum cooling; for the vertical cooling, similar pick-ups may be used where the upper and lower loop signals are subtracted before amplification.

No detailed design work has yet been done on these systems : it seems clear, however, that it will not be difficult to reach the required performance with simple means, comparable to those used in the ISR experiments. The output power required will be quite low and filters will not be needed.

In fact, it may be necessary to limit the reduction of the amplitudes in order not to increase the incoherent tune shift in the SPS beyond what can be tolerated (see Section 10).

7. VACUUM FOR THE COOLING RING

7.1 Influence of the rest gas

The rest gas will have the following effects on the circulating antiprotons :

i) Multiple Coulomb scattering will counteract the cooling of the horizontal and vertical emittance.

ii) Particles will be lost by single Coulomb scattering and nuclear interactions.

iii) The beam will lose energy due to ionisation.

iv) The positive ions created and attracted by the beam (neutralization) will increase effects i) and ii). Their density may under certain circumstances exceed the initial rest gas density.

v) The neutralization will influence the betatron tunes.

vi) Coupled ion - antiproton oscillations may cause a slow blow-up of the stack.

Analysis shows that effects i), iv) and vi) are the most important and that they determine both the pressure and the neutralization factor required. None of these effects can be calculated with high precision. The nominal design figures

$$p < 10^{-10} \text{ Torr (nitrogen equivalent)}$$
$$\eta < 0.03$$

were therefore chosen with a certain safety margin, also taking into account that no great saving would be made by increasing them even by an order of magnitude.

With these values, we expect that all effects mentioned will be sufficiently small :

i) The heating rate for the final stack with $E = \pi \times 10^{-6}$ rad.m will be 5×10^{-6} s^{-1}, i.e. 60 times less than the cooling rate. A gas composition of 90% H_2, 10% N_2 or CO is assumed.

ii) The single scattering lifetime will be about 1620 h, the nuclear interaction lifetime, 6000 hours.

iii) The relative energy loss will be 10^{-4} during 24 hours.

iv) The ion density inside the final stack with $\eta \simeq 0.03$ will be roughly equal to six times the original gas density, thus increasing effects i) and ii) by a factor 7.

v) The neutralization will reduce the vertical tune shift by about 10^{-3}.

vi) This effect was calculated using the theory existing for electron-proton oscillations [15,16]. The high mass of the ions (assumed to be H_2) compared to electrons reduces their oscillation frequency in the potential well to a value less than the betatron frequency. Taking into account Landau damping due to the tune spread present in the stack, we should be below the instability threshold with $\eta = 0.03$. Moreover, even if this were not true (the theory being approximative), the growth rate would be considerably below the cooling rate.

7.2 Vacuum system layout and characteristics

The pressure requirement is such that a combination of titanium sublimation (PS) and sputter ion pumps (PI) are required. Furthermore vacuum annealed austenitic high tensile stainless steel will be required for the chambers so that specific degassing rates of 2×10^{-13} Torr ℓ s^{-1} cm^{-2} can be attained. This combination along with in-situ bakeouts should ensure the sort of performance which has become normal at the ISR. The bakeout temperature needs not exceed 300°C.

Figure 7.1 shows the vacuum system layout over one quadrant of the cooling ring. The injection region is illustrated in Fig. 7.2. It should present no major difficulty because the septum magnet is designed such that it is placed outside the vacuum system. The sputter ion pumps should have a speed of 200 to 500 $\ell\, s^{-1}$ and the sublimation pumps around 2000 ℓ s^{-1}. There will be four sector valves (VS) placed at the regions where the beam sizes are a minimum. The beam stay-clear apertures in these

regions are somewhat smaller than the apertures of the enlarged ISR sector valves. Simple gate valves (GV) (in the form of shutters) may need to be added in the larger aperture regions of the vacuum sectors.

Pump-down during bakeout will be carried out by means of 100 ℓs^{-1} turbo-molecular pumps (PT); a minimum of two per quadrant is necessary and maybe a third if laboratory tests indicate that during the 24 hours of a bakeout the minimum pressure at 300°C is inadequate.

Vacuum gauges are distributed throughout the ring to facilitate leak detection. Two residual gas analysers per quadrant will be installed near to the potential sources of heavy gas species. It is important that the final gas composition contains at least 90% H_2 with the minimum possible of heavier molecules.

The maximum distance between pumps is 5 metres in the short bending magnets where the vacuum chamber conductance is around 1300 $m\ell s^{-1}$. The distance between pumps in the long bending magnets is 8 m where the conductance is only 610 $m\ell s^{-1}$. The highest pressure occurring in the bending magnets is expected to be well below 10^{-10} Torr.

These estimates are based on a specific degassing rate of 2×10^{-13} $T\ell s^{-1}$ cm^{-2}. .This will necessitate prebaking all parts of the stainless steel chambers at 950°C for up to ten hours in a vacuum furnace at a pressure of 10^{-6} Torr.

No details of the large tanks in the straight-sections are given because little is yet known of their vacuum characteristics. They will be supplied with enough pumping capability to maintain the average pressure at less than 10^{-10} Torr. Special precautions will be needed in those places containing ferrite or other porous materials.

All such tanks will be subjected to a low pressure limit test to ensure that they meet the vacuum requirements.

7.3 Clearing

The low value of η implies the use of ion clearing fields throughout the vacuum chamber. A similar arrangement to that used in the ISR with a pair of clearing electrodes at the exit of each bending magnet is expected to reduce the value of η to below 0.03 for a cool beam at a pressure of $< 10^{-10}$ Torr. The ions drift out of the magnet due to forces exerted by the "crossed" electric fields of the beam and the magnetic bending field. During the early stages of cooling and stacking with relatively feeble antiproton beam densities, the electric fields in the beam are not high enough to produce adequate drift velocities. In these early stages the η values are expected to approach unity in the bending magnets without affecting the heating rate due to Coulomb scattering on the ions. This, because, at that stage both the emittance E and the number of antiprotons N are such that the ion density is a factor of many hundreds less than that encountered by a cool beam.

The straight sections between magnets will also be equipped with clearing electrodes to avoid trapping ions in the cool beam potential of around 15 Volts with respect to the vacuum chamber walls. The voltage on all the clearing electrodes will need to be somewhat in excess of the cool beam potential.

8. INSTRUMENTATION AND CONTROLS

8.1 Introduction

During normal operation, the beam-derived signals driving the stochastic cooling systems contain information on several important beam parameters (see Section 6). Most of the additional diagnostic equipment is needed to facilitate the initial running-in and subsequent setting-up for operation.

The low intensity of an injected $\bar{p}$ pulse (2×10^7 $\bar{p}$pp) renders observation difficult. It is therefore assumed that most of the setting-up is done with p beams of an intensity permitting easy observation. After polarity reversal of the magnetic elements, the $\bar{p}$ should then behave in the same way. However, whenever possible, the $\bar{p}$ beams will be observed directly.

The proposed diagnostic systems are described below, and their locations shown in Figure 8.1.

8.1.1 Scintillator screens + TV

Scintillator screens will be used to detect the beam in the injection and ejection channels. This requires screens at the following locations :

- entrance to septum
- exit from septum
- entrance to injection kicker.

To observe the first-turn trajectory, a combined screen and beam stopper to prevent multiple traversals will be located

- after nearly 1 turn.

The scintillator screens are 1 mm thick doped alumina plates. The cameras are a radiation resistant version, developed at the PS. The sensitivity, as tested on the PS Booster, is 2×10^9 p/cm^2, and with a

special Vidicon tube, as used for ICE, it should be possible to see about 10^8 p/cm^2. The p test beam will then be easily visible and possibly also the pions accompanying the antiprotons. The ejection of a small $\bar{p}$ stack (10^9 $\bar{p}$) could be observed at the entrance and exit of the septum.

8.1.2 Beam transformers

The beam transformers will be similar to those used on the ISR and the SPS, with three ferromagnetic toroids : one is used in a magnetic amplifier circuit to extend the measurements down to d.c., a second feeds an integration circuit to extend the bandwidth upwards to a few MHz, and a third forms an independent passive transformer with a bandwidth of $\sim$ 100 MHz.

A version of the SPS beam transformer, improved for use on ICE, has reached a resolution of 5 μA at frequencies below 1 Hz and about 50 μA at the high frequency end. This just permits observation of the injected $\bar{p}$ beam and is adequate to observe the slow increase in stack intensity.

For operational reliability, 2 beam transformers will be installed at places where the required aperture is small.

8.1.3 Schottky signals

Schottky signals caused by statistical fluctuations in the proton beam current are not only the basis for stochastic cooling but also offer a convenient means of beam observation [17]. Spectrum analysis of a harmonic band of the current fluctuation gives the square root of the particle density versus revolution frequency, i.e. the particle density versus momentum. Furthermore, spectrum analysis of betatron sidebands will yield the vertical and radial Q values of narrow $\Delta p/p$ beams in the machine. By placing beams at various radial positions, complete working lines (Q_V, Q_H versus $\Delta p/p$) can be measured. This can be done with a single injected proton beam, positioned by phase displacement acceleration.

Perturbation and phase sensitive detection techniques, recently tried out in the ISR, will be used. It will also be possible to measure the Q values versus momentum in the antiproton stack.

Measurements of RMS betatron oscillation amplitudes versus momentum inside the stack are possible from betatron sidebands, once the working lines (Q_V, Q_H versus $\Delta p/p$) and the particle density versus $\Delta p/p$ are known.

Computer treatment of Schottky profiles is required to extract the beam parameters mentioned.

Pick-ups of the coupling loop type will be provided for these measurements in one of the straight sections where $\alpha_p = 0$.

8.1.4 Position pick-up electrodes

A total of 12 pick-up stations, each containing horizontal and vertical electrodes, will be mounted in somewhat enlarged pump connections, distributed regularly around the ring.

Conventional diagonally divided electrodes are proposed. They have good linearity and allow single turn observation. However, only bunched beams are seen.

Even with high input impedance head amplifiers mounted directly on the feed-throughs (as done for ICE) one probably cannot obtain sufficient sensitivity to measure a single injected $\bar{p}$ beam. Thus the exploration of the closed orbits as a function of momentum will have to be done with p beams. In this case, the signals are large enough to be transported over coaxial cables before amplification and the active electronics can be in a radiation free environment. The total bandwidth will be 100 kHz to 30 MHz.

The procedure by which the final stack is ejected in 6 batches can be clearly observed.

8.1.5 Measurement targets

Measurement targets similar to the ones installed on the PS Booster are foreseen. Where the target is flipped into the beam, all particles with an amplitude greater than the distance from the target edge to the closed orbit are intercepted. In this way, one can measure the integral of the amplitude distribution.

The vertical target will be placed at high α_p, so that the vertical amplitude distribution as a function of momentum can be studied by adjusting the horizontal position before flipping the target vertically.

In the horizontal plane a similar measurement is not possible. The target will be located at $\alpha_p \approx 0$ and average over all momenta will be measured.

8.1.6 Non-destructive profile monitors

At present, two non-destructive profile detectors are being developed and built for ICE, the Rubbia type and the Vosicki type. Both extract the electrons, liberated by the beam particles from the residual gas, by means of a transverse electric field with a magnetic field in the same direction to obtain good spatial resolution.

In the Rubbia detector, the electrons are post-accelerated to about 50 keV and penetrate through a thin foil into a wire chamber, operated in counting mode. The wires are spaced at 1 mm intervals so that a profile can be obtained with good resolution.

In the Vosicki detector, the electrons impinge with about 40 keV on a thin layer of scintillator. The light is observed with a wide-aperture lens, an image intensifier and a TV camera.

The decision whether to build one of these two devices will depend on the experience in ICE. A space of 2 x 1 m will be reserved.

8.1.7 Q measurement

It is important for the understanding and control of beam behaviour to measure the horizontal and vertical tunes to an accuracy of $\pm$ 0.001.

A kicker with a rectangular pulse lasting a fraction of a revolution will excite coherent oscillations with an amplitude of a few mm. The signal derived from a position PU will contain the frequencies

$$f_m = |m \pm Q| \, f_{rev}$$

where m is the mode number. Selecting two modes by filtering, and measuring the frequency gives the fractional part of Q. Alternatively, one can measure one mode and f_{rev}, but this is possible only with bunched beams.

Pulsing the kicker only in one plane and observing the oscillations in both planes allows the coupling between the planes to be determined. The Q kicker will occupy about 1 m.

8.1.8 Beam loss monitors

During the running-in period, it is useful to know where and at what time the beam is lost. Later on, the same information may be used to minimize the losses.

A simple beam loss detector (developed at FNAL and also used on the PS Booster) consists of a can of liquid scintillator in which a small photo-multiplier is immersed. The loss of 10^7 p or $\bar{p}$ can be detected with a bandwidth near 100 MHz.

In total, 24 of these detectors are foreseen.

8.2 Controls

The control system of the cooling ring will be similar to the systems in use at the SPS and in construction for the PS. It will essentially consist of a control computer, interface equipment, a simple terminal for local control and a data link to the PS message handling computer. In this way the ring can be operated from the PS Control Centre after the initial running-in period.

Although a detailed list of the possible commands and data acquisitions does not yet exist, it seems probable that a single computer will be sufficient, both because of the concentration of all equipment in the same area and because of the d.c. operation of most components. Data acquisition from cycle to cycle will only be required for some purposes such as beam diagnostics where the rate is limited by the operator's capacity for interpretation.

The tight construction schedule will not permit the development of any appreciable amount of software in assembly language. Existing software (operating system, data modules) will therefore be adopted except for the specific application programs that will be written in the interpreter language NODAL.

The local control terminal will include disk storage for control programmes and a simple video unit for graphic displays. Analogue waveform displays will be provided in the standard way, with switching controlled by software. Transmission of these signals to the PS Control Room will also be provided .

The access to the ring building will initially be controlled from the local control room. After running-in, this will be transferred to the PS Control Centre.

9. BUILDINGS

9.1 Introduction

The building for the antiproton ring is determined by a few basic requirements. The general area must be such as to allow the 26 GeV/c protons from the PS to be led to the production target, and the cooled antiprotons at 3.5 GeV/c to be conveyed both to the SPS and to the ISR. This fixes the location alongside the transfer line TT2 (Fig. 1.1), which allows the cooled antiprotons to be injected in the reverse direction in the SPS via TT2a and TT60 or into ring 1 of the ISR. In addition, it keeps open the possibility of injecting antiprotons in the normal direction in the SPS, should the need arise.

The choice of location on the North side of TT2 was determined both by the lower ground level, requiring less excavation, and to avoid blocking the passage along TT2 with the switching magnets.

9.2 Main Halls

The basic layout of the building has been determined by a variety of boundary conditions. Firstly the majority of the civil engineering work, the subsequent installation and maintenance of the machine must be able to procede independently of the operation of TT2, since both the SPS and ISR are filled via this line. This requirement leads to the need for a minimum of 4 m of concrete and rock between TT2 itself and the excavation.

The production target area should be well separated and shielded from the machine, so as to avoid radiation damage of the machine components and so that the building housing the machine needs little or no shielding.

There must be good access to the building for large and very heavy components and direct communications across the ring for the stochastic cooling signals. For these reasons the building consists of a rectangular

hall of 65 x 58 m partially submerged in the molasse rock, with a road access at one end (Fig. 9.1). This contains the ring itself, the area inside the ring will serve for most of the large power supplies, etc. as well as for the direct connections required by the stochastic cooling. To reduce the amount of excavation required, and avoid an excessively long or steep access road, the building has a floor level 1.9 m above that of TT2. This corresponds to a floor level about 7 m below the surface of the molasse, so that lateral shielding will not be required, although it will be necessary to close the access road during machine operation.

9.3 Target tunnel

The antiproton production target is located about mid-way along a 30 m long tunnel, 3 m high and 6 m wide which leads into the semi-underground hall housing the cooling ring.

The beam pipe enters this area through a 80 cm diameter hole bored in the molasse which connects with a small gallery constructed alongside TT2 (Fig. 4.2).

This effectively separates the access and operation of the machines from that of TT2.

The proton beam entering the target tunnel is inclined upwards by about 2^{o} to allow for the 1.9 m higher floor level of the building. The beam is deflected into the horizontal plane, then accuretely steered and focused by a quadrupole triplet onto a tungsten target 10 cm long and less than 3 mm in diameter. The antiprotons produced are then collected by a small magnetic focusing horn of about 45 cm length and matched into the 3.5 GeV/c line for transfer to the cooling ring. The antiprotons are deflected 4.5^{o} to the left and the non-interacted protons continue almost straight on ($\sim \frac{1}{2}^{o}$ right) into a beam dump.

Since the target and beam dump area and components will become highly activated, considerable attention has been devoted to the conceptual layout.

The antiproton production system can be divided into three parts having quite different characters :

i) a conventional proton beam transport system with little or no beam loss and consisting of conventional elements;

ii) the target zone itself, with very high radiation levels and potentially fragile components such as the target and magnetic focusing horn;

iii) the collimator and beam dump area, again with high radiation levels but containing large mainly passive elements which are expected to have very high reliability.

The design philosophy is to minimize both the number and complexity of components in the high radiation areas, isolate them from adjacent areas and arrange for easy access to components. Thus the arrangement foreseen consists of a curtain of 80 cm thick shielding blocks suspended from the roof, separating the beam line from the rest of the tunnel, and a 30 cm thick wall just upstream of the target, to separate the first two areas.

All cables, cooling water pipes, etc. will be situated on the East wall and connections made by crossing the tunnel in transverse ducts.

In area i) normal access for maintenance will be possible due to the shielding alongside areas ii) and iii) and just upstream of the target.

In area ii) components will be pre-aligned on marble bases, and enclosed in marble whenever possible. These assemblies could for instance be moved into position on a removable trolley and lowered onto precision supports.

The electrical and cooling supplies pass via the marble base as indicated in Fig. 9.2 , so that all connections and disconnections, except for the vacuum pipe, can be made with the shielding curtain in place. It should be noted, however, that the target + horn assembly will be in air and so need no vacuum pipe connections. Thus, as presently envisaged, area i) ends with a piece of beam pipe through the 30 cm shielding wall, containing a vacuum window.

Wherever vacuum disconnects are necessary, it is foreseen to use quick disconnect flanges which can be operated with special tools.

In area ii), the beam dump and collimator are foreseen as installations fixed once and for all which would not be touched afterwards. If however some repair or modification should be needed, the shielding followed by the equipment would then be moved into the hall.

The shielding layout is shown in Fig. 9.3. This gives access to the tunnel via a labyrinth for personnel. For equipment and vehicle access, a removable plug is planned.

Initial calculations based on 5×10^{18} protons per year show that with this layout, the maximum dose received by the cables, etc. on the East wall of the tunnel is about 1 Mrad per year, and the maximum level in the passageway 24 hours after shutting off the beam is 20 mrad/hour (Fig. 9.4).

After stacking and cooling, the beam re-enters TT2 via a pipe through the molasse. For injection counterclockwise in the SPS, a connection will be made between TT2A and TT60 (Fig. 4.9).

9.4 Services

To house the cooling plant, electrical sub-station and local control room, a surface building is located along the East side of the hall. This is of conventional construction with a double floor which connects to an existing technical gallery. The total installed power will be about 5 MW and the machine components will be cooled by a conventional demineralized water circuit with a supply pressure of 25 bars and a total flow rate of about 4 m^3/minute. This will be cooled via heat exchangers and primary water from cooling towers.

The ventilation system foreseen will operate closed circuit during machine operation with the addition of a small supply of fresh air to maintain a slight overpressure in the building and to compensate for leaks. To avoid excessive heat loss, the walls and roof of the building will have additional thermal installation.

As presently envisaged, the building will be equipped with two 5 ton cranes, each with a span of 32 m covering a half of the hall, but the metallic structure is designed to support their possible replacement by 50 ton cranes.

10. SPS ASPECTS

This chapter delas with the modifications and additions necessary to the SPS. Extra hardware for the low beta insertion, the RF systems and for diagnostic purposes are described and intensity, lifetime and stability limits discussed. As a foreword we describe the status of the SPS machine development studies related to the proposal.

10.1 Results of SPS machine development studies

Studies relevant to the $p\bar{p}$ proposal have been carried out in machine development sessions on the SPS throughout 1977. Results to date are encouraging.

i) A normal circulating beam at 200 GeV has been stored for periods of more than an hour. The decay time during storage is in excess of 15 hours, consistent with a measured average pressure of 5×10^{-9} Torr. At the design energy of 270 GeV the decay time should be double this figure. The key to obtaining long-lived beams is careful control of chromaticity to keep the Q spread small, and careful tuning to avoid fifth order stop bands.

ii) A single bunch 5 ns long containing more than 10^{11} protons has been injected. The space-charge Q spread caused beam to be lost to betatron resonances as predicted by theory. At the start of acceleration, 300 ms after injection, 6×10^{10} protons are left and of these, 3×10^{10} pass transition to reach high energy. This reproduces the space charge conditions for the design luminosity of 10^{30} cm^2 s^{-1}.

iii) No transverse instabilities causing beam loss have so far been encountered, although we are within a factor three of the bunch population needed to reach design luminosity.

iv) Single bunches have been stored at 200 GeV, though in these preliminary experiments only 10^{10} protons were accelerated; an intensity per bunch midway between that normally accelerated in the SPS and that required by the new scheme. No adverse effects were seen.

v) Preliminary measurements of beam growth during storage are within the theoretical estimates quoted below.

vi) The CPS has injected 3.5 GeV/c protons into the SPS and injection parameters adjusted to obtain a centered closed orbit with only one or two millimeters of distortion, an optimum Q value and zero chromaticity. In spite of the rather large transverse and longitudinal emittances of the proton beam, roughly twice that to be expected when antiprotons are injected, beam decay times of almost one second were obtained. It is expected that this decay, thought to be due to non linear resonances, will be considerably extended when smaller emittances are injected and when measures are applied to compensate the stop bands.

Further experimental investigation will be needed to develop the 3.5 GeV/c injection scheme and study the effects of the low beta insertion. These early experiments must also be translated into an operationally reliable procedure.

10.2 Intensity limitations

10.2.1 Single particle phenomena

The antiprotons, injected at 3.5 GeV/c, are three times more sensitive to remanent field imperfections in the SPS guide field than the protons, injected at 10 GeV/c. Careful correction of closed orbit and betatron resonances will be required and facilities installed in the SPS but rarely used because of its good magnetic purity will no doubt have to be brought into operation. The SPS at 3.5 GeV behaves rather like the FNAL main ring. One can therefore hope, with some confidence, that an acceptance of :

$$A_V/\pi = 1 \text{ mm mrad}$$

$$A_H/\pi = 1.4 \text{ mm mrad}$$

can be made available even at 3.5 GeV/c.

The invariant emittances of the antiproton beam assumed at injection and used as a basis for calculation of space charge Q shift correspond both to the physical acceptance of the transfer channel and the SPS physical acceptance assumed. They are :

$$E_V \beta\gamma/\pi = 3.73 \text{ mm.mrad}$$

$$E_H \beta\gamma/\pi = 5.22 \text{ mm.mrad}$$

One must expect some dilution of these emittances during acceleration and for the calculation of luminosity, beam-beam Q shift and gas scattering dilution at 270 GeV/c, larger antiproton invarient emittances are assumed. They are :

$$E_V \beta\gamma/\pi = 5.5 \text{ mm.mrad}$$

$$E_H \beta\gamma/\pi = 11.0 \text{ mm.mrad}$$

Because the proton beam undergoes fewer manipulations and is injected at a higher energy we assume a value based upon experience with the SPS which at all energies has an invarient value of :

$$E_V \beta\gamma/\pi = 10.0 \text{ mm.mrad}$$

$$E_H \beta\gamma/\pi = 20.0 \text{ mm.mrad}$$

10.2.2 Transverse collective phenomena

Possible limitations on beam intensity due to transverse collective phenomena were thoroughly studied during the design of the SPS. Reference 18 contains a complete review of possible instabilities. Experience with large accelerators leads us to believe this review to be valid, both qualitatively and, apart from minor reservations, quantitatively.

In its $p\bar{p}$ storage mode the SPS will be loaded with six antiproton bunches and six proton bunches, each containing 10^{11} particles. The mean current in each beam averaged over the circumference is low by SPS standards and collective effects which depend on mean current or are driven

by impedances whose time constants are comparable to, or longer than a revolution period, are not expected to be troublesome. One can therefore discount :

i) The low frequency transverse instability or "resistive wall effect" which appears in the SPS at 15 mA mean current (2×10^{12} particles) at a frequency below 1 MHz.

ii) The high frequency transverse instability at 460 MHz, which appears with over 5×10^{12} particles circulating, and which is driven by parasitic deflecting modes in the rf cavities whose bandwidth, 15 kHz, indicates a time constant of more than one revolution.

Since there is ample time between the passage of bunches for ions and electrons to diffuse away, the effects mentioned in Reference 18 due to neutralization may also be discounted.

Although the mean $p\bar{p}$ current is low, the local current or bunch population is high, 10^{11} compared with 2×10^{9} per bunch in normal SPS operation. The two remaining collective phenomena, which Reference 18 warns us to be beware of, are single bunch instability and space charge Q spread.

10.2.3 Single bunch transverse instabilities

Reference 18 contains a prediction by Sacherer for this effect. At 2×10^{9} protons per bunch, the rise time should be 80 ms falling to just over 1 msec for bunches of 10^{11} particles. We would expect this "head tail" effect to just overcome the Landau damping present in the beam and appear at a threshold 10^{11} protons per 200 MHz bunch. Sacherer's calculation assumes that the only transverse impedance driving the effect is that of the vacuum tube itself.

Having succeeded in injecting 10^{11} protons into the SPS in a single bunch and in accelerating 60% of this to transition, we feel reasonably confident that the single bunch limit is close to Sacherer's 1972 estimate.

Gareyte has shown that the sensitivity of the CPS to single bunch instabilities is much larger than that calculated from the impedance of the pipe itself and high frequency impedances presented by major discontinuities in vacuum chamber geometry have been invoked to explain this. We can only conclude from SPS experiments that such additional impedances should not be scaled up with the machine radius and that in the SPS they no more than double the effect of the pipe itself.

However, it would be too optimistic to hope that we will reach the design luminosity without having to deal with the lowest mode of the instability. Our single bunch experiments already show an unexplained loss at transition which may be due to single bunch instability. Careful chromaticity control should deal with any such difficulty.

10.2.4 Laslett Q shift

The effect of the Laslett Q shift is negligible in normal operation with 10^{13} protons spread around the 7 km of SPS circumference. But because it depends on local current density it becomes a force to be reckoned with in the proton-antiproton application. Although only 6×10^{11} particles circulate in each beam they are eventually compressed into a total beam length of only 30 m. At 10 GeV/c, this would produce an unacceptable Q shift of 0.15 and at 3.5 GeV/c, because the effect is proportional to $1/\gamma^2$ for a given invariant emittance, the Q shift would be ten times larger.

In a bunched beam there is a change in ΔQ as particles pass from the intense centre of the bunch to the rarefied ends. A particle with maximum synchrotron amplitudes will pass twice per synchrotron period from a Q value which is depressed by ΔQ, back to the unperturbed Q of the lattice. Even if one retunes the lattice by some fraction of ΔQ to restore the centre of probability of the Q distribution, a Q spread remains whose full width equals ΔQ which must fit between neighbouring stop-bands. The problem is similar to that of the Q spread due to SPS chromaticity combined with momentum spread. Experiments have shown that, in a machine of this size, significant fractions of injected beam begin to be lost if the chromatic Q spread exceeds 0.05 full width.

It is principally for these reasons that we propose to inject the antiprotons into the long buckets of a 2.6 MHz low frequency RF system at 3.5 GeV/c. Protons are also injected into these long buckets at 10 GeV/c and only at 18 GeV/c are the bunches squeezed into the short 200 MHz buckets in which they are accelerated and stored at 270 GeV/c. The details of these RF manipulations are described in Section 10.5. At each stage the bunches are compressed only when their γ has risen sufficiently for the Q shift to be acceptable at a higher line density. Table 10.1 shows the Q shift expected at each stage. The most serious Q shift is encountered by antiprotons at 3.5 GeV/c but it is still somewhat smaller than the Q shift calculated for the single bunch simulation performed recently in the SPS.

TABLE 10.1

Q shift due to space charge

	p (GeV/c)	Total beam (units of 10^{11})	Bunch length (m)	Number of bunches	ΔQ	
					$\bar{p}$	p
at injection	3.5	6	80	6	0.06	-
for h = 60	18	6	11.5	6	0.016	0.006
after compression	18	6	1.4	24	0.032	0.012
after merging 4 bunches into 1	270	6	1.4	4	0.0006	
SPS simulation experiment	10	0.6	1.4	1		0.08

(Emittances are the low energy values defined in Section 10.2.1).

In the single bunch test 6 x 10^{10} protons out of more than 10^{11} loaded into a single 200 MHz bunch at 10 GeV/c survived a 360 ms dwell time at this energy to be accelerated to transition. Losses were exponential as one would expect from repeated crossing of betatron resonances caused by Q spread. They rose steadily with injected intensity rather than appearing suddenly as an instability threshold and we are confident that the simulation reproduced the space charge Q shift phenomena to be expected in this proposal.

10.2.5 Longitudinal instabilities in the SPS

The filling time of the SPS 200 MHz cavities is 560 nanoseconds, less than 3% of a revolution period and much longer than the bunch length. Transient effects due to the sudden arrival of such a dense packet of charge deserve further study but meanwhile we take comfort from the successful acceleration of single bunches which already contain between 3 and 6.10^{10} protons.

Similar arguments lead us to expect that the beam will not be longitudinally unstable due to the impedance of other cavity-like objects in the ring.

At low energy, while the antiproton bunches are rather long and under the influence of low frequency rf systems, the 200 MHz cavities remain a potential source of microwave instability. Their impedance at these frequencies must be reduced by a factor 40 to a Z/n of about 20 ohms. This is a value comparable with other parasitic impedances around the ring. If broad band amplifiers and cavities (190 to 210 MHz) can be installed, they may be used as a feedback loop to compensate beam induced voltages in the cavities to an accuracy of 2%. The design of these systems is under way to damp instabilities in normal SPS operation but is still at a rudimentary stage.

At 270 GeV, single bunches containing almost 10^{10} protons have been stored, but it has yet to be demonstrated that bunches of 10^{11} particles will remain stable. Bunch areas of at least 550 mrad are theoretically necessary and the expected area of 3 to 4 radians should be safe.

10.3 Scattering and SPS vacuum

10.3.1 The SPS vacuum

The SPS vacuum is considerably better than its design value. During the last six months, careful surveys of the pressure measured at ion pumps around the ring and at pressure gauges between the pumps show an average of 7×10^{-7} Torr dropping to 5×10^{-9} Torr as pressure bumps due to small leaks have been progressively eliminated. Eventually we expect the average pressure to be no higher than that of the best sextant (i.e. 2×10^{-9} Torr).

Approximately half the pumping ports in the SPS were deliberately left without ion pumps when the present system was installed, and by mounting extra pumps on these ports one might drop the pressure even further to 10^{-9} Torr. Further improvements, particularly in rate of pump down, are to be expected if heating elements are attached to vacuum tubes to allow a mild bake-out. The benefits of baking are under study.

10.3.2 Beam loss lifetime

Estimates of nuclear scattering beam loss depend upon gas composition and further losses due to Coulomb diffusion to the walls depend on assumed aperture stop radius for the machine, but one can estimate these effects and scale them from measurements at higher pressure made at FNAL. Both methods agree and predict lifetimes at 5×10^{-9} Torr (N2 equivalent) of 40 hours at 200 GeV and 50 hours at 270 GeV. At 2×10^{-9} Torr lifetimes should be several days. With careful chromaticity compensation and Q tuning, SPS experiments have achieved decay rates of only 2% in the first hour at 5×10^{-9} Torr and at 200 GeV. The natural 1/e life time corresponding to this decay is 25 hours; we seem within striking distance of the theoretical lifetime.

10.3.3 Emittance growth and degradation of luminosity due to scattering

The Coulomb scattering due to the residual gas may be calculated exactly using Molières solution of the diffusion equation :

$$\theta_e(t) = \sqrt{\theta_0^2 + \frac{0.27\ Pt}{p_0^2}}$$

where : θ_e is the rms divergence after time, t.
θ_2 is the initial value of θ.
P is the gas pressure in Torr assuming N_2.
p_0 is the momentum of the stored particles in GeV/c.

Suppose a small scattering angle $\delta\theta$, is produced at a point in the machine where the betatron function is $\beta(s)$, and observed as a displacement, $\delta\sigma$, at a reference point where $\beta=\hat{\beta}$ which is distant in phase from the scattering event by $\Delta\psi$. Then, from a well known expression in Courant and Snyder :

$$\delta\sigma^2 = \delta\theta^2\hat{\beta}\beta(s)\ \sin\Delta\psi$$

To calculate the mean square displacement due to all such events wherever they occur in β or ψ we must take the mean of the above expression

$$\overline{\delta\sigma^2} = \frac{\delta\theta^2_{rms}\ \hat{\beta}\ \overline{\beta}}{2}$$

This, combined with the first expression gives a formula for the increase in the standard deviation, or half width at half height, of a Gaussian shaped beam profile observed at $\hat{\beta}$ (at other points in the ring the dilation, like the beam itself, scales as $\beta^{\frac{1}{2}}$)

$$\sigma(t) = \sqrt{\tau_o^2 + \frac{0.27\ \hat{\beta}\ \overline{\beta}\ Pt}{2p_o^2}}$$

We notice that σ^2 grows linearly with time

$$\frac{d(\sigma^2)}{dt} = \frac{0.27\ \hat{\beta}\ \bar{\beta}\ P}{2p_o^2}$$

Extensive measurements of scattering dilation have been made at FNAL [19] at elevated vacuum pressures above 10^{-7} Torr where this effect predominates. The results clearly demonstrate the expected pressure and energy dependence and curves of σ^2 versus time exhibit the expected linear slope. Putting their measured value for the slope in the above equation gives a pressure of 3.10^{-7} Torr for the FNAL main ring vacuum. This value is consistent with other estimates and measurements of their vacuum pressure. There exists of course the usual uncertainty of a factor 2 in such estimates in the absence of a gas analysis.

We can therefore with some confidence predict the growth rate for the SPS. Taking :

$\bar{\beta}$ = 55 m $P = 2.10^{-9}$ Torr (N_2 equivalent)

$\hat{\beta}$ = 110 m p_o = 270 GeV

one predicts :

$$d(\sigma^2)/dt = 2.2\ 10^{-11}\ m^2/s$$

In 24 hours the growth is $(1.39\ mm)^2$ and taking normalised emittances of 20 π mm.mrad horizontally and 10 π mm.mrad vertically corresponding to σ's of 1.4 and 1.0 mm respectively, the luminosity, inversely proportional to the product of the two σ's, drops by a factor 2.4.

Bearing in mind that we have assumed pessimistically that at these low pressure the gas is nitrogen while gas analysis suggests at least half is a partial pressure of lighter and much less dangerous elements, we conclude that the emittance growth of the beam will be tolerable at 2.10^{-9} Torr.

Remembering that the antiproton beam may have a smaller emittance initially and that one may find that optimum luminosity is achieved in practice with fewer protons within a smaller emittance, we still feel that a further reduction of residual pressure obtained by adding pumps may well be a valuable investment.

10.3.4 Beam-beam interaction

The design luminosity is ultimately limited by the electromagnetic forces on a particle as it passes through the colliding bunch of the other beam. The forces are of a non-linear nature and can drive destructive non-linear stopbands just like imperfections in the guide field. Solution of the non-linear problem is complex and depends on particle distributions in all three phase planes of both beams. A calculable measure of their strength, however, is the linear Q shift. Experience with the ISR shows that if decay rates due to related non-linear driving forces are to be smaller than 10 hours, this Q shift must be less than 0.01.

Assuming elliptical beam cross sections, Gaussian distributions, frontal collisions and v = c, the tune shift is

$$\Delta Q = \frac{r_p N}{\pi \gamma} \left[\frac{\beta_v}{(a+b)b} \right]_{\text{average}}$$

where r_p is the proton radius
N is the number of particles
a is the RMS beam half width
b is the RMS beam half height

Examination of this expression shows that it is independent of momentum for an invarient emittance and of the azimuthal structure of the beams.

The formula assumes that the n bunches of each beam collide in 2 n points around the ring. The quantitiy in brackets is averaged over

all these meeting points and since both numerator and denominator scale as beta, contribution from the low beta interaction point will be no more important than those from each of the 11 other meeting points. Small differences arise only from the aspect ratio of the beams at the different points.

The worst beam-beam Q shift is that experienced by protons in the vertical plane as they traverse the antiproton beam whose normalised emittances are 5 and 10 mm.mrad. The calculated value at full luminosity is a Q shift of 0.064 and much larger than may be tolerated. We must aim to prevent collisions at the unwanted meeting points by displacing the beams tranversely. ISR calculations[20] suggest a separation of 7.5 rms beam half widths is sufficient to reduce the non-linear forces by an order of magnitude. At 270 GeV this corresponds to 8 mm at maximum beta.

The orbit separation must be produced by electrostatic deflectors which, unlike magnetic deflectors, produce orbit deformations of opposite sign for the two beams. One such deflector 5 m long and operating at a field of 60 kV/cm will produce a deformation in each orbit of 6 mm amplitude which has the form of a sine wave of azimuthal frequency Q = 26.6. Since this frequency is unrelated to the 12 fold symmetry of the meeting points, one expects the average separation at meeting points to be the necessary 8 mm.

For quite independent reasons, namely to scan the beams across each other at the low beta points vertically and radially in order to determine luminosity and measure backgrounds, four such electrostatic deflectors will be installed in each plane close to the low beta section. Each quartet can be used to steer the beam at the low beta location and at the same time produce the necessary orbit distortion elsewhere in the ring.

With the beams separated at all but the low beta section, the Q shift is reduced to a tolerable 0.009.

10.4 The low beta insertion

10.4.1 The long straight sections

The lattice of the SPS has six long straight sections formed by simply omitting 20 dipole magnets without perturbing the regular focusing pattern. Of the six, one, LSS5, is almost unused and can be modified by adding quadrupoles to produce a low beta in both horizontal and vertical phase planes. A similar modification may also be made in LSS4 if the beam dump system, which occupies some of the space, is displaced to another long straight section.

10.4.2 The low beta insertion

Fig. 10.1 and Table 10.2 show the modifications to the focusing structure and beam dynamics at the insertion. The programme AGS[21] has been used to arrive at this solution. The low beta values are : 4.7 m horizontally and 1.0 m vertically, and the momentum compaction function, α_p, is essentially zero over the whole of the long straight section. The normal lattice quadrupoles in the neighbourhood of the insertion are left in place, but are modified in strength to form an integral part of the insertion design. The entire half cell between quadrupoles Q517 and Q518 is left free of obstruction for experimental equipment at the interaction region. This total free space is 29 m. The asymmetry of the design stems from the fact that one is producing minima in the beta functions at points where such extrema do not exist in the unperturbed lattice. To produce a symmetric solution, a normal SPS quadrupole would have to be removed.

10.4.3 Effect on SPS dynamics

The insertion inevitably perturbs the dynamics of the SPS. To obtain a low value at the intersection point, beta must be allowed to rise to five or six times the normal maximum of 100 m on either side of the insersection. If the insertion were to be switched on throughout the acceleration cycle of the SPS, quadrupoles and bending magnets about the insertion would need to be enlarged in aperture to allow the passage of the large emittance beam at 10 GeV/c or 3.5 GeV/c.

Furthermore, the modifications to beta functions make the phase advance over the long straight section very different from that at other straight sections. A superperiodicity of one is introduced and systematic sextupole and decapole errors, principally in the remanent fields of the dipole magnets, become capable of driving all third and fifth integer betatron resonances. The dislocation also breaks the regular pattern of 72 chromaticity correcting sextupoles which could then excite all third integer resonances.

It is expected that at 270 GeV the effect of remanent fields will be weak enough and the emittance small enough for these effects to be tolerable, given some modification to the pattern of correcting sextupoles. The problem has yet to be studied with computer simulation. But at 10 GeV/c, where the SPS is known to already be sensitive, even to non-systematic betatron resonances, one can be sure that such a dislocation to the optics is intolerable. Injection at 3.5 GeV/c and space charge Q-shift would only make things worse.

10.4.4 The "in-flight" insertion

We propose to circumvent this problem of aperture and stopbands at low energy as follows. The SPS will accelerate to 270 GeV with the seven extra quadrupoles of the insertion switched off, and with its full complement of normal quadrupoles in series. Once the beam is stored at 270 GeV, individual supplies, powering the extra quadrupoles, and active shunts by-passing nine SPS quadrupoles whose strengths are to be modified, are ramped to slowly transform the unperturbed machine into the configuration shown in Fig. 10.1. That a continuity of solutions exists between unperturbed and perturbed configurations, must be checked, but such "in-flight" transformations have been applied to SPEAR and ISR with success. Some further modification and additions to the proposed quadrupole locations may prove necessary to ensure this continuity.

Altogether nine SPS quadrupoles must be equipped with active shunts. Five of them are only trimmed by a small amount. The others must be

altered considerably and in the case of 516 and 518 reversed in polarity. This will require stout cables from the active shunts. The seven extra quadrupoles (Q1 through 7) must also be powered individually through cables from the surface.

The lengths and apertures of all quadrupoles are standard values for the SPS and all strengths are velow the saturation limit. Nevertheless, several of the quadrupoles must run DC at full field and new coils with larger cooling holes may have to be constructed and installed. An alternative solution is to install more quadrupoles at the risk of obstructing space otherwise left free for experimental equipment.

TABLE 10.2

Quadrupole modifications

$$k = \frac{(dBy/dx)}{B\rho}$$

Normal SPS locations

Number	k (m^{-2})	
513	0.0123	weak active shunts (3) + main bus
514	-0.0141	
516*	0.0108	
517	0.025	strong active shunts + main bus (3)
518*		
519	0.0118	
520	-0.007	
522	-0.0142	weak active shunts + main bus (2)
533	0.0123	

Extra quadrupoles

Q1	0.006	individual power supplies (5)
2	-0.0196	
3		
4	0.0215	
5	0.0229	
6	-0.0198	
7		

(k = 0.015 m^{-2} is a standard SPS strength)

* Reversed

10.4.5 Insertion design procedure

The first step in calculating a system to produce the required values of β_H, β_B and α_p and their derivatives at the centre of the insertion is to slightly modify the strength of quadrupoles 513, 514, 522 and 523. These are within the bending structure on each side of the insertion and may be adjusted to make α_p zero throughout the long straight section [22].

The second step is to place three quadrupoles next to Q517 and three next to Q518 to form, together with these quadrupoles, strong doublet lenses which pinch beta to a minimum in both planes. To achieve sufficient perturbation, each member of the doublet is really two quadrupoles.

With modifications to the strength of 519 and 520 downstream and 516 plus an extra quadrupole, Q1, upstream, eight variables are available, sufficient to match β_H, β_V plus their derivatives into each side of the lattice. All the quadrupoles varied in this second phase are within the bending free region and so the initial α_p match is not perturbed. Note that normal quadrupoles 516 and 518 have opposite polarity from their normal configuration. Their active shunts must provide about twice the normal quadrupole current.

Finally, one adjusts the strength of all the other lattice quadrupoles to restore Q, perturbed by the additional phase advance introduced by the insertion. After a second iteration of this procedure, AGS gives a consistent solution.

10.4.6 Errors and tolerances

We have studied the effects of errors in the focusing strength of the insertion quadrupoles. An error of 3×10^{-4} in a quadrupole at a high beta point causes a 2% modulation of the beta function around the ring and doubles the half-integer stopband width due to gradient errors in the unperturbed machine. To be safe, bearing in mind that there are several such quadrupoles with errors weighted according to β, it would seem reasonable to ask for a gradient precision of 10^{-4} or better.

It seems one can make quite large changes to the Q of the machine of the order of unity by means of the normal SPS quadrupoles, without disturbing the low β, low α_p condition.

A large number of solutions exist and one may shift the location of the intersection point by several metres or provide larger betas or different aspect ratios without moving quadrupoles. However, to produce a significantly lower beta, more quadrupole strength and better precision would be required.

10.5 RF systems for the SPS

The present SPS RF system has a nominal frequency of 200 MHz and, when augmented as is planned in the present SPS improvement programme, will supply a peak voltage per turn of 8.8 MV. One half of this is available for p and $\bar{p}$ each. A single bunch riding in a stationary bucket formed by the RF system will have a length less than 5 ns. This is consistent with the experimenters need for a short interaction region and a high luminosity. Each stored beam will consist of six such bunches equally distributed in azimuth and each containing a nominal 10^{11} particles.

One may calculate the phase space area of these bunches from the momentum spread obtained in the cooling ring. In Section 2.7, we show that the momentum spread has a minimum value mainly determined by the necessity of limiting the intra-beam scattering. Although the bunch area thus calculated is small enough to fit in at 270 GeV stationary bucket, it is too large to be accelerated in a single 200 MHz bucket in the critical region just above transition where the bucket area for a given voltage is considerably reduced.

We propose to overcome this difficulty by sharing the longitudinal phase space area of the bunch among four consecutive 200 MHz buckets during the acceleration process and then merging them into a single bunch at high energy. A special 16.9 MHz RF system is required for this manipulation.

A second special RF system tunable to 2.6 and 9.1 MHz is required to cover the low energy part of the acceleration cycle from 3.5 to 18 GeV/c. In Section 10.2.4 we show how serious the Laslett space charge Q shift can be in this energy region if one attemps to keep 10^{11} particles in short bunches. Even when 80 m long bunches of antiprotons are injected into the buckets of the proposed 2.6 MHz low energy RF system, the line density is high enough to produce a Q spread of 0.055.

The parameters of these two new RF systems and the conditions prevailing at critical points in the acceleration process are to be found in Table 10.3. Details of the manipulations are described below.

10.5.1 Acceleration from 3.5 to 18 GeV/c

Six long bunches of antiprotons, each with an area of 12 mrad, a length of 80 m and a momentum spread of $\pm$ 6.7 x 10^{-4} are extracted in turn from the cooling ring and deposited in 2.6 MHz buckets in the SPS. The 2.6 MHz RF system proposed consists of four CPS type ferrite tuned cavities giving a maximum total voltage of 80 kV and operating at a harmonic number of 60.

Initially the space charge Q spread is 0.055 but as acceleration proceeds this falls as $1/\gamma^2$ and one can afford to increase the acceleration rate, thus shortening the bunches. Nevertheless acceleration to 18 GeV/c will take more than 10 s and considerable improvements will have to be made in 3.5 GeV/c beam lifetime if a large fraction of the antiprotons are to survive.

10.5.2 Injection of protons

Protons will be injected at a momentum in the range 10 to 14 GeV/c and the acceleration of the antiprotons will be arrested for 3.25 s to allow the SPS kicker to fire and recover six times, transferring six CPS bunches into equally spaced slots around the SPS circumference. The proton bunches will be matched to the buckets of the low frequency RF system by voltage manipulations in the CPS. Care must be taken not

to kick out antiprotons and the collision point of the two opposing beams must be some distance from the long straight sections, at this time.

10.5.3 Manipulations at 18 GeV/c

Following injection of protons the low frequency RF system accelerates both beams to 18 GeV/c where the Laslett Q spread has fallen to the level where one may compress the low frequency bunches into the four 200 MHz buckets which will take them to high energy.

During acceleration from 3.5 to 18 GeV/c the low frequency bunches have shrunk to a length of 11.5 m. Their momentum spread is $\pm 10^{-3}$ and they are rather prone to longitudinal instability ($Z/n = 48\ \Omega$). To fit into four 200 MHz buckets each bunch must be compressed to less than 6 m length. This may be done by suddenly increasing the RF voltage so that the long shallow bunch rotates in a much taller bucket until after one quarter of a synchrotron revolution it becomes short and tall. This process of bunch compression has worked successfully in the CPS.

Unfortunately the four CPS cavities do not provide sufficient voltage for this manoeuver at a harmonic number of 60. However, the bunches are short enough at 18 GeV/c to fit in a bucket produced by retuning the cavities to harmonic number 210. The details of this change in harmonic number are as follows. The beam is held at harmonic number 60 with three of the four cavities giving their full voltage of 60 kV. The fourth cavity is tuned to h = 210 and powered to 20 kV, a voltage which matches the bunch at this higher harmonic number. The first three cavities may then be switched off and retuned to h = 210, leaving the beam under the control of the fourth cavity. By then rapidly raising the additional three cavities to their peak Volts, an 80 kV bucket is formed in which the bunch rotates. All cavities are then switched off and the 5.7 m long bunch adiabatically captured in four adjacent 200 MHz buckets in which it is accelerated to full energy.

10.5.4 Acceleration to 270 GeV/c

The SPS 200 MHz travelling wave cavities accelerate only in one direction. Particles passing in the opposite direction see only a small resultant perturbation.

By the time the $\bar{p}$-p scheme is implemented, the SPS will have been equipped with four cavities as part of the programme to increase intensity and repetition rate. Each pair of cavities will provide almost as much voltage per turn as those presently installed. One has only to connect one pair in the opposite sense to the other for antiprotons. In this way, the two beams may be treated separately. They may be given slightly different frequencies so that the interaction point where bunches clash can be made to migrate to a different point in the ring. With six bunches, there will be twelve such interaction points. At injection these should be remote from the long straight sections to avoid kicking out antiprotons as protons are fed in. As acceleration proceeds they will be made to migrate to be coincident with the experiments in the long straight section(s).

An alternative method of using the cavities is to pump RF power from one end as the protons pass, and from the other end as antiprotons pass. This is possible because the filling time of the cavity is only one thirtieth of a turn. In this way the full voltage of the four cavities may be applied to each beam providing large bucket areas. This mode of operation however would require there to be five rather than six bunches in each beam. With six bunches the two beams would arrive simultaneously at the cavities which like the low beta point are located in a long straight section and therefore at an interaction point.

10.5.5 Compressing four bunches into one

At high energy the high frequency RF system has sufficient bucket area to contain each train of four bunches in a single bucket. The transformation is made by a bunch rotation similar to that made at 18 GeV/c. The 200 MHz is momentarily switched off and large buckets formed by a 16.9 MHz system in which the four bunches rotate (Fig. 10.2) from being a string along the phase axis until they extend along the momentum axis

of longitudinal phase space. The voltage required is 1 MV and the RF system to produce it at this frequency is expensive. Nevertheless this final manipulation is necessary to achieve the design luminosity.

Once rotated the four bunches, superimposed in time, may be captured in a single 200 MHz bucket by switching back to the normal RF system.

10.5.6 Longitudinal instability

Intense bunches are inevitably prone to longitudinal instabilities and care must be taken to ensure that the RF systems not active at any given time are "shorted" to present a minimum impedance to the beam. The danger points are just before the two bunch rotations where Z/n of 20 to 50 Ohms can produce an instability.

10.6 Diagnostics

10.6.1 Present equipment in SPS

The SPS is equipped with instrumentation designed to monitor a continuous beam with 200 MHz structure at intensities in the range of 10^{11} to 10^{13} protons (800 μA to 80 mA). Detectors and instrumentation include :

i) Beam current transformers (BCT) with a noise and long term drift of 240 μA (3 x 10^{10} protons).

ii) Closed orbit measurement systems using 216 electrostatic pick-ups looking at the 200 MHz structure of the beam and capable of 1 mm accuracy at 10^{11} ppp (800 μA).

iii) Q measurement systems which operate by kicking the beam and processing the signals from broad-band electrostatic pick-ups. The signal is sampled at the revolution frequency through a gate which is presently long compared with a single bunch. Fourier analysis determines the fractional part of Q and indicates the Q spread.

TABLE 10.3

RF parameters for the SPS

Particles per bunch	10^{11}	
γ_{tr}	24	
$E_V\beta\gamma = E_H\beta\gamma/2$	$3.73\pi.10^{-6}$	rad m

a) SPS low frequency - low energy 3.5 GeV/c → 18 GeV/c

RF frequency (h = 60)	2.6	MHz
Area of 12 mrad cooling ring bunch in SPS	16.4	mrad
Length of bunch	±122.7	deg
Length of trapping bucket	±130	deg
Blown-up bunch area	17.6	mrad
RF voltage for trapping	12.68	kV
Longitudinal stability $(Z/n)_{max}$	∿2200	Ω
Incoherent Q spread	-0.055	
Initial ϕ_s (const.bunch length)	12	deg
Initial RF voltage for acceleration	17.1	kV

b) Injection of p bunches from PS

Momentum	10-14	GeV/c
Bunch area in PS (h = 20) corresp. to 17.6 mrad in SPS (h = 60)	65	mrad

c) Change of h = 60 to h = 120 in the SPS (typical)

Momentum	18	GeV/c
Voltage on h = 60	60	kV
Bunch length	±18	deg
Voltage on h = 210	21	kV
RF frequency at h = 210	9.1	MHz
Blown-up bunch area (h = 210)	65	mrad
Bunch length in m	11.5	m
Bunch height in Δp/p before filamentation	$\pm 9.4 . 10^{-4}$	
Z/n before change of h } = worst case	48	Ω
ΔQ before change of h } = worst case	-0.014	

d) First bunch compression in the SPS

Momentum	18	GeV/c
Maximum V_{RF} on h = 210	80	kV
Time of $\frac{1}{4}$ rotation	15	ms
Bunch length after rotation	5.67	m
ΔQ after rotation	-0.028	

e) Adiabatic trapping on h = 4620

Momentum	18	GeV/c
Number of filled buckets	4	
Number of particles in each of two inner buckets	34	%
Number of particles in each of two outer buckets (for parabolic distrib.)	16	%
Bunch area of each of the inner bunches on h = 4620	$\sim$500	mrad
V_{RF} on h = 4620 for 500 mrad	1350	V
ΔQ after trapping	-.035	

f) Acceleration in the SPS

		*)	
Number of accelerating tanks	2	4	
Maximum bucket area at 18 GeV/c (ϕ_s = 0)	900	1250	mrad
Maximum stable phase angle ϕ_s for 500 mrad	16.5	25.5	deg
Acceleration rate for ϕ_s max. at 18 GeV/c	50	160	GeV/c/s
Maximum stab. phase angle at $\sqrt{3}.\ \gamma_{tr}$ (39 GeV/c)	25	33	deg
Accel. rate for $\phi_s = 25/33^o$ at 39 GeV/c	80	200	GeV/c/s
Bunch length for ϕ_s max. at 18 GeV/c	1	0.85	m
$\Delta\dot{Q}$ (1/0.85 m, 18 GeV/c)	-0.053	-0.062	
Max. bucket area at 270 GeV/c (h = 4620)	2.63	3.72	rad

g) Bunch compression in the SPS

Momentum		270	GeV/c
Harmonic number		390	
Frequency		16.9	MHz
RF voltage		1000	kV
Time of $\frac{1}{4}$ rotation		9.6	ms
Longitudinal stability for inner bunches	before rotation	26	Ω
" " " outer "	before rotation	$\sim$18	Ω
Blown-up bunch area after rotation		2.6/3.7	rad
Longitudinal stability after rotation		240/490	Ω

* not possible with 6 bunches

iv) Wide-band transverse and longitudinal pick-ups with a response which is flat into the GHz range, give either continuous or sampled pictures of bunch configuration revealing longitudinal and transverse high frequency instabilities. These signals can also be used for spectrum analysis to determine $\Delta p/p$ in an unmodulated beam.

v) Precision Ionization Beam Scanners (IBS) which measure horizontal and vertical beam profiles with a resolution of better than 1 mm above 5×10^{12} ppp.

vi) Beam scrapers and fast ejection profile detectors capable of measuring beam distributions destructively as a check on IBS profiles.

Before single bunches of protons and antiprotons are injected, the SPS will be tuned for 3.5 GeV/c and 10 or 14 GeV/c injection and acceleration with continuous beams of protons. All these devices will then be employed since one must rely heavily on this preliminary tuning when the machine is switched first to single bunch mode and finally to accelerate and store the antiprotons.

This kind of mode switching without disturbing injection and SPS acceleration conditions, presents a major operational challenge to the SPS and has yet to be developed as a technique.

10.6.2 Special requirements for observation of single-bunch and coasting beams

Even if one relies heavily on mode switching, some improvements to the SPS diagnostics will be required for machine studies leading up to $p\bar{p}$ operation, to check mode switching and to monitor the $p\bar{p}$ beams once injected. Some improvements include :

i) Beam current transformers

Considerable improvements have been made to the SPS type beam current transformers with a view to installation in ICE and the APR. Improvements to the magnetic amplifier and integrating current transformer have reduced the noise/long-term drift level to 5 μA. These improvements will be incorporated in some of the existing BCT's to meet the need to monitor the acceleration and coasting lifetime of single proton and antiproton bunches.

ii) Closed orbit monitoring and correction

At present, it is customary to use closed orbit dipoles to correct both remanent field errors and misalignment errors at injection. The admixture of these two components will be different at the two injection energies, 3.5 GeV/c and 10 GeV/c. While in principle one can provide exact correction at both energies by correcting only the remanent field errors with dipoles and adjusting lattice alignment, this has yet to be proved practicable. Meanwhile, one should keep open the possibility of adding time-dependent reference generators to the closed orbit dipole supplies.

Once one has corrected the orbit at the two energies in continuous beam mode, it is unlikely to change during mode switching. Nevertheless, a few more sensitive position monitors may be needed to check that the injection orbit is still the same in the single-bunch mode. The increase in sensitivity required is not a large one; closed orbits have already been measured at the 10^{11} level. Sensitivity may be increased by driving a high impedance rather than a matched load at the expense of placing electronics close to the beam.

iii) Q measurement

While we have already managed to measure Q with single bunches of 10^{11} protons the signal to noise ratio may be considerably improved by shortening the gate length. By locating the detectors correctly, one

may hope to distinguish between the signals from the passage of the protons and antiprotons.

The technique, being detrimental to the beam if not destructive, is not suitable for repeated monitoring of coasting conditions or for checking the transition from an unperturbed machine as the low-β insertion is powered. Continuously active, non-destructive techniques, similar to those used at the ISR, should be studied for this application.

iv) Wide-band observations

Single densely populated bunches will give more signal strength above 200 MHz than is available at present. We have already demonstrated that with sampling scope techniques, the development of the length of a single bunch can be monitored during coasting. It would be useful to reject noise with a gate compatible with spectrum analysis techniques.

v) Profile detectors

The Ionization Beam Scanner is limited by noise to intensities above a few 10^{12} ppp. Moreover, even the high precision version of this device requires a local vacuum bump of a few x 10^{-6} Torr.m, comparable to the total residual gas in the whole ring. We shall certainly require at least three of these precise IBS's to study beam growth with continuous beams, but to monitor bunched beams we must look to devices being developed for ICE (Section 8.1.6). These integrate over an extended time (50 ms) and can operate at gas pressures of 10^{-9} Torr and beam intensities as low as 10^{10} particles per APR circumference, and seem to meet the SPS requirements. One version of this device, in which electrons from beam-gas collisions are imaged in a wire chamber, seems particularly promising from the point of view of computer acquisition.

Such devices should be installed at locations where the p and $\bar{p}$ beams are separated : they may thus distinguish the profiles of the two beams, an essential requirement if one is to understand the causes of poor luminosity.

10.6.3 Beam separation

One needs to be able to separate the beams at the low beta point to measure luminosity. About 5 m of electrostatic field of 60 kV/cm is needed to separate the beams by twice their full width at 270 GeV. Two such electrostatic devices are required in each plane on either side of the low beta point, but in high beta locations. Their phase advance to the centre of the insertion should be an odd multiple of $\pi/4$. There must be another high beta location where one can locate profile mode monitors between each pair of deflectors at an odd multiple of $\pi/2$ in phase from the deflectors. The medium straight sections, where two magnets are missing on either side of the long straight section, are obvious possible locations for the deflectors but some modification to the insertion may be necessary to obtain the right phase advance.

Distribution (open)

Distribution (of abstracts)
PS, ISR and SPS Scientific Staff

/ed

11. REFERENCES

1. C. Rubbia, unpublished.
   See also K. Hübner, D. Möhl, L. Thorndahl, P. Strolin, Estimates of ISR luminosities with cooled beams, ISR Workshop Oct. 1976, PS/DL/Note 76-27.

2. J.I. Budker et al., Experimental study of electron cooling, Institute for Nuclear Physics, Novosibirsk, Preprint 76-33. Translation : Brookhaven, BNL-TR-635.

   J.I. Budker et al., New experimental results of electron cooling, Institute for Nuclear Physics, Novosibirsk, Preprint 76-32. Translation : CERN, PS/DL/Note 76-25.

3. F. Bonaudi et al., Antiprotons in the SPS, CERN/DG-2. Preliminary description of the $p\bar{p}$ facility, SPS/DI/PP/Int.Note 77-9-

4. B. Autin, Dispersion suppression in the antiproton ring (in preparation).

5. A. Piwinski, Intra-beam scattering, Proc. IXth Conf. on High Energy Acc. (1974) 405.

6. E. Keil, W. Schnell, Concerning longitudinal instability in the ISR, CERN ISR-TH-RF/69-48 (1969).

7. P. Sievers, private communication.

8. D. Dekkers et al., Experimental study of particle production at small angles in nucleon-nucleon collisions at 19 and 23 GeV/c, Phys. Rev. 137, B962 (1965).

9. G. Bellettini et al., Proton-nuclei cross-sections at 20 GeV, Nucl. Phys. 79 (1966) 609.

10. S. Van der Meer, Influence of bad mixing on stochastic acceleration, SPS/DI/PPInt.Note 77-8 (CERN).

11. F. Sacherer, L. Thorndahl, S. Van der Meer, Some contributions to the theory of momentum cooling (in preparation).

12. R.B. Palmer, BNL, private communication (1975).

13. G. Carron, L. Thorndahl, Stochastic cooling of momentum spread by filter techniques in the cooling ring, ISR-RF/LT/ps (Ttechnical Note, Jan. 1977).

14. G. Carron, L. Faltin, W. Schnell, L. Thorndahl , Experiments with stochastic cooling in the ISR (1977 Particle Accelerator Conference, Chicago).

15. H.G. Hereward, Coherent instability due to electrons in a coasting proton beam, CERN 71-15.

16. E. Keil, Intersecting storage rings, CERN 72-14.

17. H.G. Hereward, Statistical phenomena - Theory
W. Schnell, Statistical phenomena - Experimental results
Proc. of the 1st Course of the Internat. School of

18. Spring study on accelerator theory (1972), AMC-1 (available from SPS Division Secretariat).

19. C.M. Ankenbrandt et al., Proc. National Conf. on High Energy Accelerators, Chicago (1977).

20. K. Hübner, private communication.

21. E. Keil et al., AGS - The ISR computer program for synchrotron design, orbit analysis and insertion matching, CERN 75-13.

22. P. Bryant, A. Hutton, private communication.

APPENDIX A

Participants in Design Study

B. Autin
B. Bianchi
R. Billinge
D. Blechschmidt
J. Brunet
B. Couchman
L. Evans
D. Fiander
G. Gravez
M. Höfert
E. Jones
H. Koziol
D. Möhl
A. Poncet
J. Rouel
C. Rubbia
F. Sacherer
G. Schröder
N. Siegel
H. Stucki
L. Thorndahl
S. van der Meer
E. Weisse
T. Wikberg
E. Wilson
C. Zettler

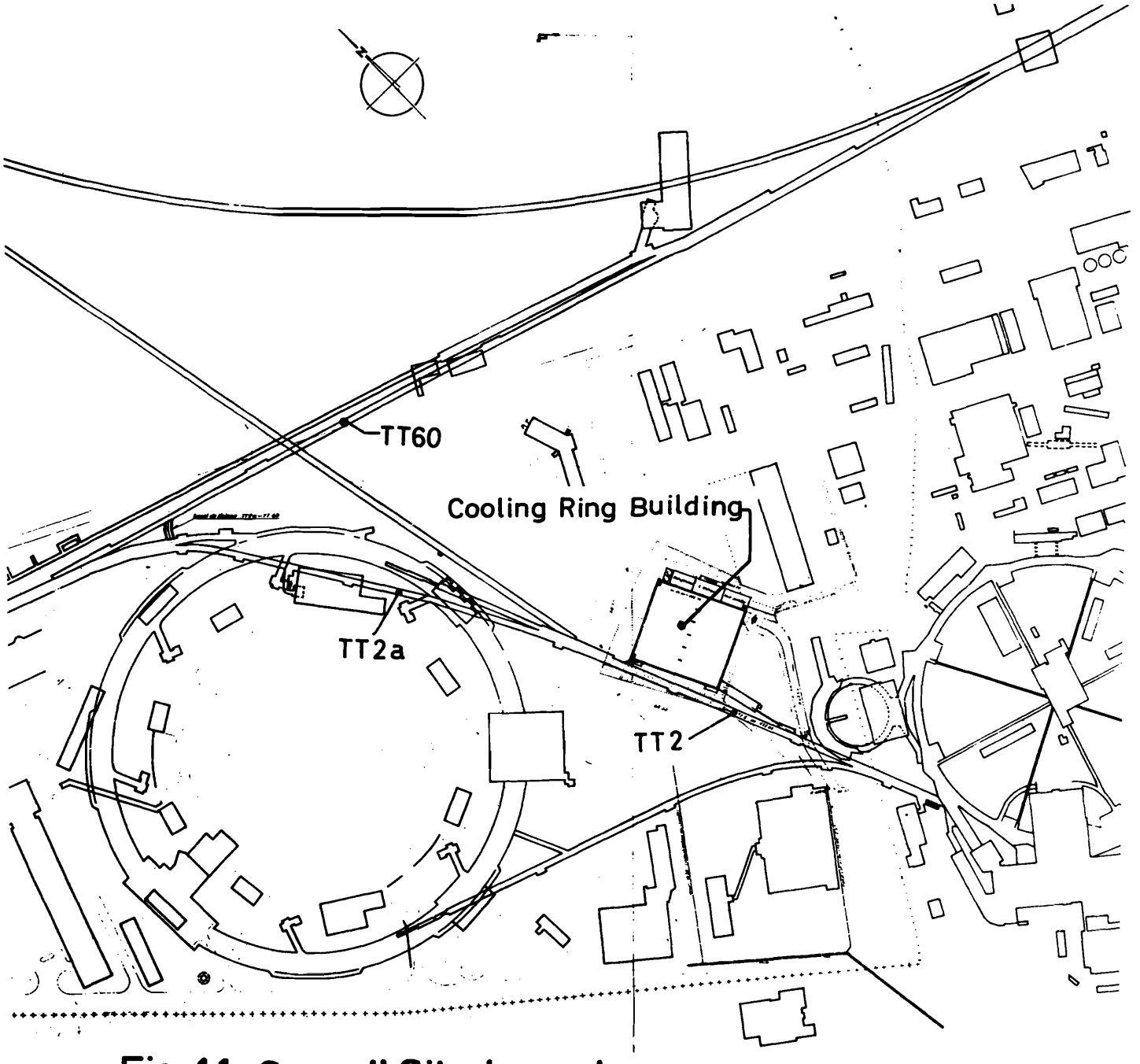

Fig. 1.1 Overall Site Layout

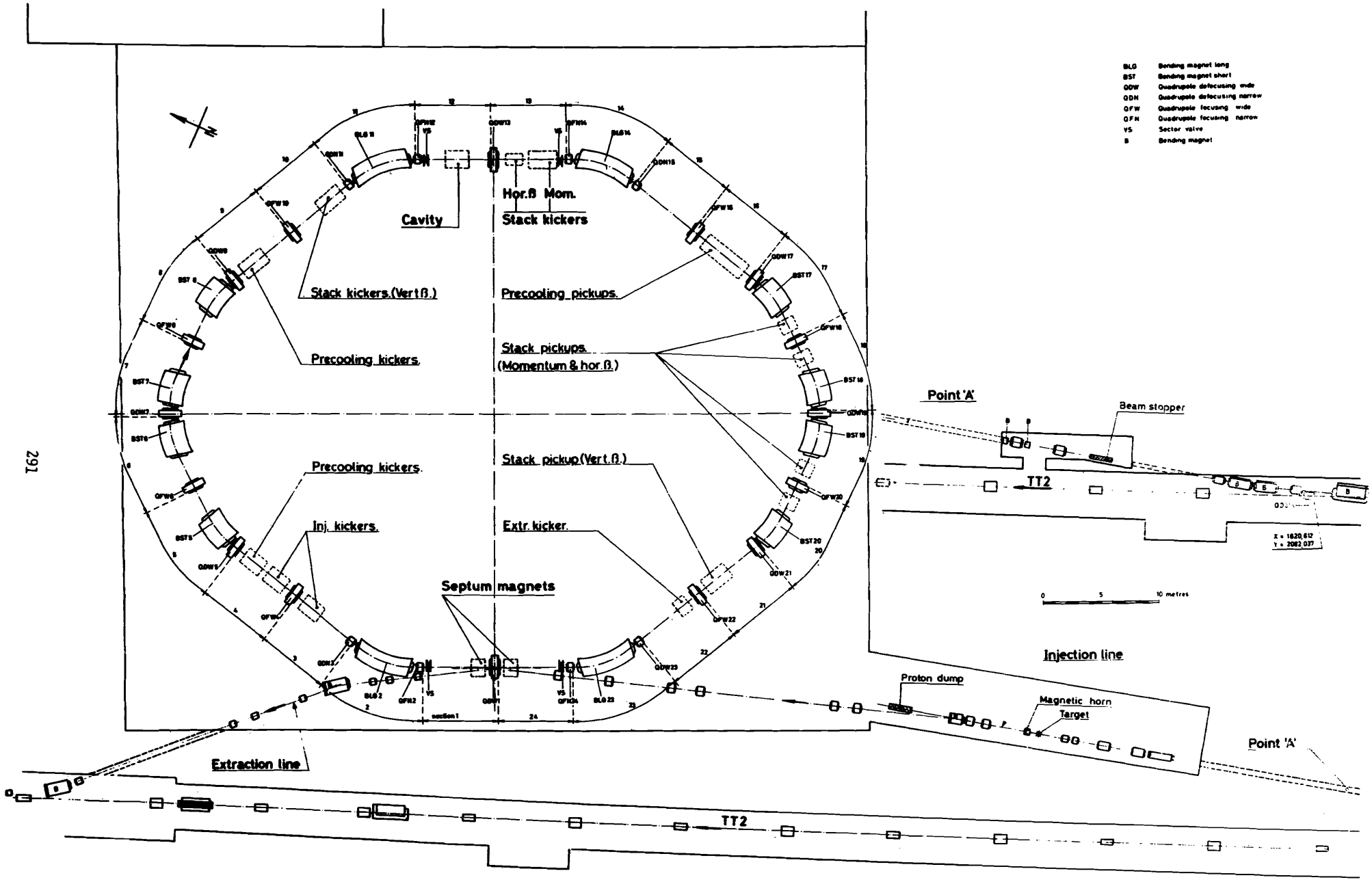

Fig. 1.2 General Layout Of The Antiproton Accumulator

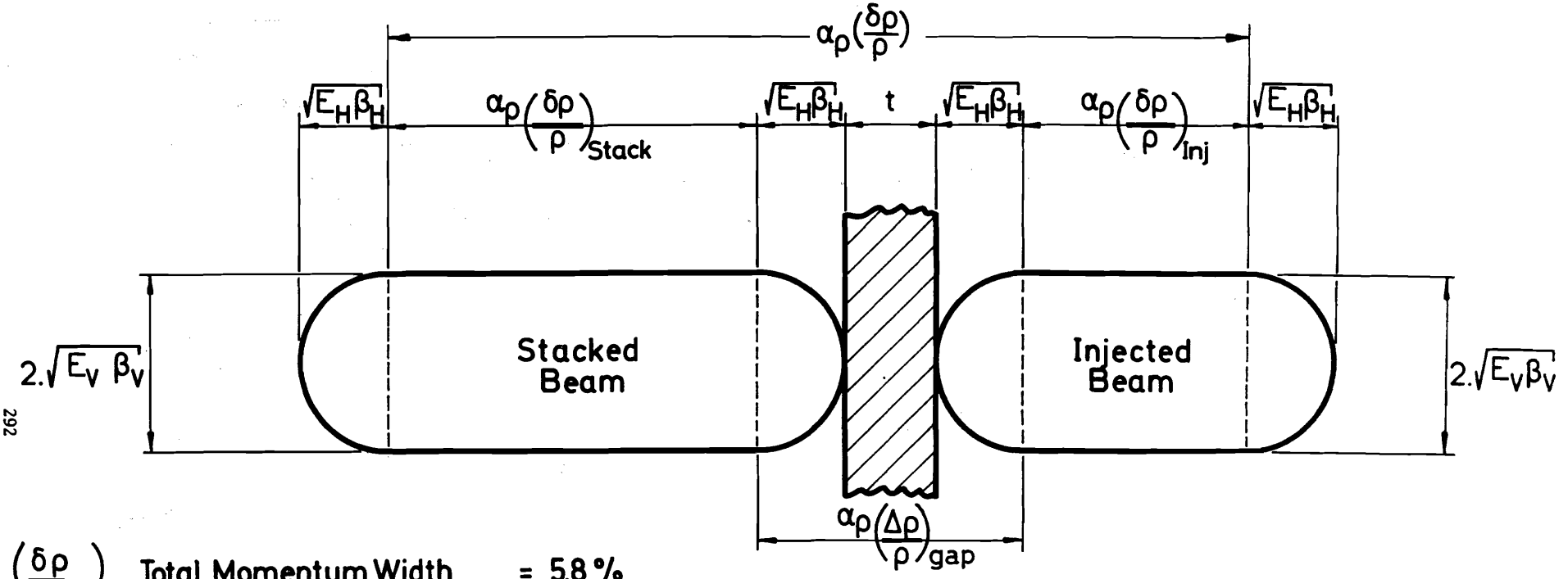

$\left(\frac{\delta\rho}{\rho}\right)$ Total Momentum Width = 5.8 %

(πE_v) Vertical Emittance = $100\,\pi\mu\vartheta m$

(πE_H) Horizontal Emittance = $100\,\pi\mu\vartheta m$

$\left(\frac{\delta\rho}{\rho}\right)_{St}$ Stack Momentum Width = 2.5 %

$\left(\frac{\delta\rho}{\rho}\right)_{Inj}$ Injected Momentum Width = 1.5 %

Fig. 2.1 Machine Acceptance

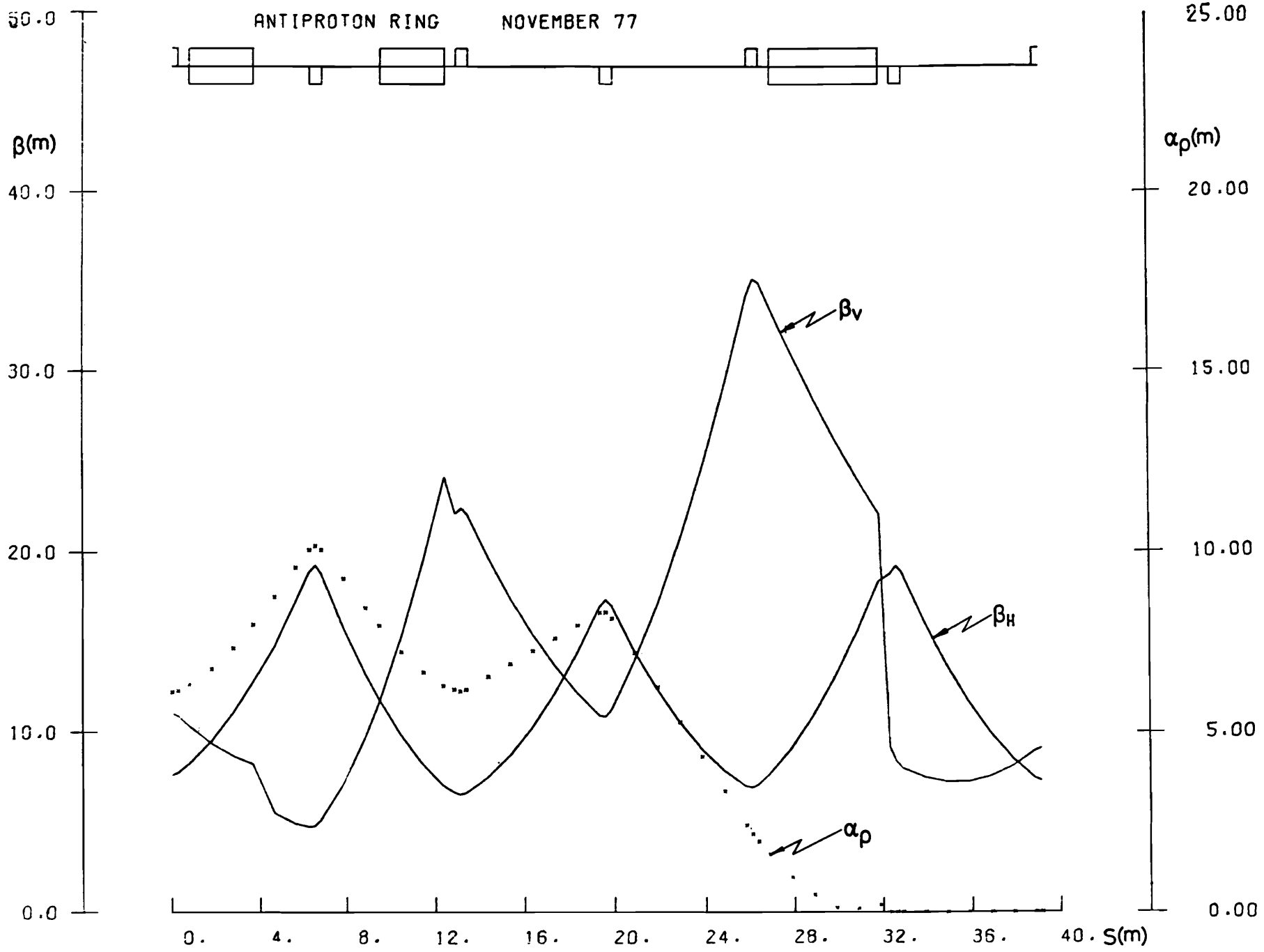

Fig. 2.2 Lattice Functions

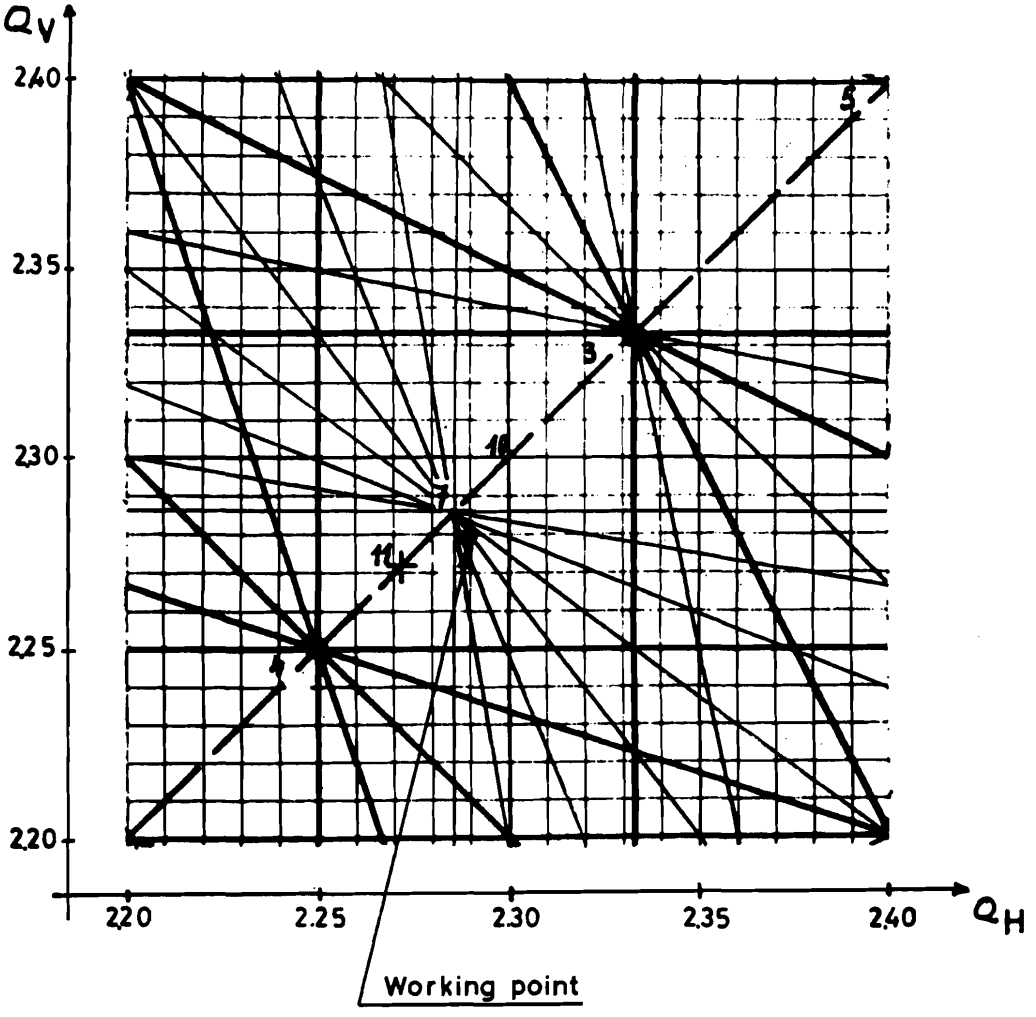

Fig. 2.3 Working Diagram

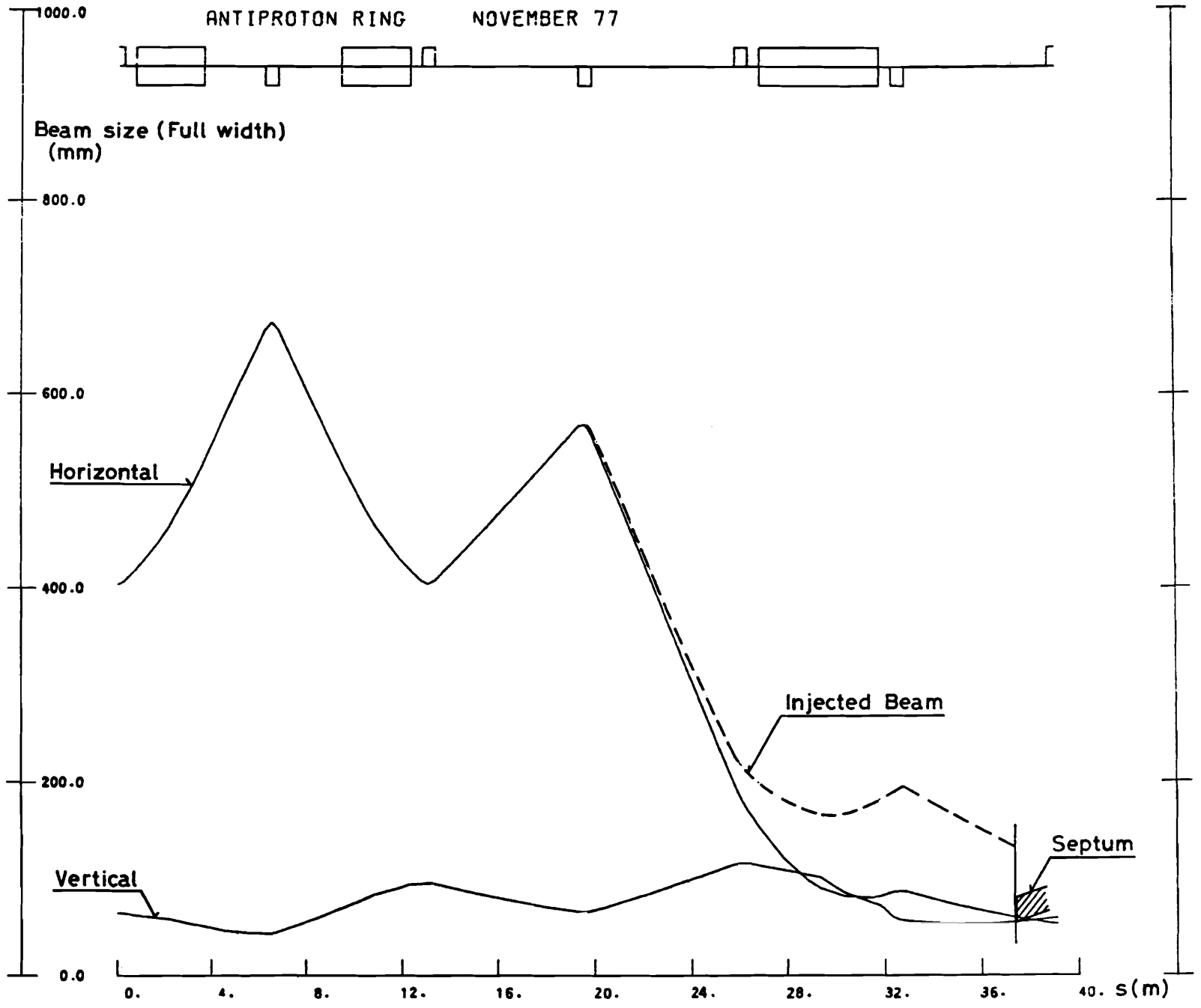

Fig. 2.4 Beam Sizes In A Quadrant

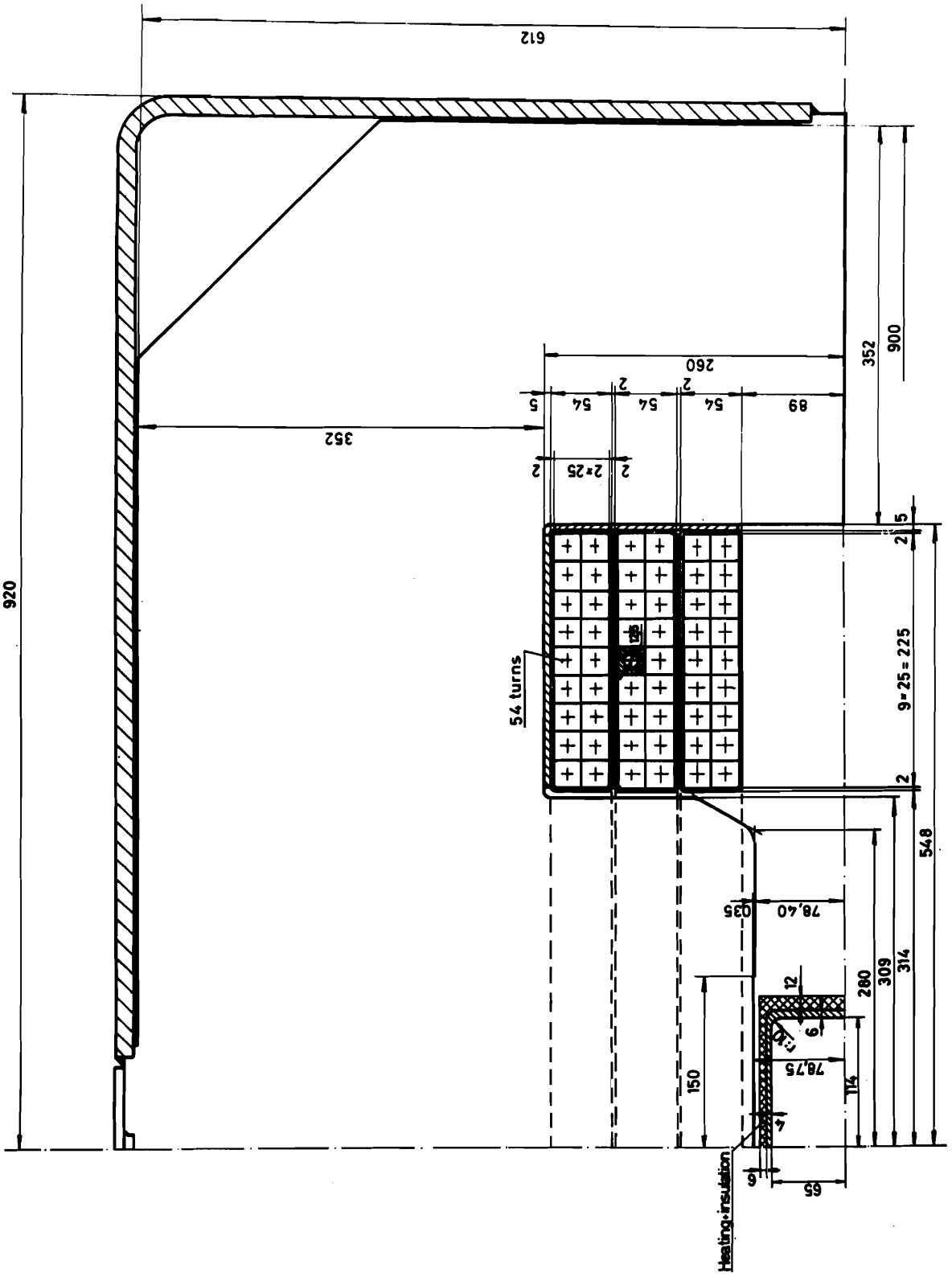

Fig. 3.1 'H' Magnet Cross Section

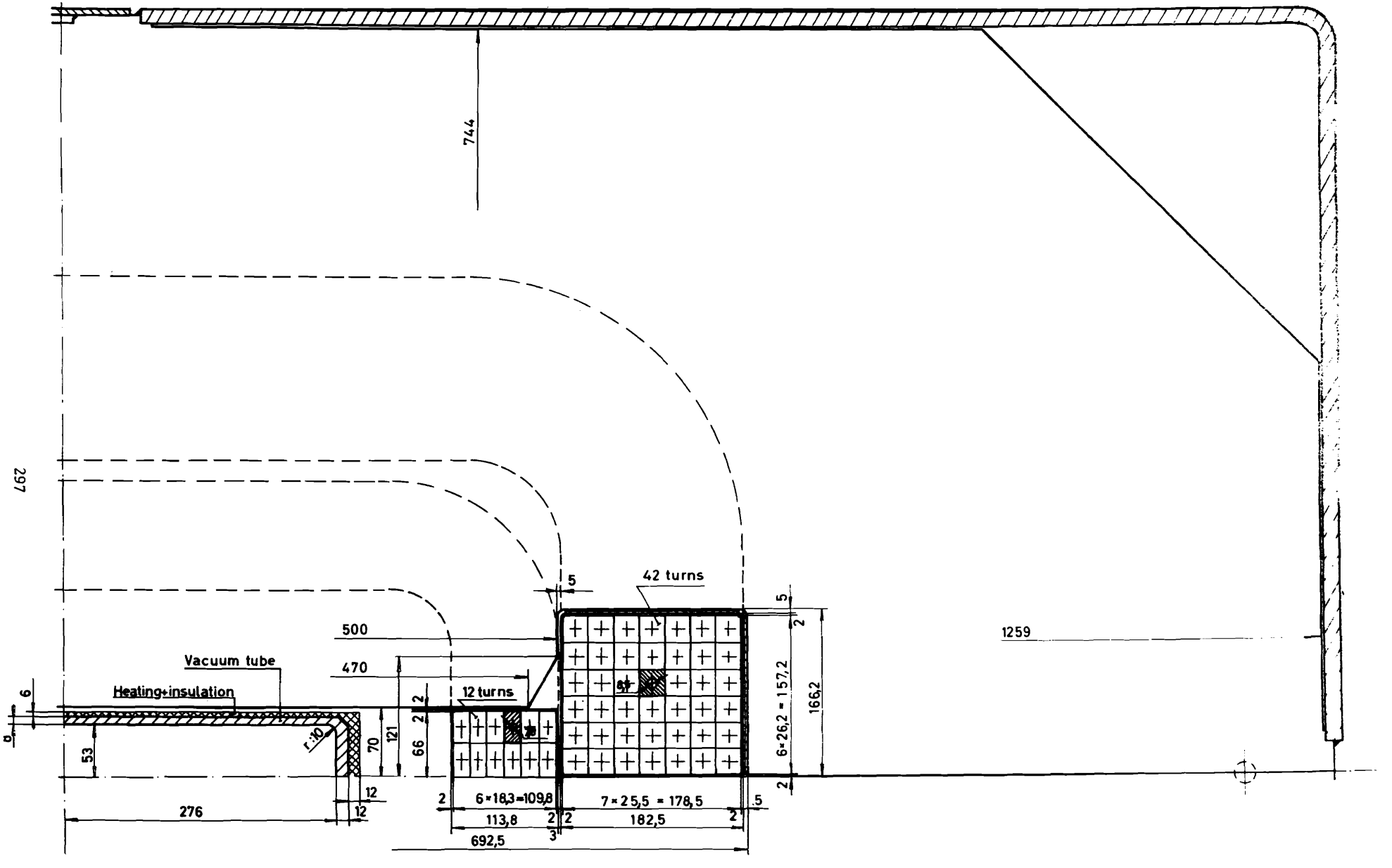

Fig. 3.2 Window-Frame Magnet. Cross Section

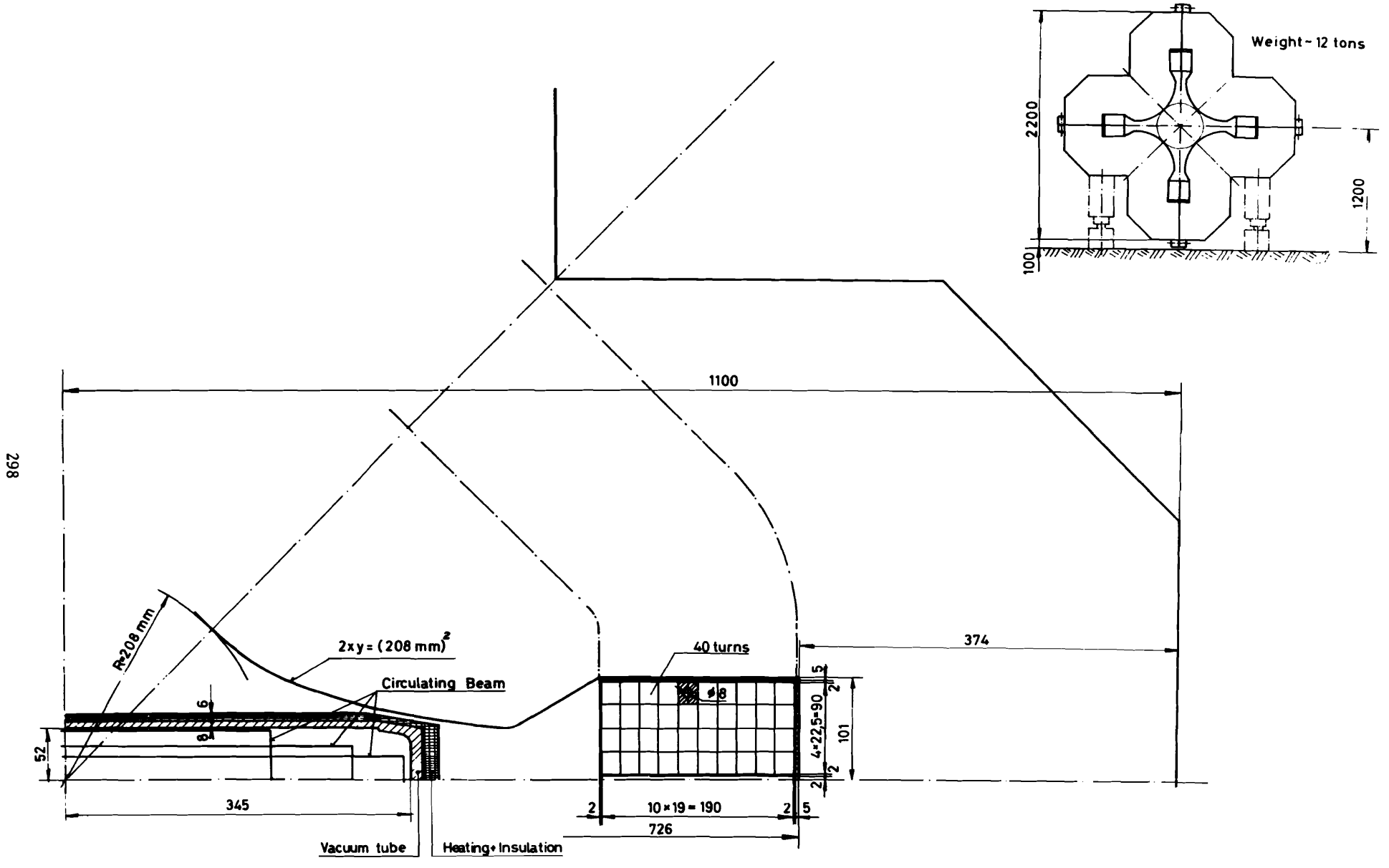

Fig. 3.3 Wide Quadrupole. Cross Section

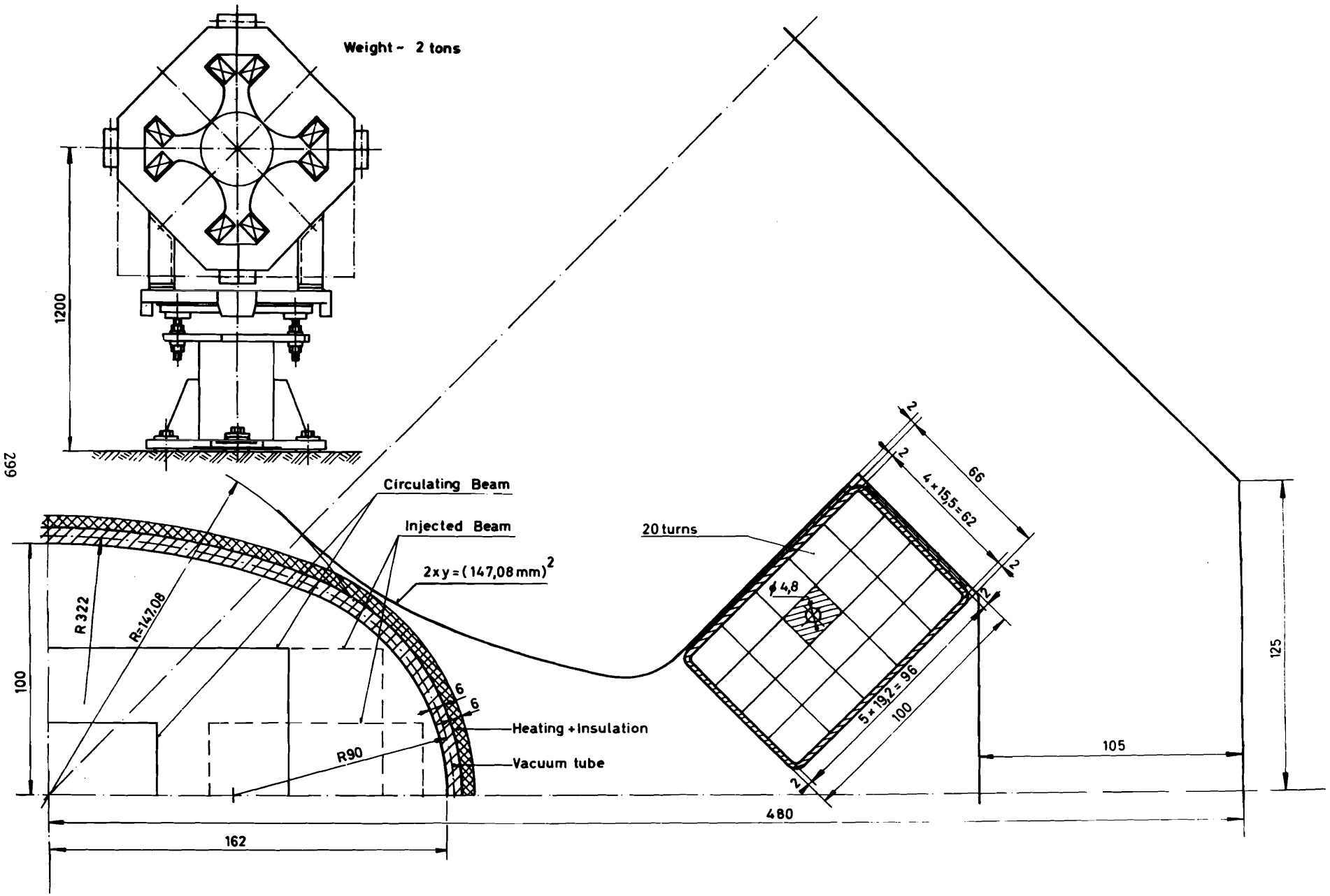

Fig. 3.4 Narrow Quadrupole. Cross Section

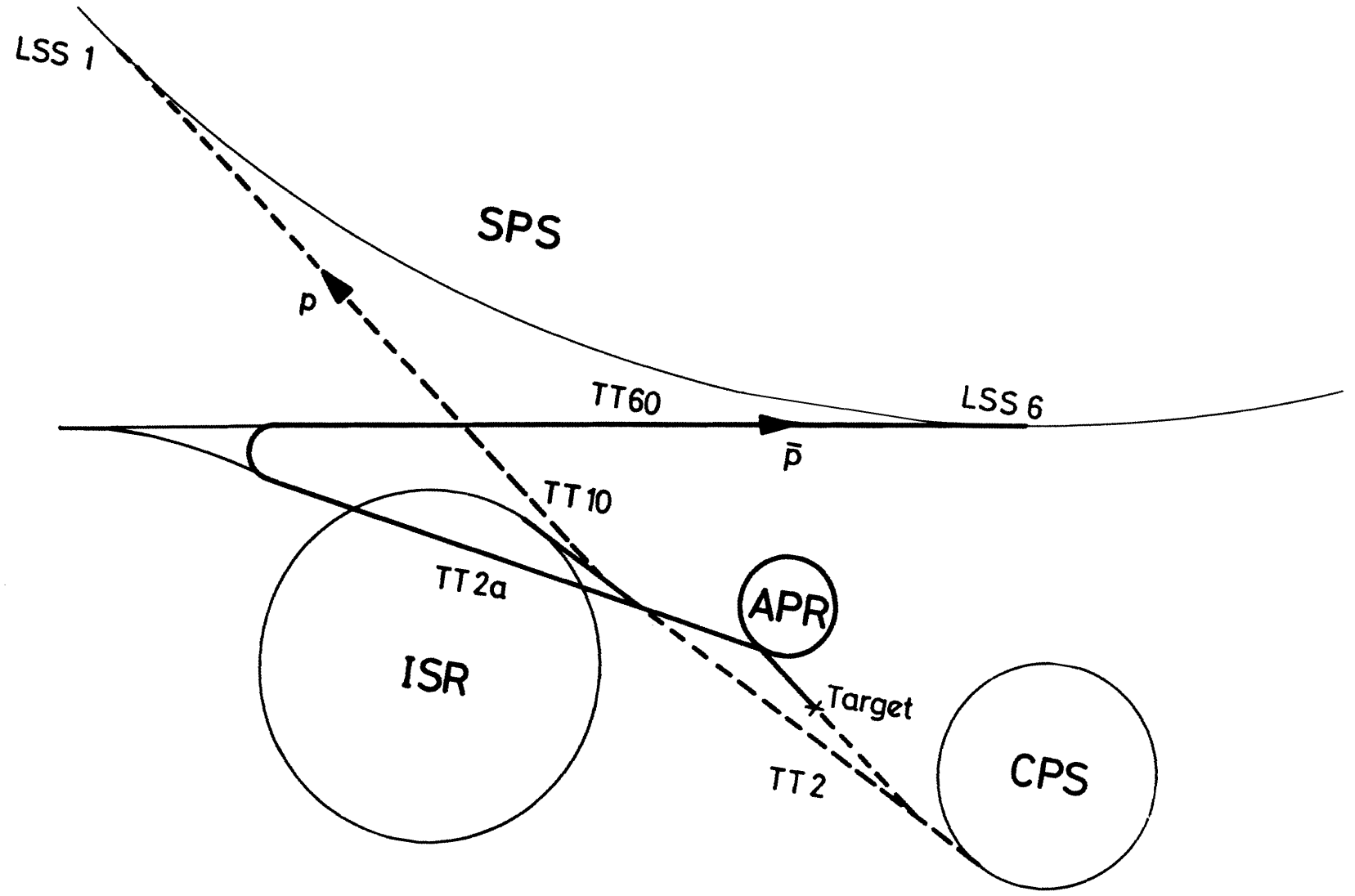

Fig. 4.1. Schematic layout of beam transfers.

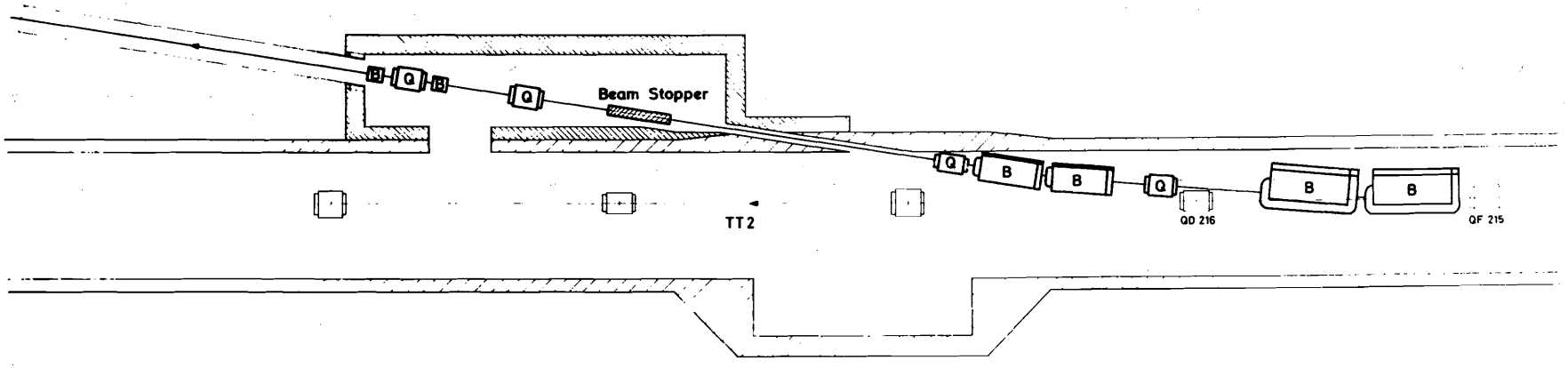

Fig. 4. 2. Layout of Branch-off TT2

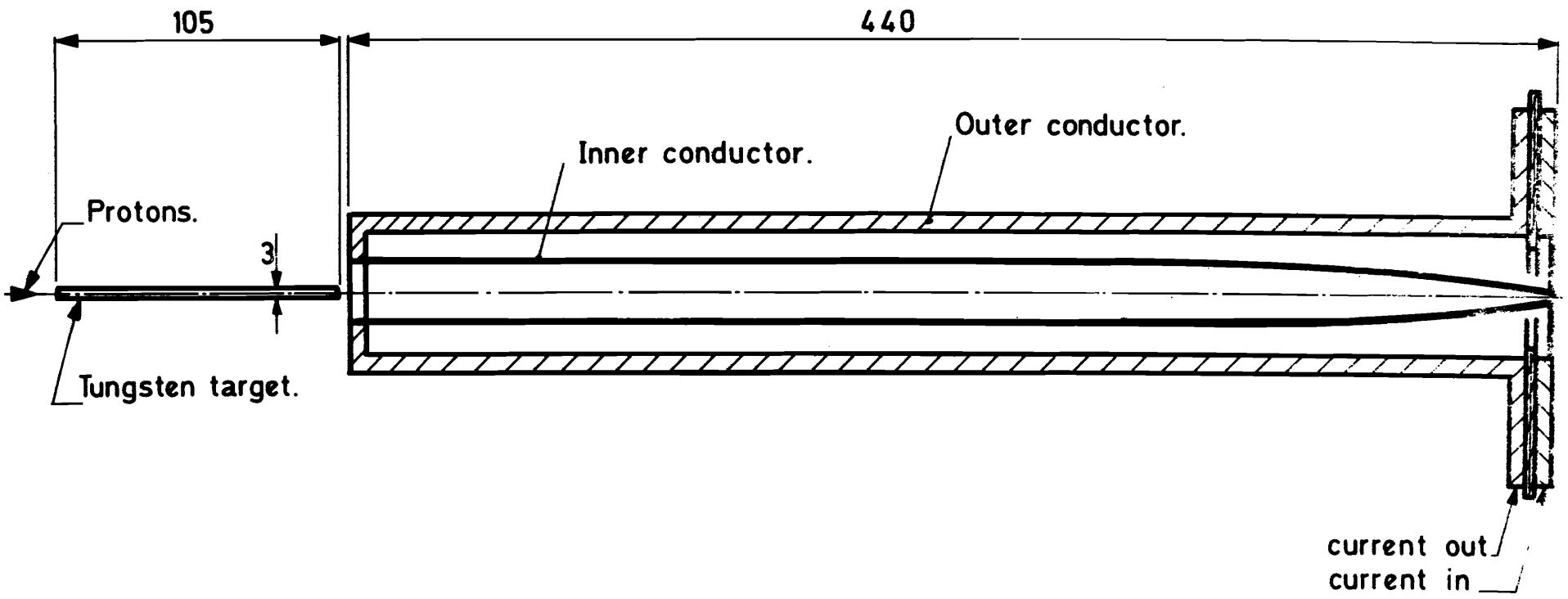

Scale 1:2

Fig. 4.3 Cross section of focusing horn.

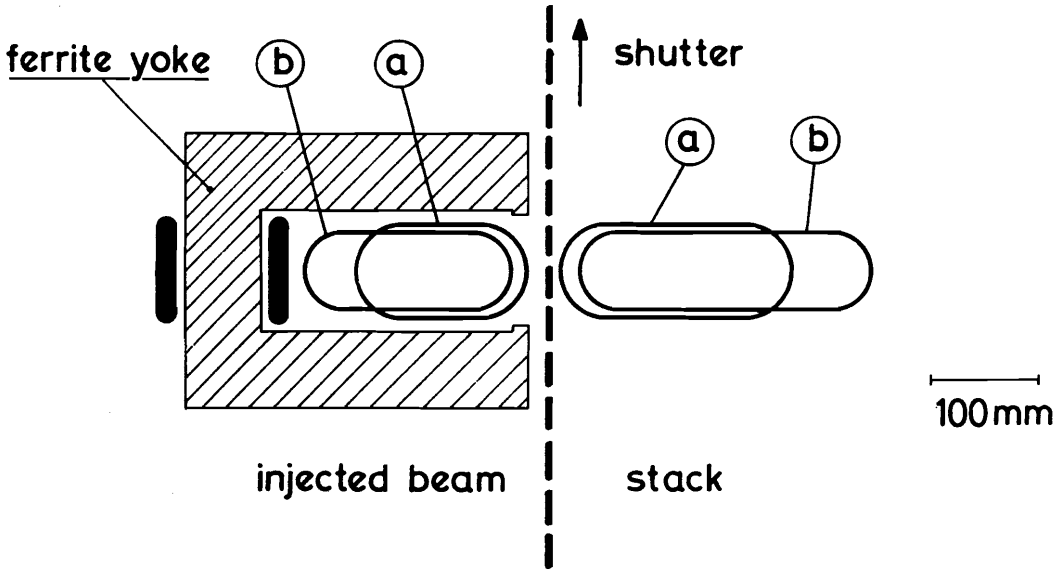

Fig. 4.4. Schematic cross section of the injection kicker; beams (a) at entrance and (b) at exit of kicker 1.

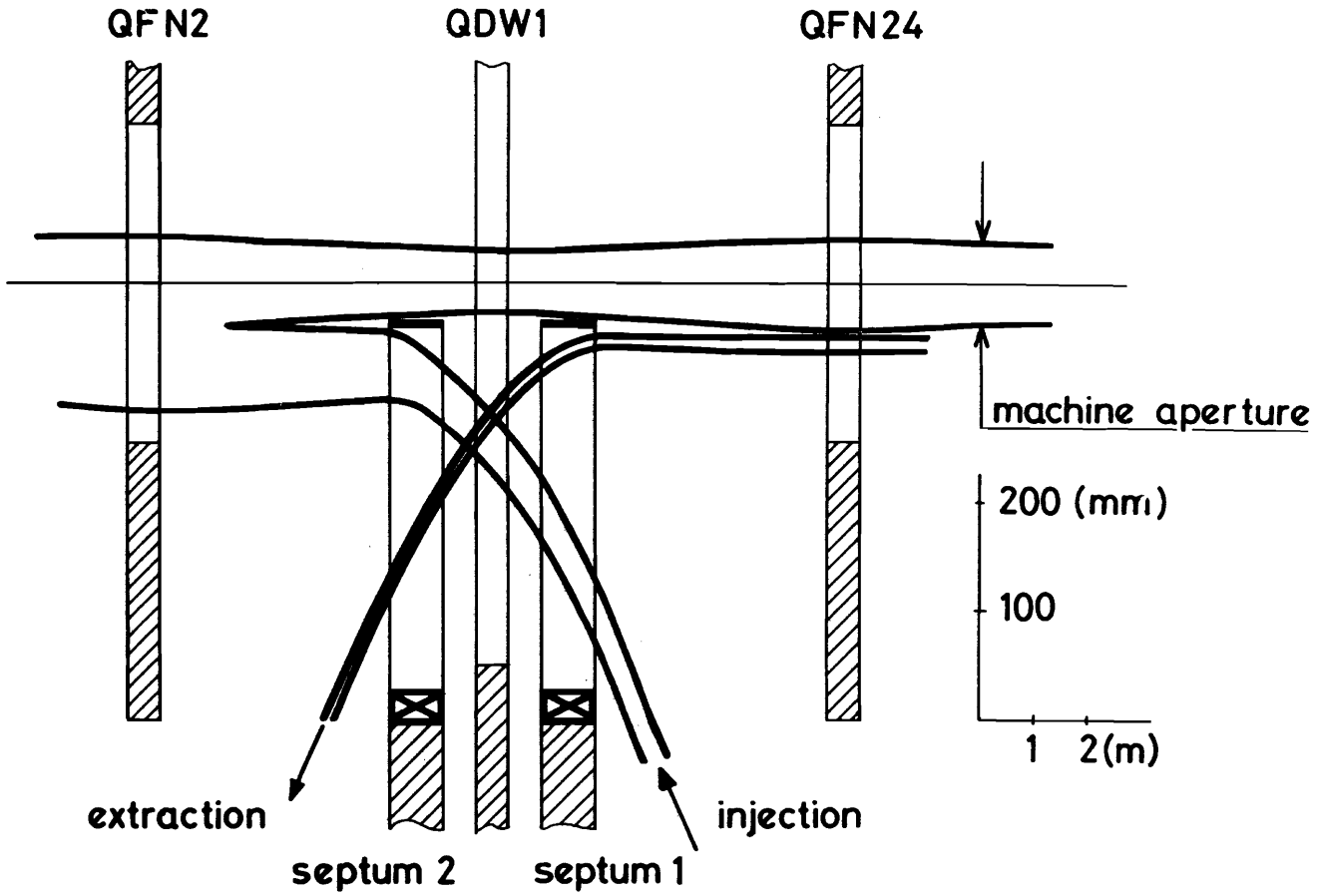

Fig.4.5. Layout of septum magnets for injection and extraction

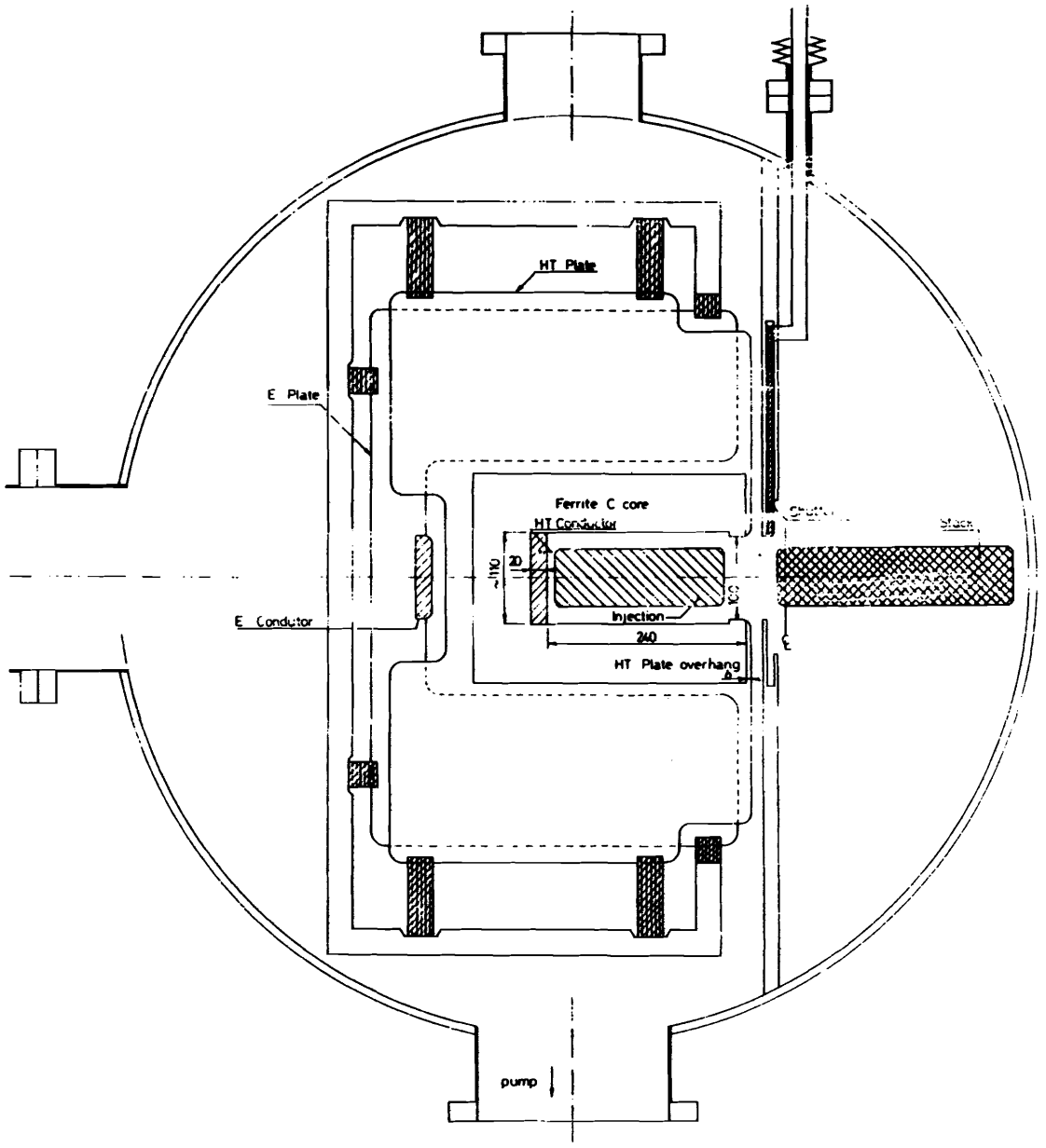

Fig.4.6 Injection Kicker. Cross Section

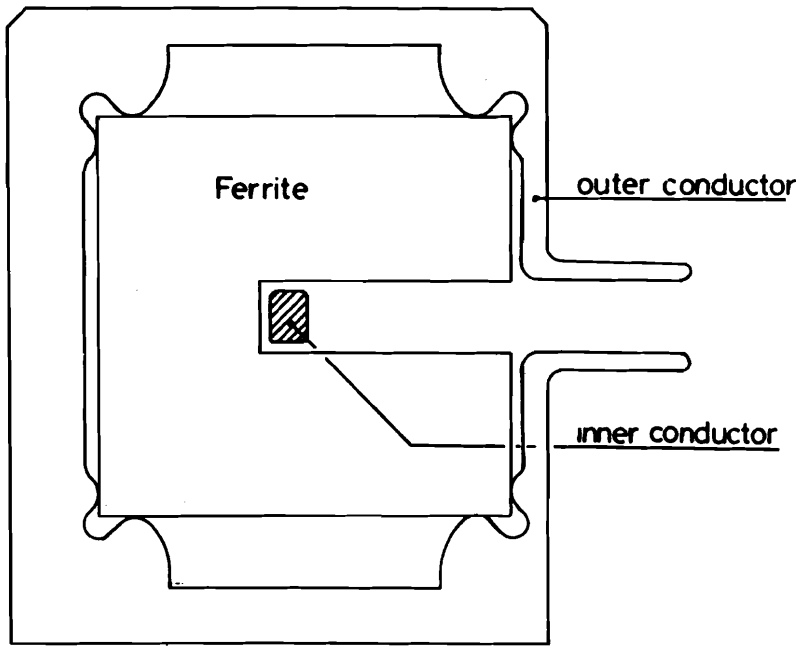

Fig.4.7 Extraction Kicker. Cross Section

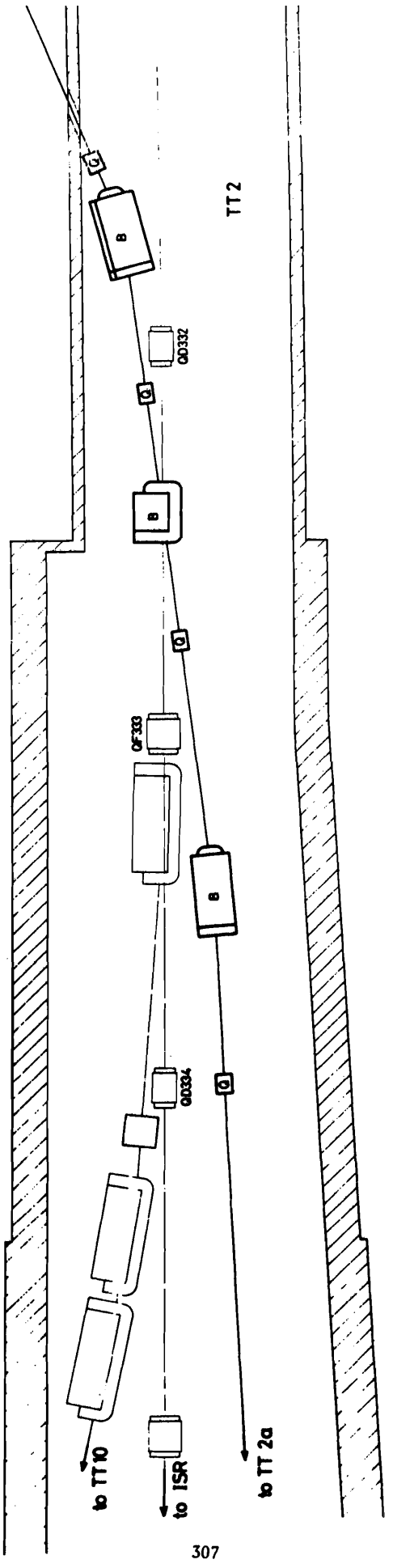

Fig. 4.8. Transfer of Antiprotons to the SPS ; Crossing TT2

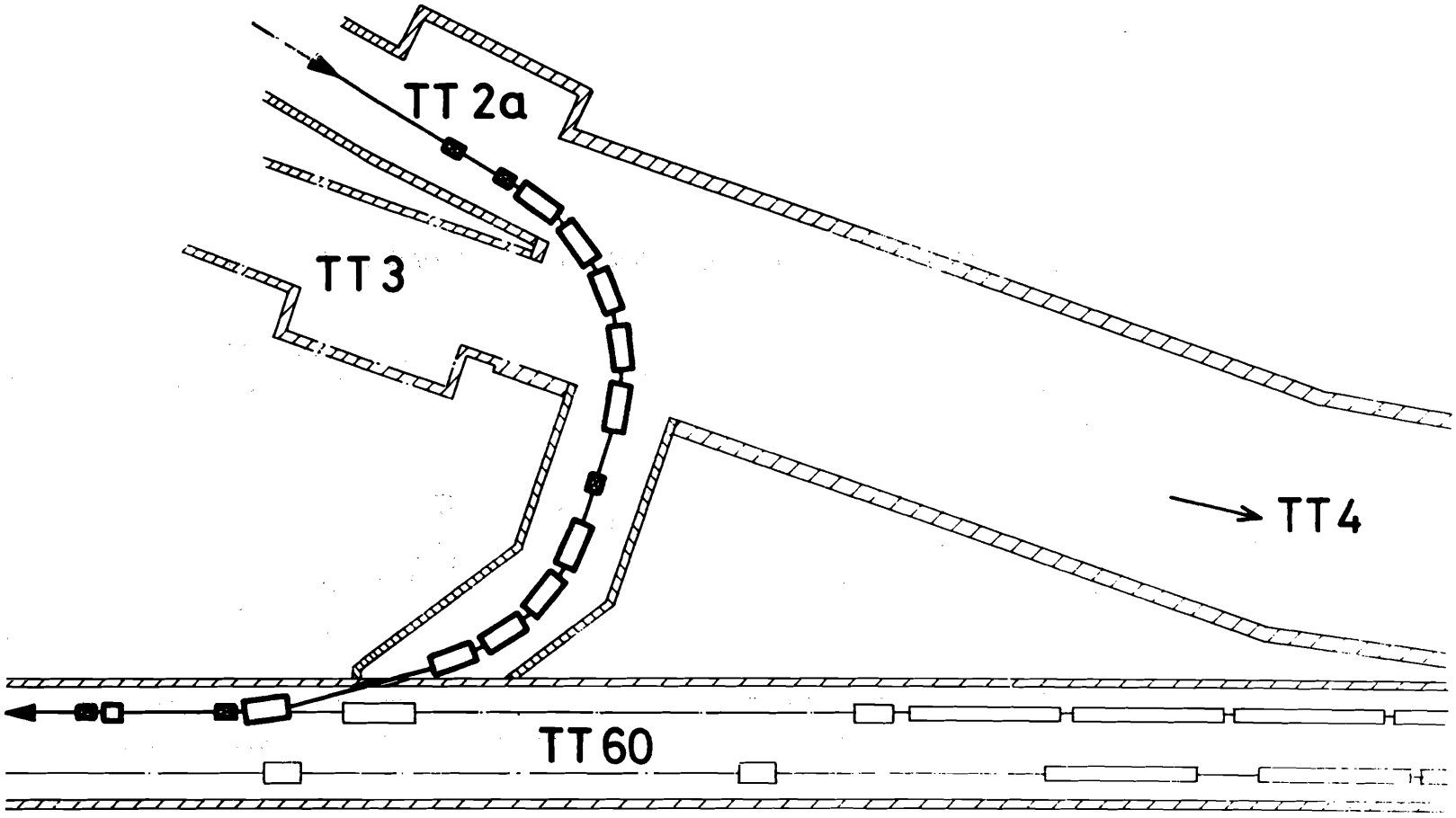

Fig. 4. 9 . Transfer of Antiprotons to the SPS ; junction TT60 - TT 2a.

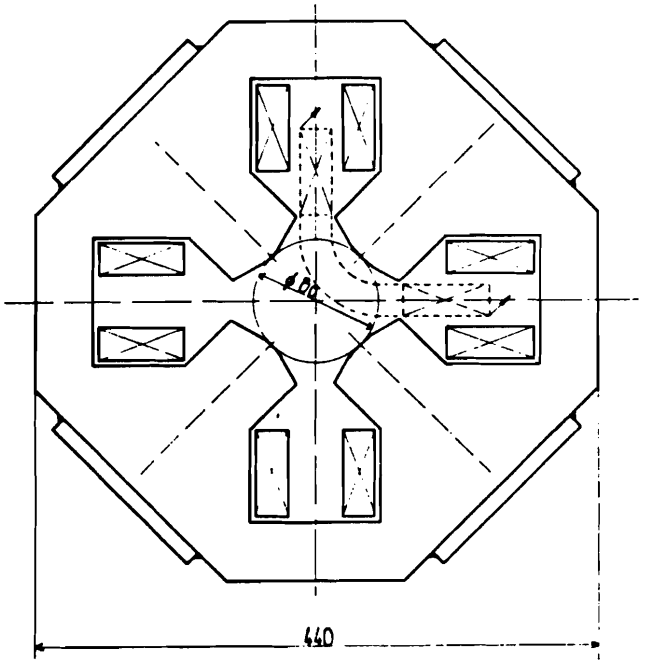

Nominal gradient	: 5 T/m
Inscribed diameter	: 80 mm
Core length	: 500 mm
Core width	: 440 mm
Number of turns per pole	: 27
Conductor	: 5 x 7.5 mm
Cooling hole diameter	: 3 mm
Nominal current	: 120 A
Power dissipation at I_{nom}	: 1440 Watt
Steel weight	: 370 kg
Copper weight	: 43 kg

Fig. 4.10 Cross-section of beam transfer quadrupole

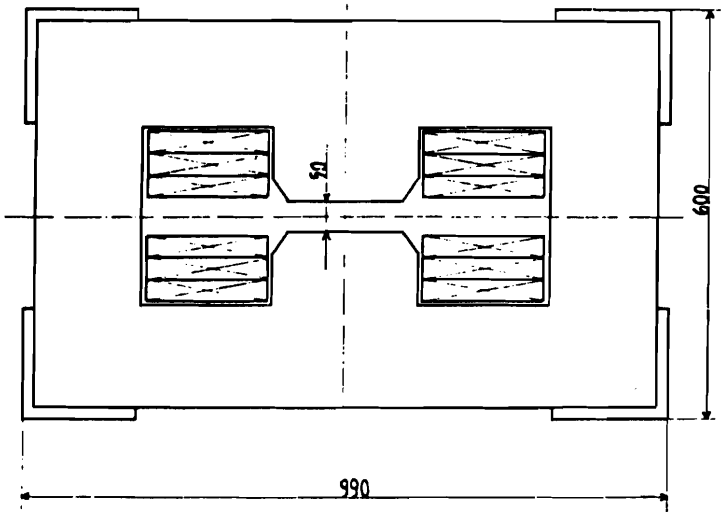

Nominal field	: 1.7 T
Gap height	: 50 mm
Core width	: 990 mm
Core height	: 600 mm
Steel length	: 1.9 m
Number of turns	: 192
Conductor	: 11 x 11 mm
Cooling hole diameter	: 6 mm
Nominal current	: 390 A
Power dissipation at I_{nom}	: 28.3 kW
Steel weight	: 6800 kg
Copper weight	: 775 kg

Fig. 4.11 Cross-section of beam transfer bending magnet

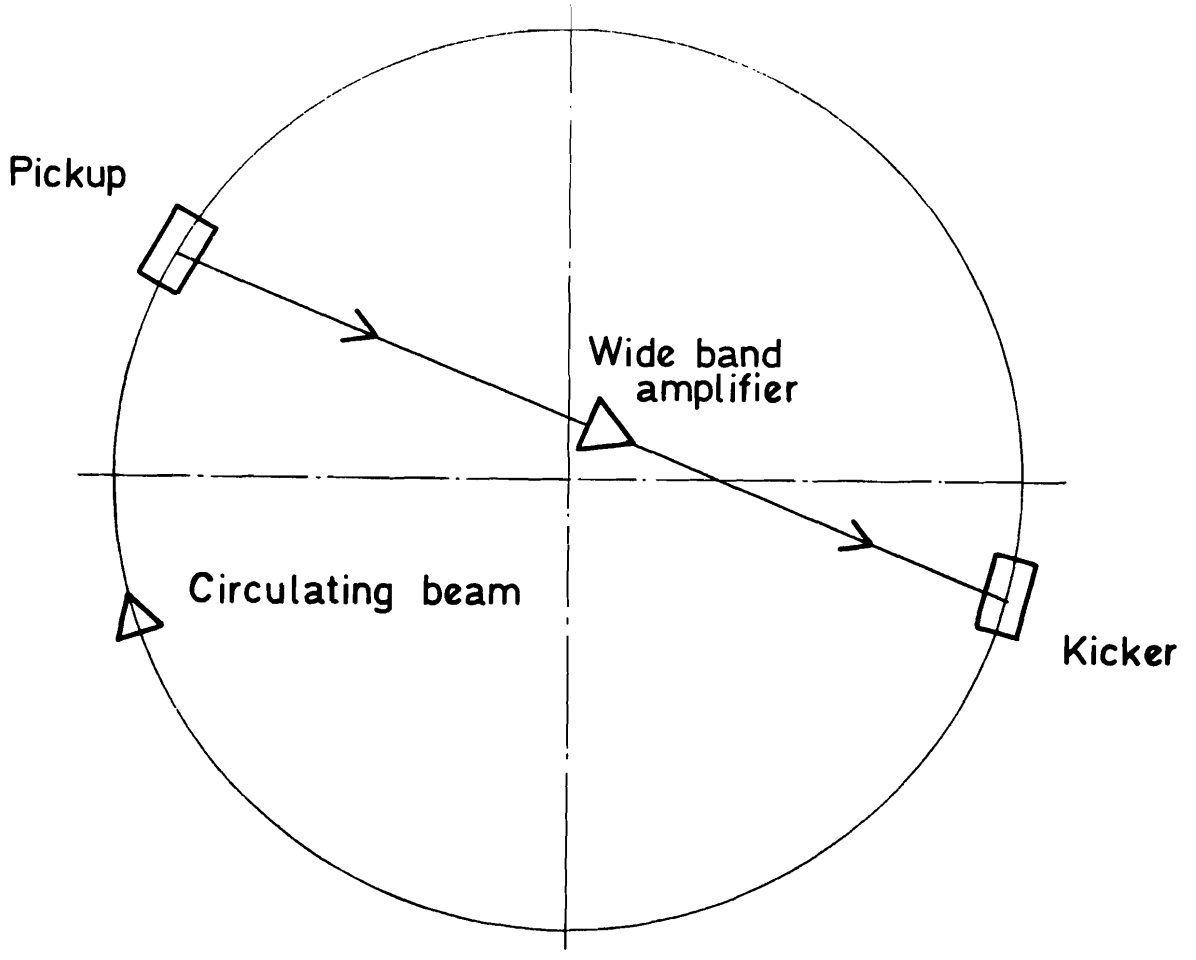

Fig. 6.1 Schematic representation of a storage ring with momentum cooling.

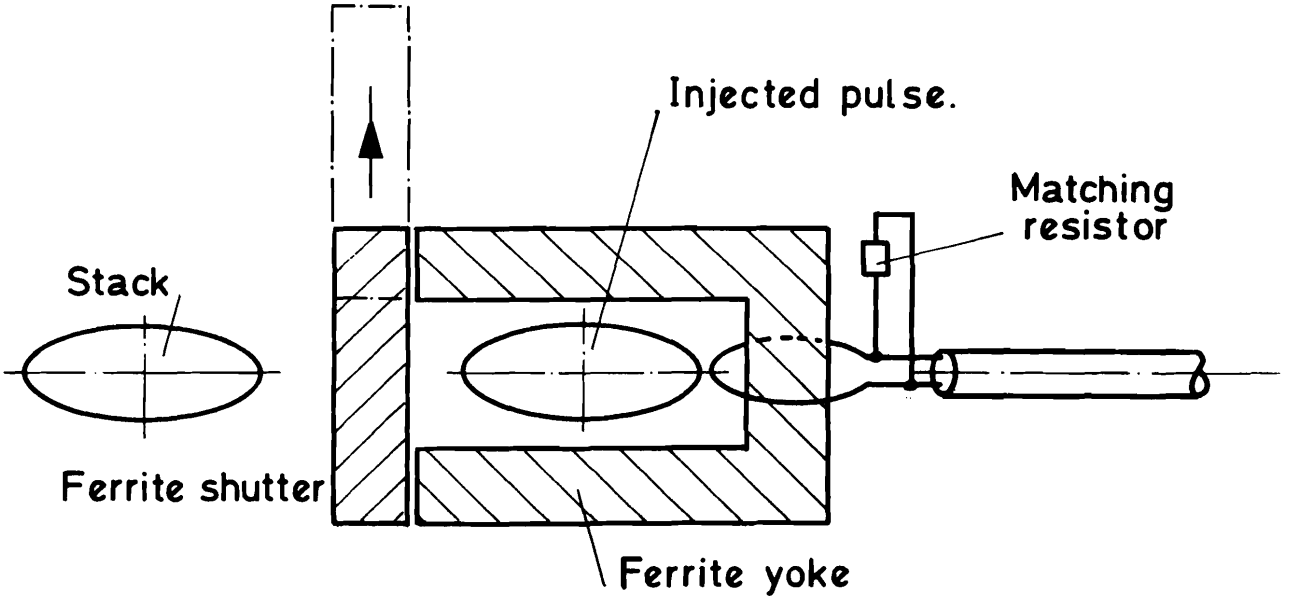

Fig. 6.2 Schematic cross section of precooling pickup or kicker.

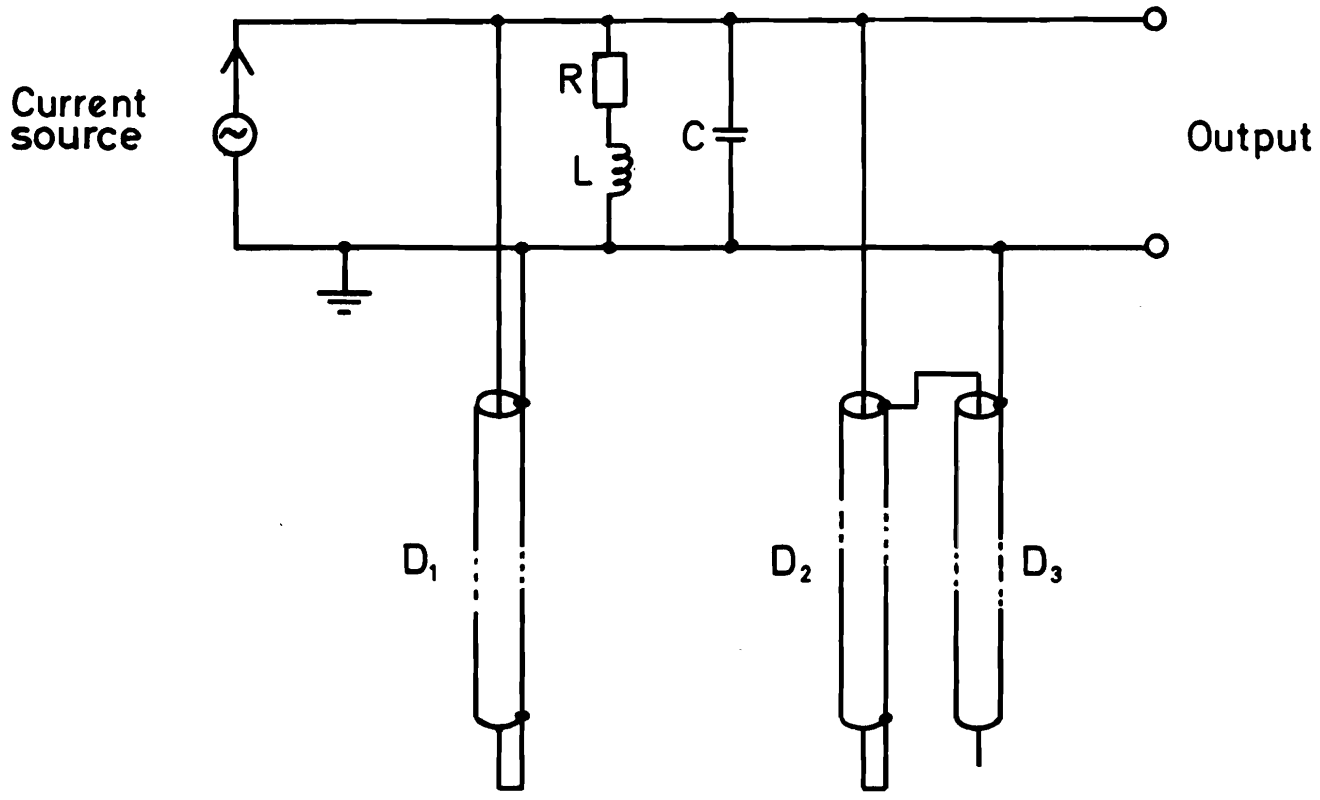

Fig. 6.3 Precooling filter

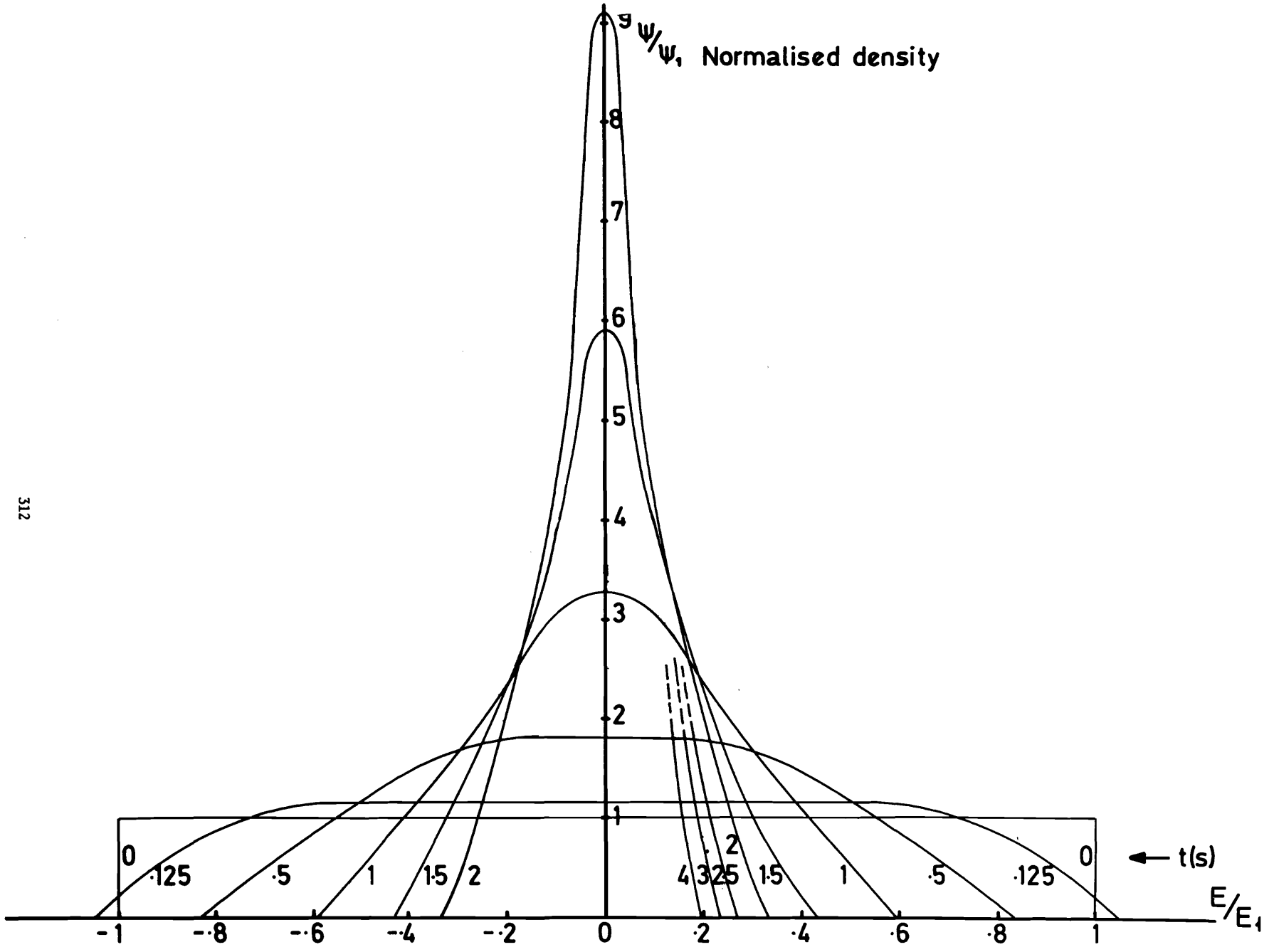

Fig. 6.4 Precooling curves.

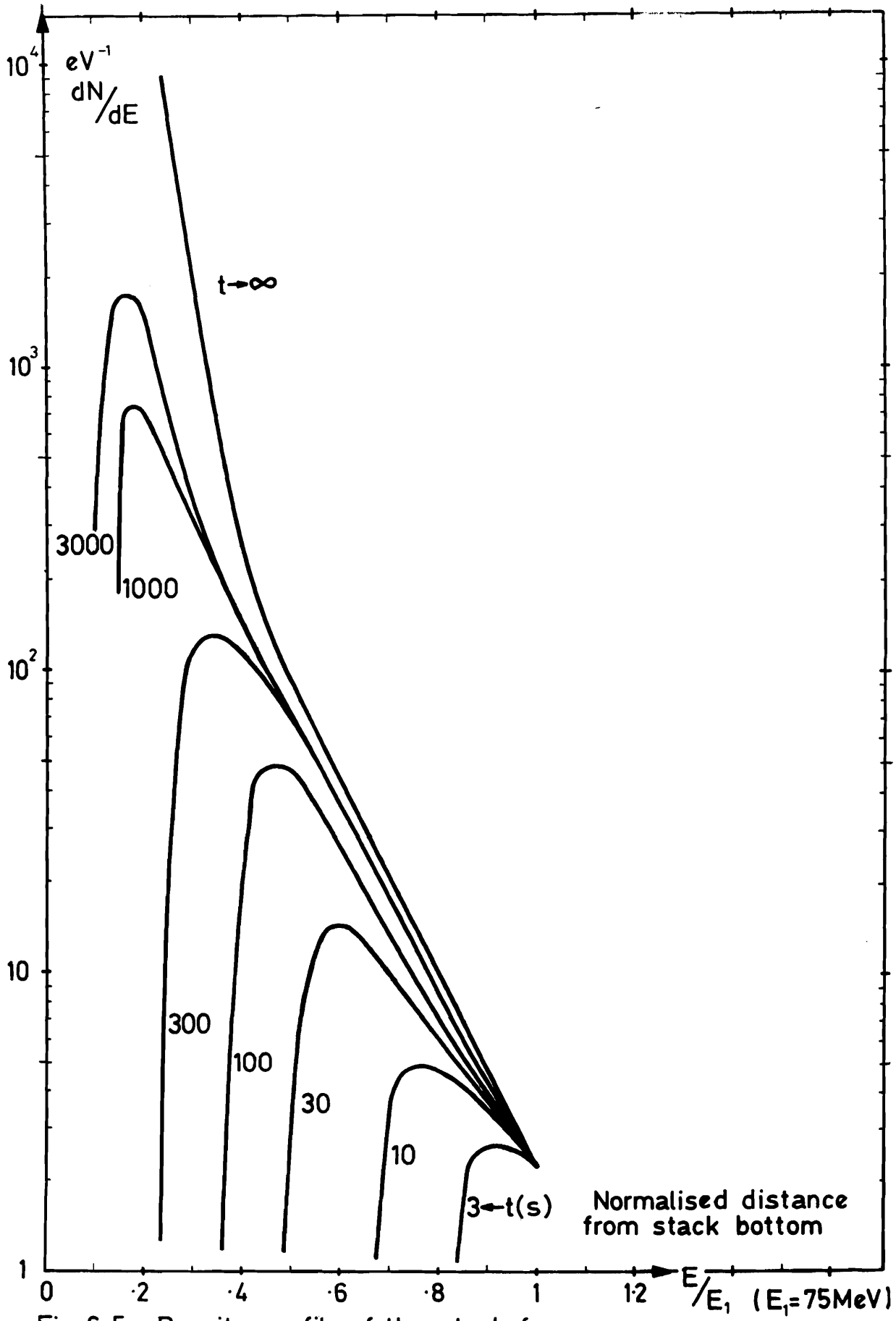

Fig. 6.5. Density profile of the stack for a constant particle flux towards the stack bottom.

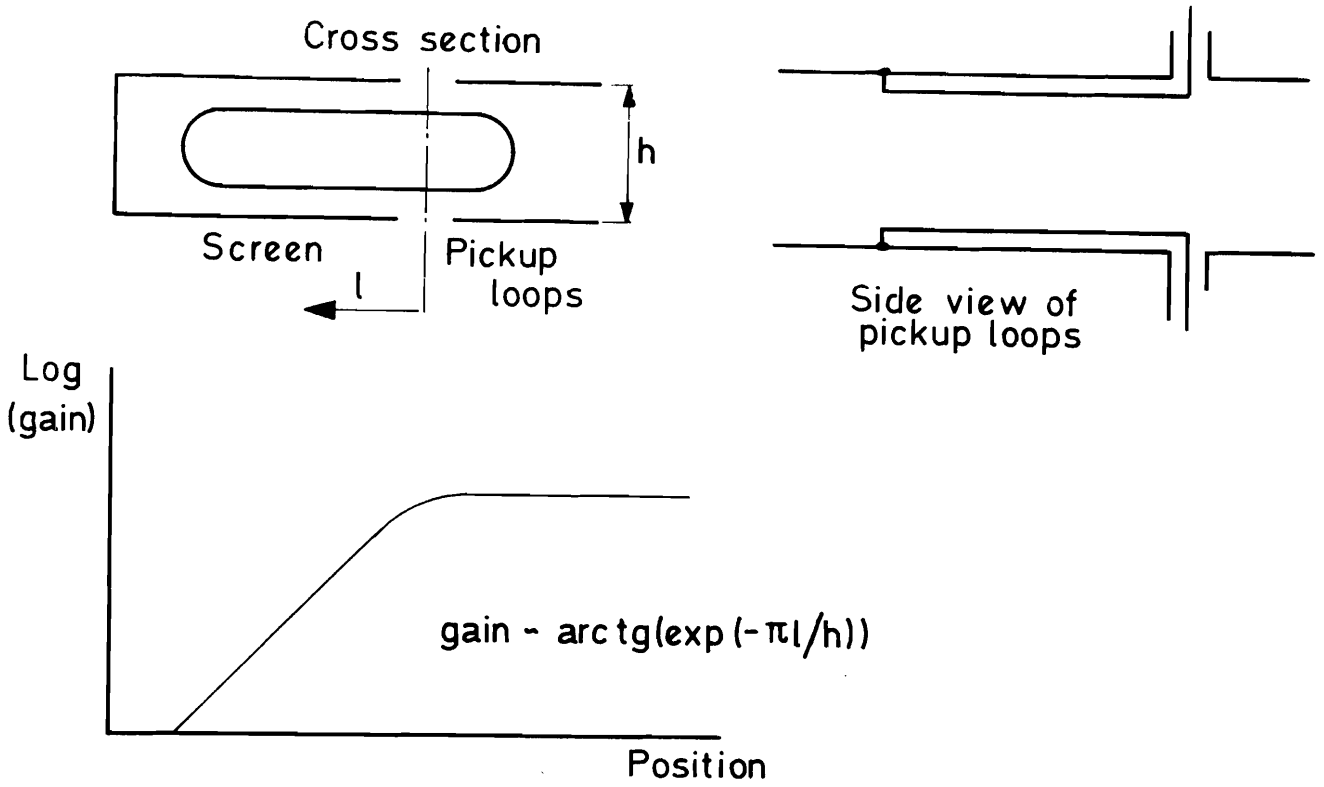

Fig.6.6 Schematic cross section and gain profile of the stack pickups.

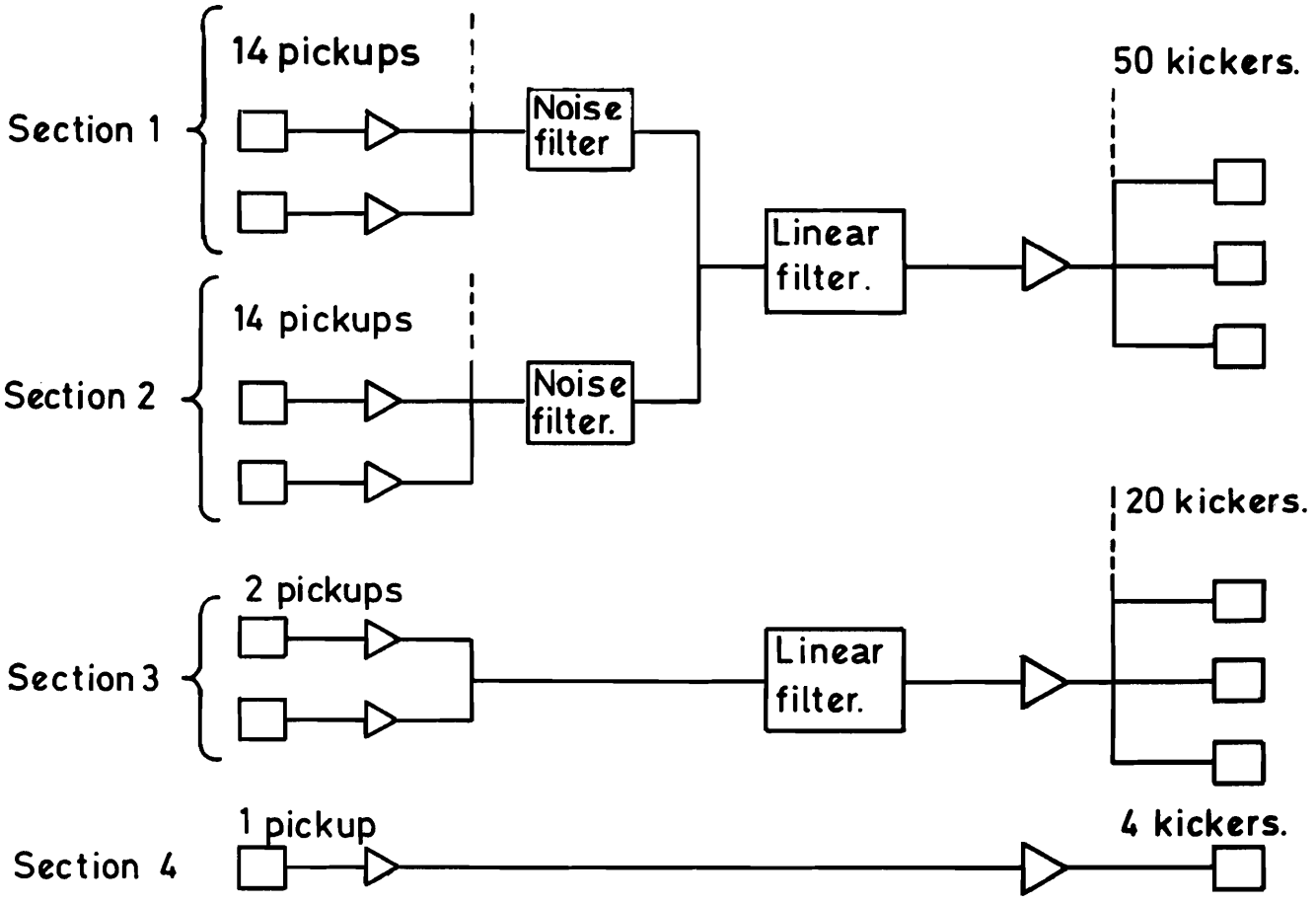

Fig.6.7 Block diagram of the stack cooling system.

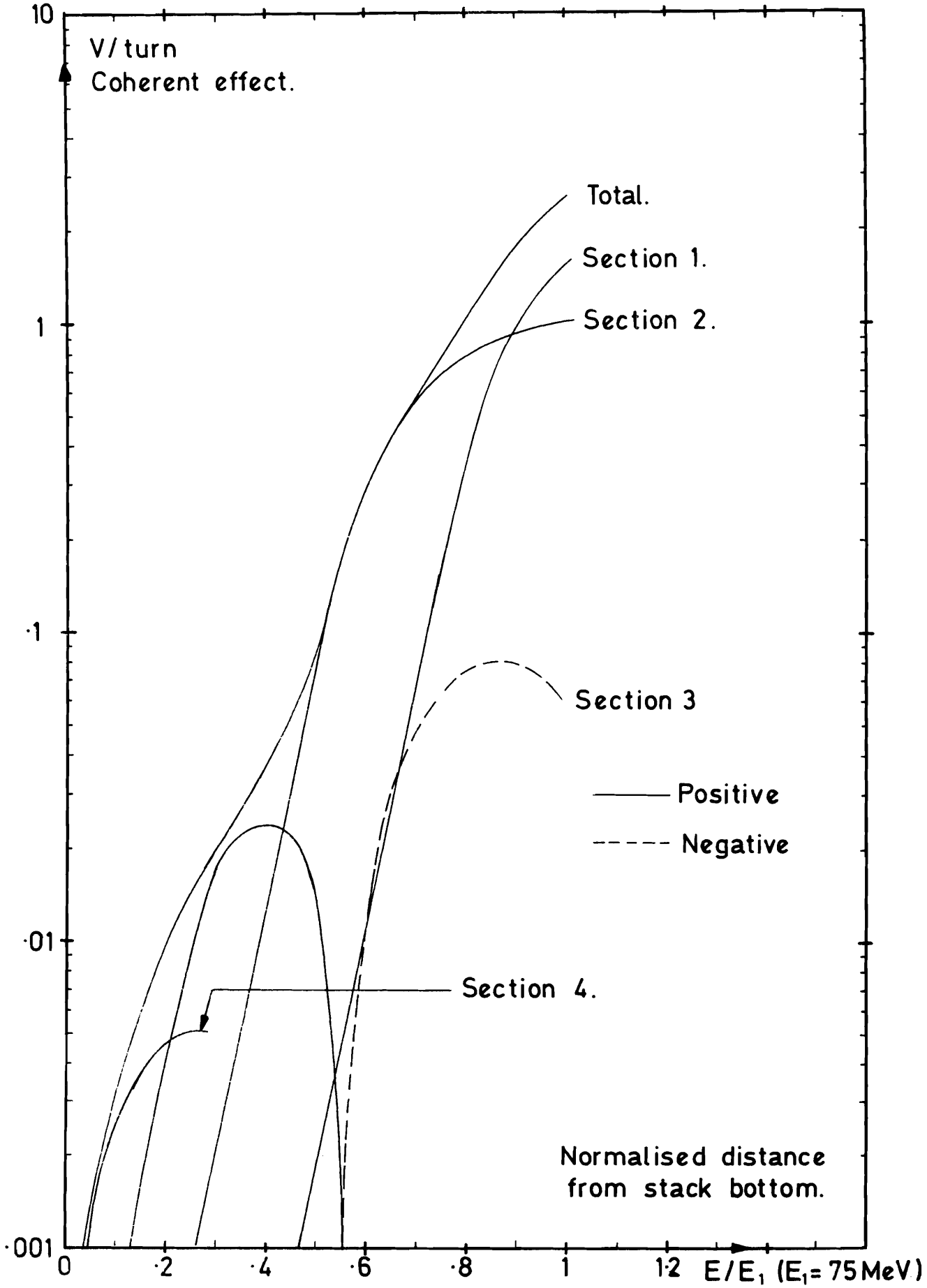

Fig. 6.8. Gain curves for stack cooling system.

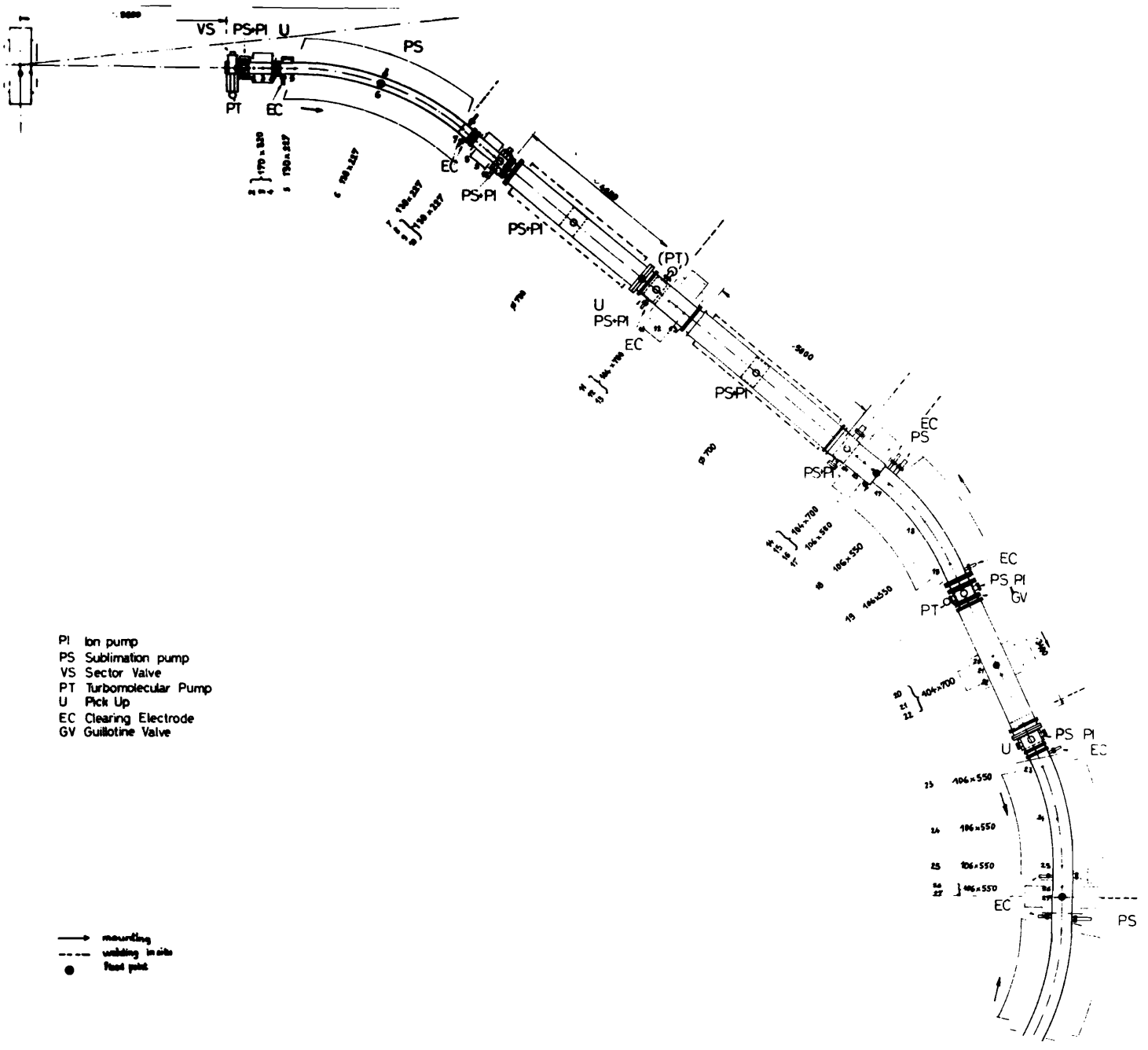

Fig. 7.1 Vacuum System Layout

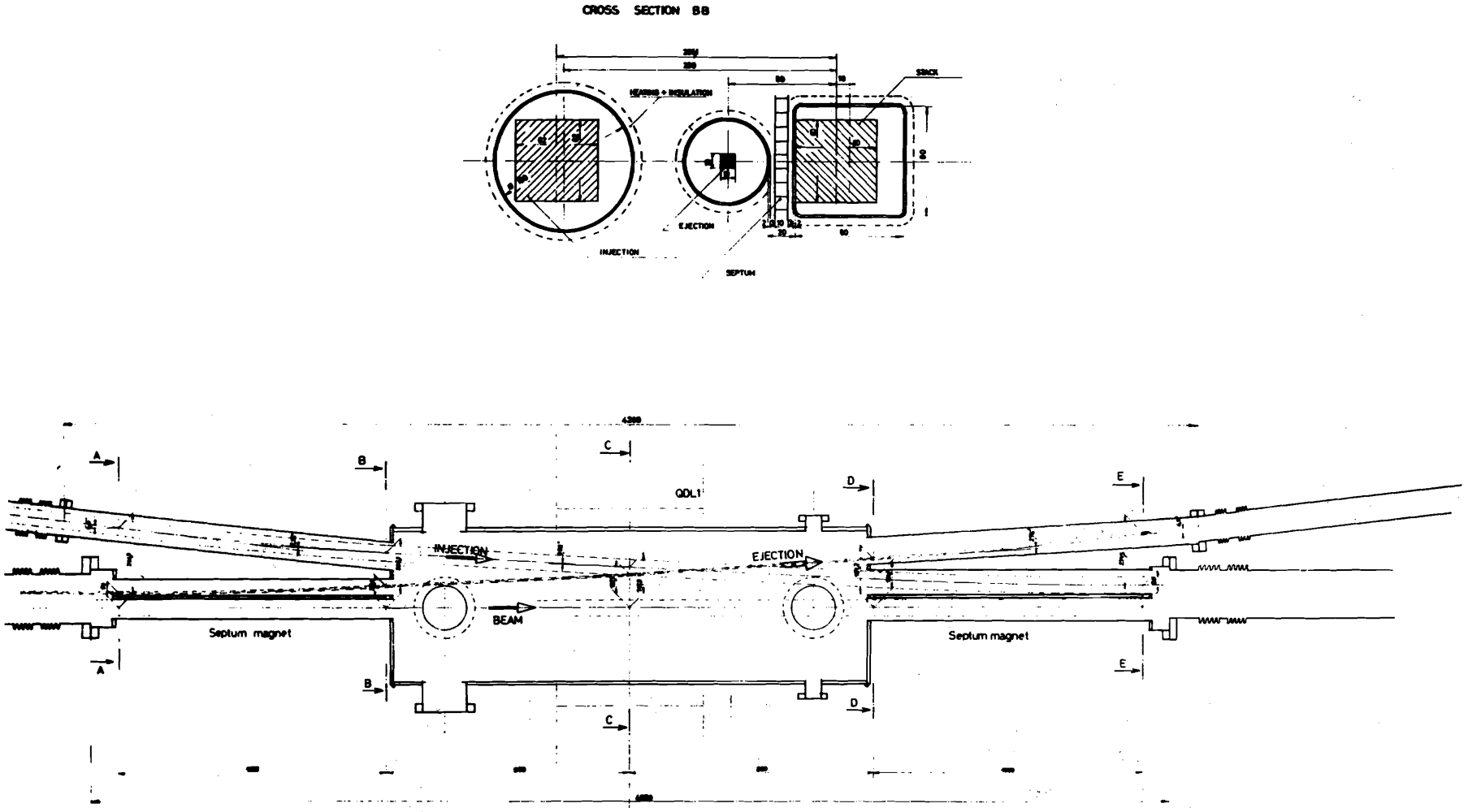

Fig. 7.2 Vacuum chamber. Injection / Extraction region

Fig. 8.1 Beam Diagnostics

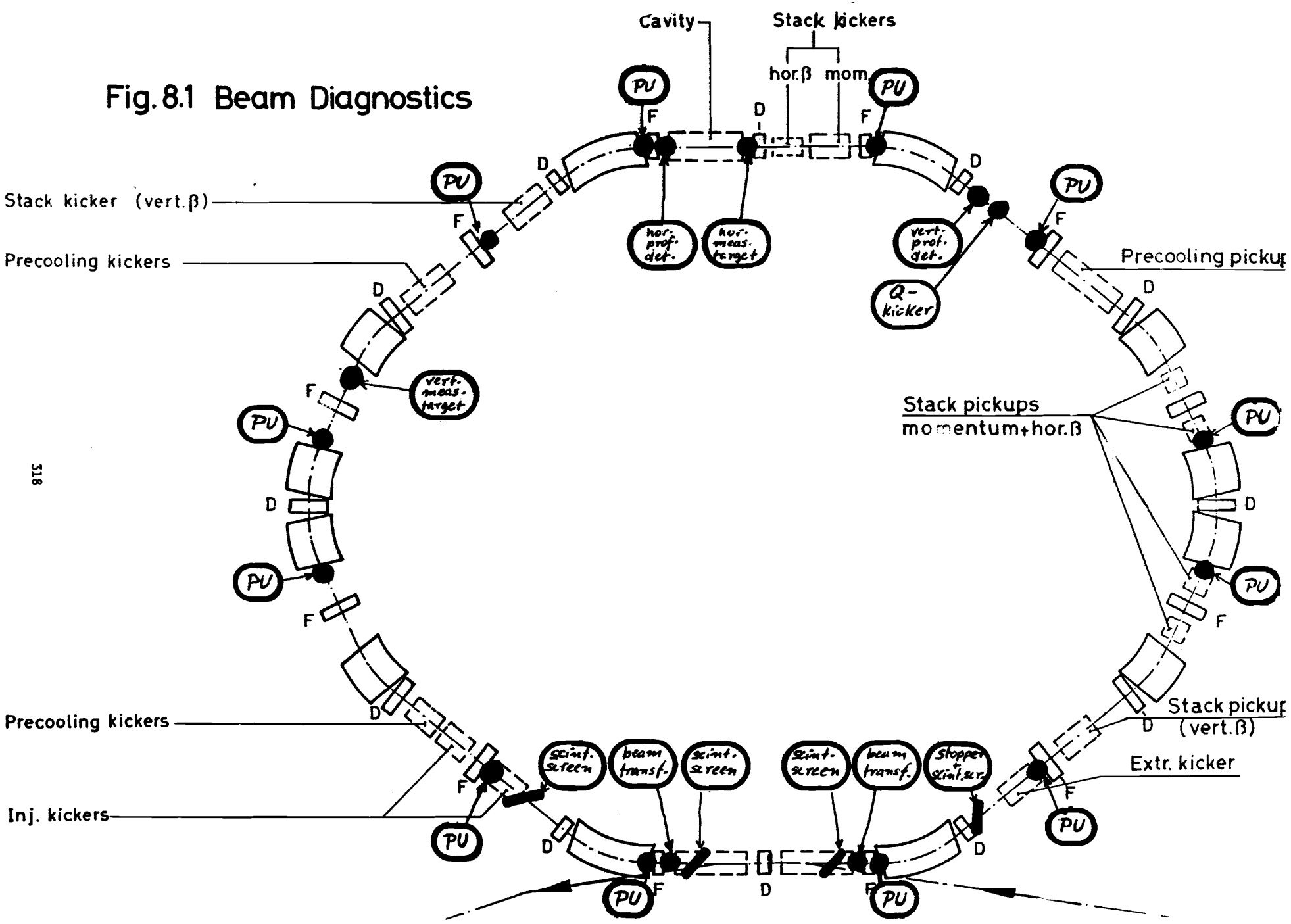

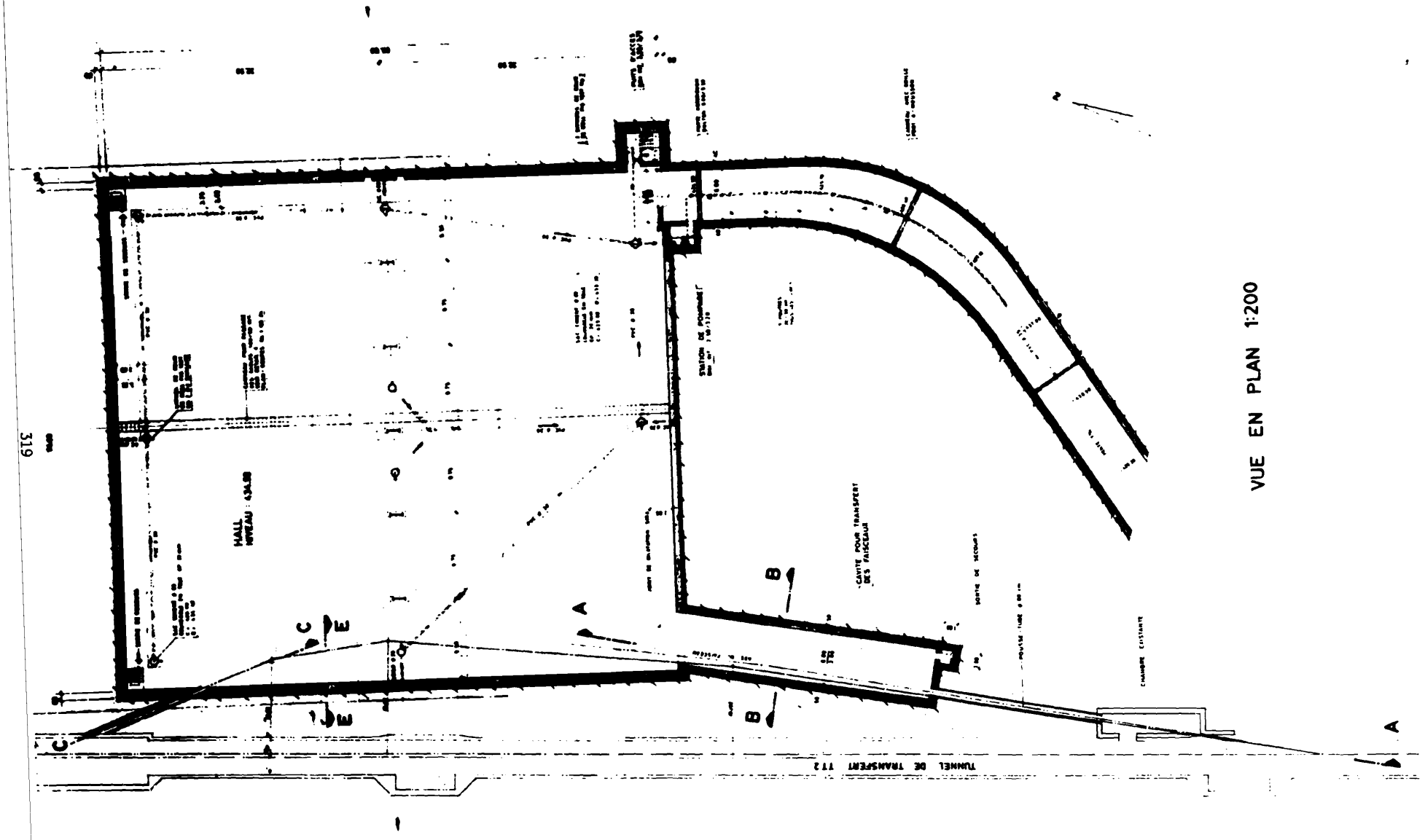

Fig. 9.1 Building Overall View

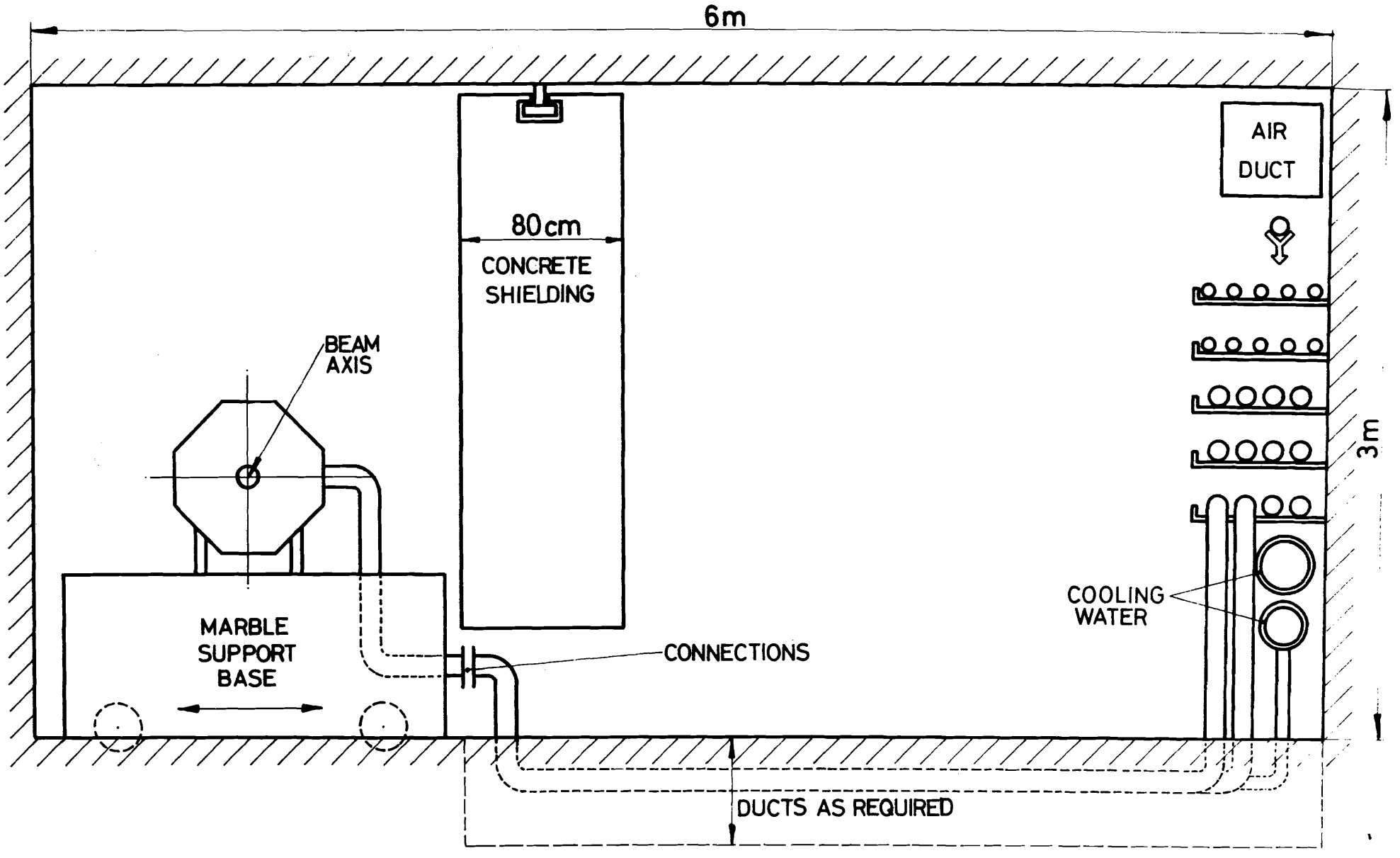

Fig. 9.2 Target area Schematic cross section

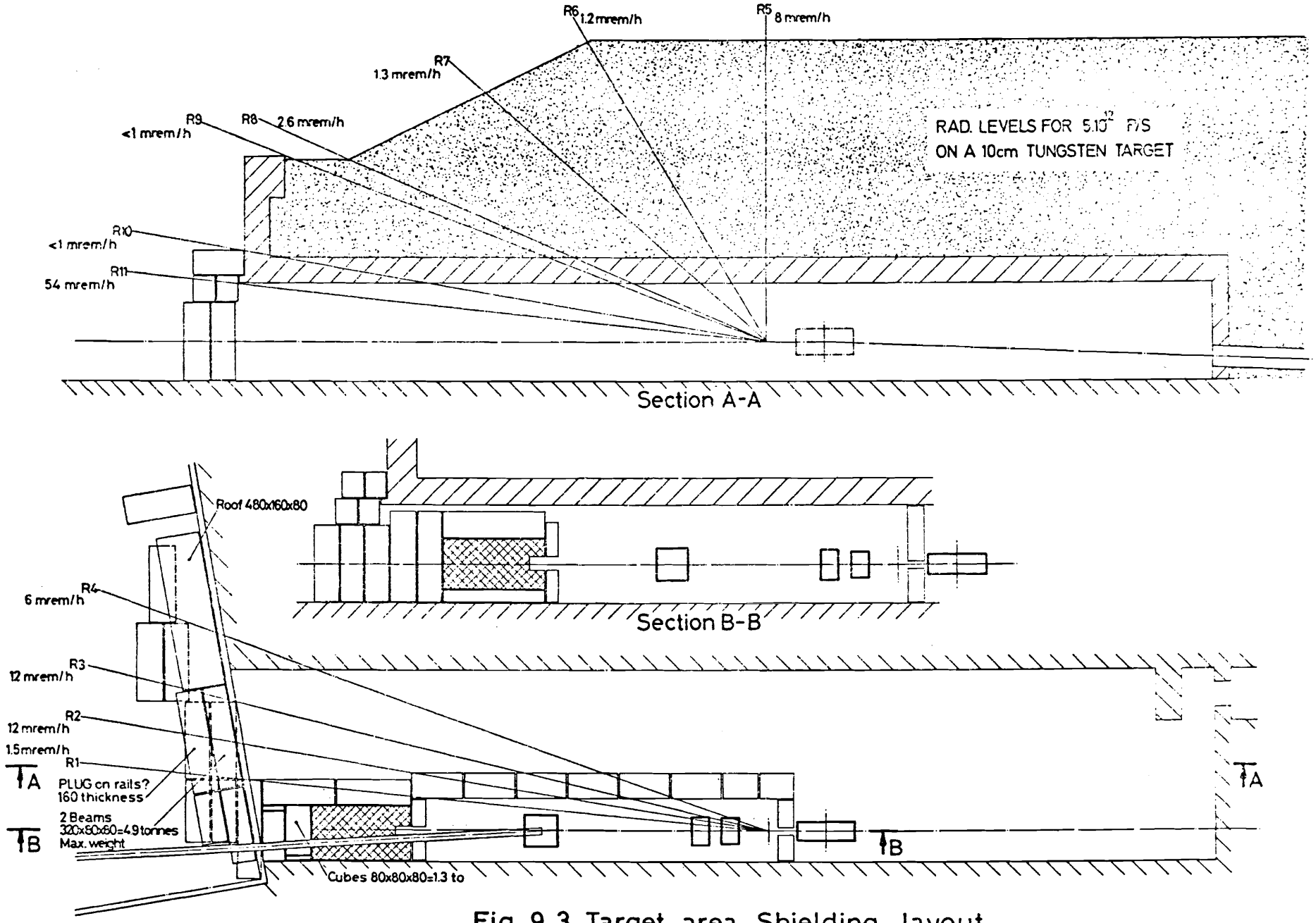

Fig. 9.3 Target area Shielding layout

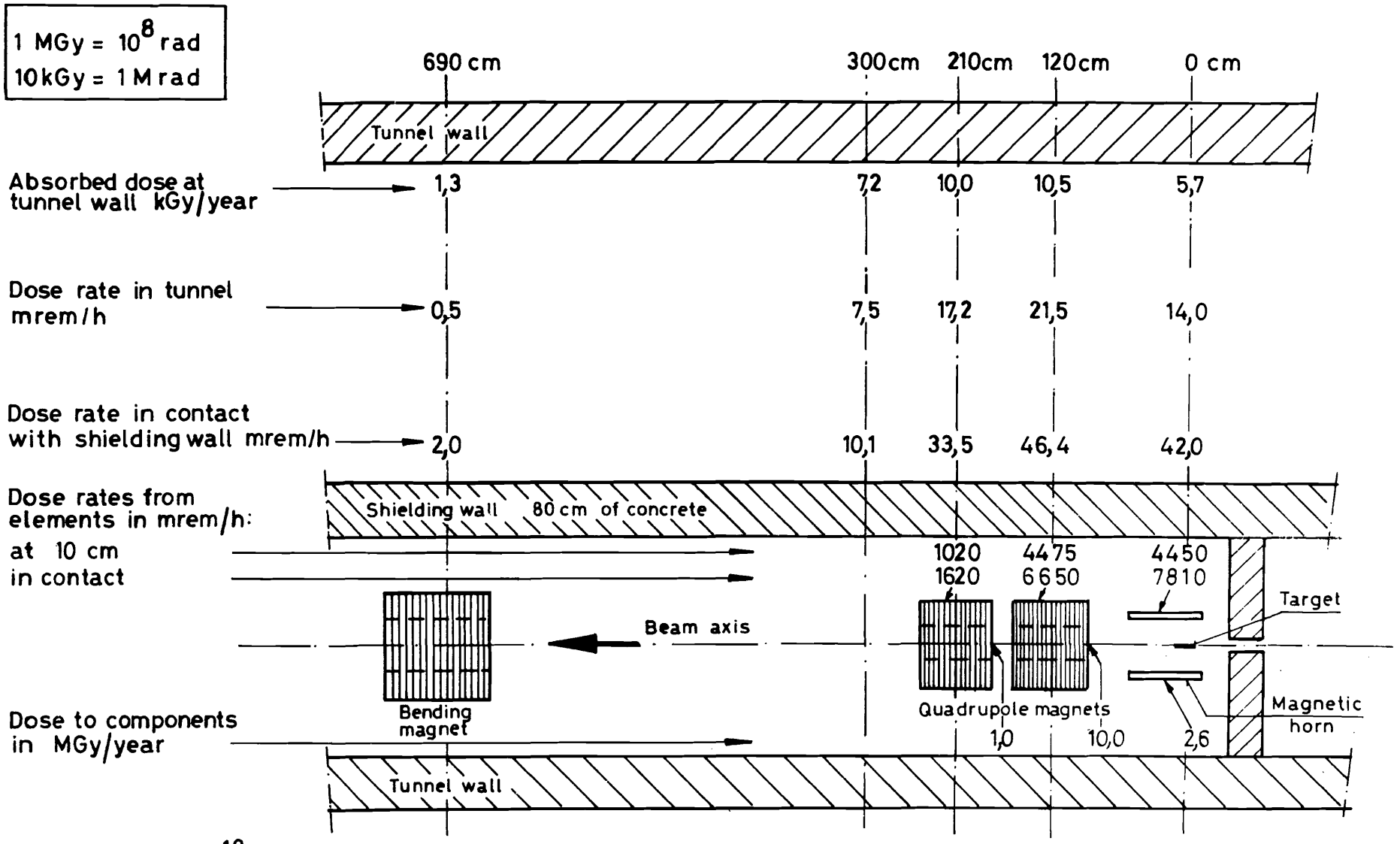

Assumption: $5 \cdot 10^{18}$ p/annum and 24h cooling!; for 2h cooling multiply dose rate figures by 3; for 15 min cooling multiply by 4,5.

Fig. 9.4 Target area Calculated radiation levels

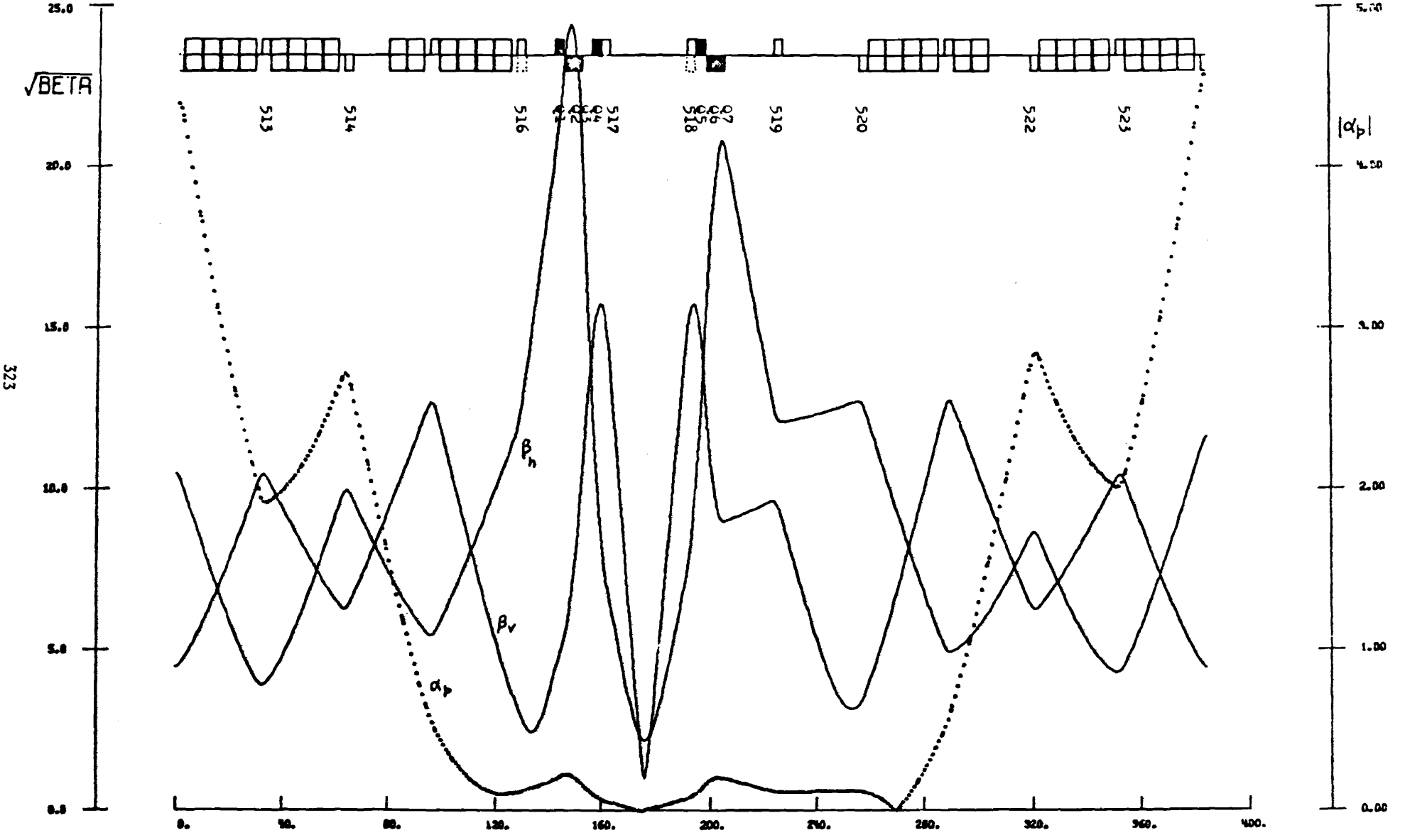

Fig. 10.1 SPS Insertion for low beta at proton-antiproton interaction point

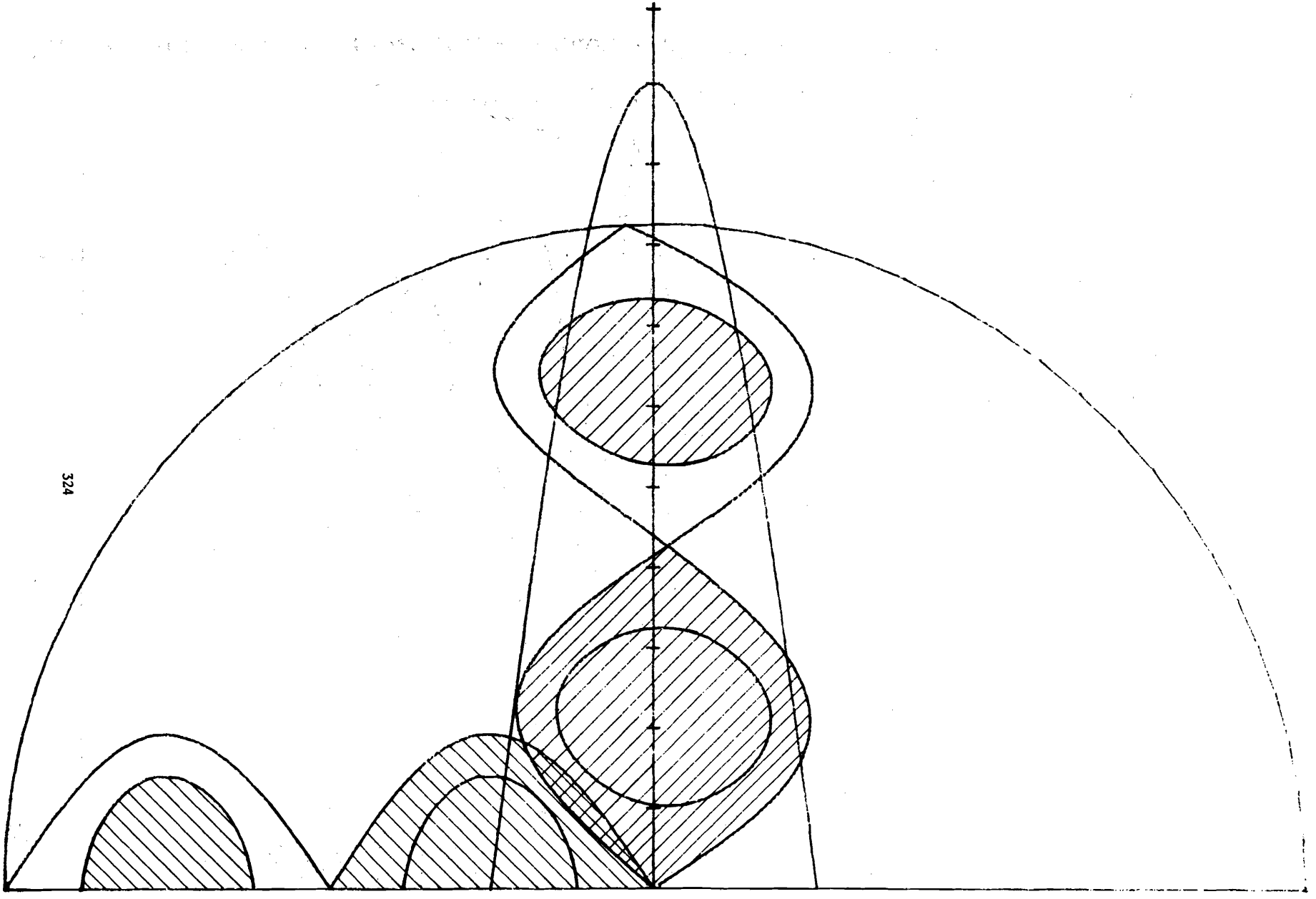

Fig. 10.2 Bunch rotation at 270 GeV.